A galanin-positive population of lumbar spinal cord neurons modulates sexual behavior and arousal

Constanze Lenschow[1,3,4], Ana Rita P. Mendes[1,3], Liliana Ferreira[1], Bertrand Lacoste[1], Camille Quilgars[2], Sandrine S. Bertrand[2] and *Susana Q. Lima[1]

1. Champalimaud Neuroscience Programme; Champalimaud Foundation, Av. Brasília, Doca de Pedrouços, 1400-038 Lisbon, Portugal.
2. INCIA, Université de Bordeaux, CNRS UMR5287, 33076 Bordeaux, France.
3. equal contribution
4. Present affiliation: Institute of Biology (House 91), Otto-von-Guericke University Magdeburg, Leipziger Straße 44, 39120 Magdeburg

*corresponding author: susana.lima@neuro.fchampalimaud.org

Graphical abstract

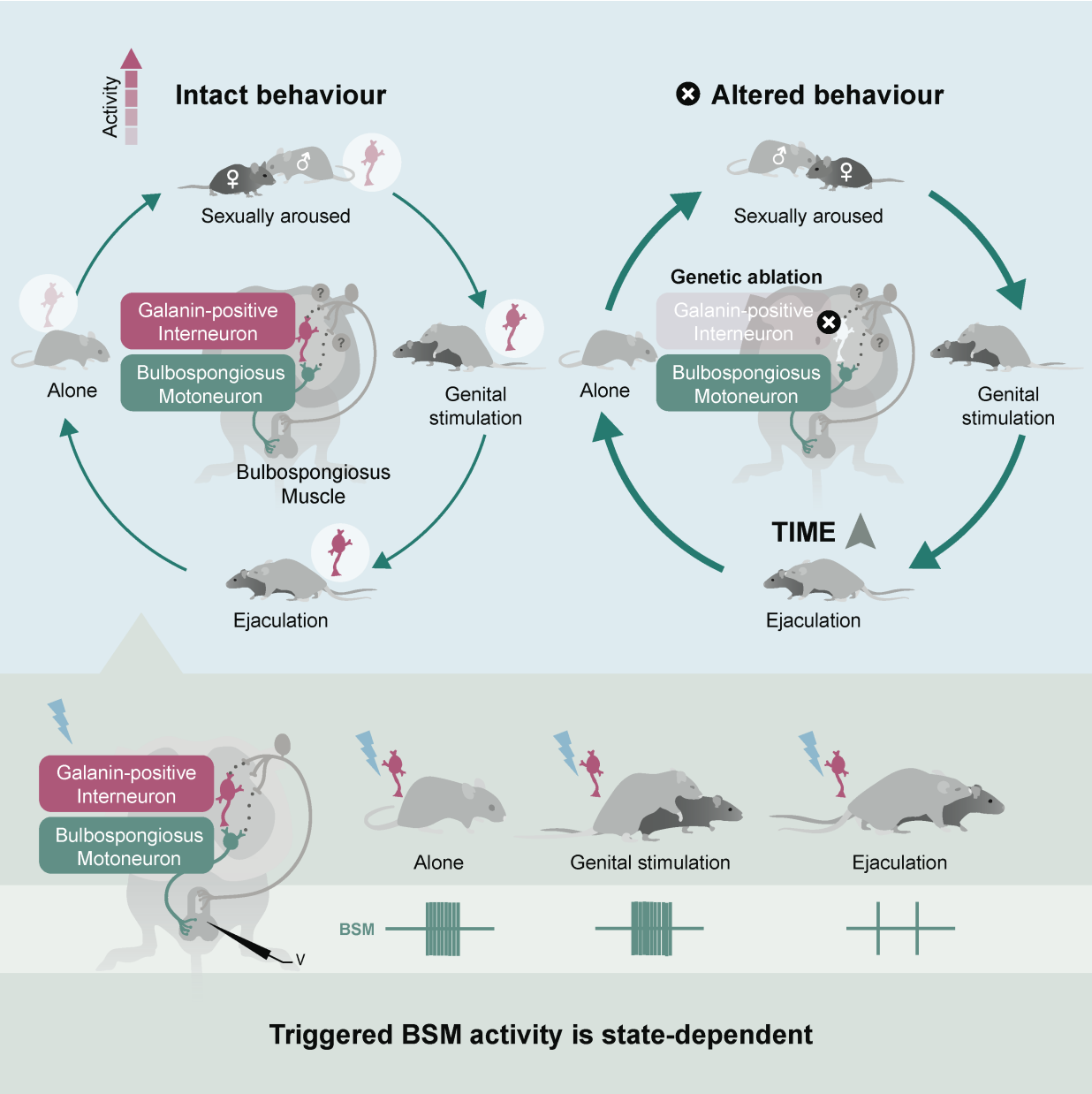

Summary
During sex, male arousal increases up to the ejaculatory threshold, allowing genital sensory input to trigger ejaculation. While copulation and arousal increase are thought to be centrally regulated, ejaculation is a reflex controlled by a spinal circuit, whose activity is strongly inhibited by descending input from the brain, bearing no role on the regulation of sexual behavior up until the arousal threshold. However, this hypothesis remains untested. To tackle this problem, we combined genetic approaches with electrophysiological and behavioral analysis to functionally map the spinal circuit controlling the main muscle involved in sperm expulsion, the bulbospongiosus muscle (BSM). We found that BSM motor neurons (BSM-MNs) receive direct synaptic input from a group of galanin-expressing (Gal+) interneurons located in the upper lumbar spinal cord. Furthermore, the Gal+ population is progressively activated during sexual behavior and receives genital sensory input. Electrical and optogenetic activation of the Gal+ neurons evoked activity in BSM-MNs and BSM after spinalization. Interestingly, these effects were dependent on the behavioral state of the male and drastically decreased with repeated stimulation. Moreover, genetic ablation of the Gal+ neurons severely impacted the latency to ejaculate and the structure of the copulatory sequence. Taken together, our results imply an unexpected involvement of the spinal cord in the control of copulatory behavior, sexual arousal and in the post-ejaculatory refractory period, in addition to its well established role in ejaculation.

Keywords: spinal cord, ejaculation, sexual behavior, bulbospongiosus muscle, electrophysiology, optogenetics, circuit mapping.

Introduction

Sex, albeit crucial for species survival and evolution, goes beyond reproduction: recreative and pleasurable sex is observed across taxa (Balcombe, 2009; Georgiadis, Kringelbach and Pfaus, 2012; Zer-Krispil *et al.*, 2018) and plays a pivotal role in the establishment of social bonds (Cappelleri *et al.*, 2007). In humans, sex can have additional effects on well-being, such as improvement of cognition (Maunder, Schoemaker and Pruessner, 2017) or prevention of disease (Leitzmann *et al.*, 2004). Moreover, sexual dysfunction can lead to great distress in individuals and their sexual partners (Carson and Gunn, 2006). Yet, despite the ubiquity of sex, its importance to well-being and its fundamental role in species survival, the mechanisms controlling sexual behavior remain poorly understood.

Sexual behavior comprises copulatory actions, including direct genital stimulation, that progressively increase sexual arousal until the "ejaculatory threshold": at this point, in mammals, penile insertion in the female's reproductive organ triggers ejaculation and sperm ejection (Lucio *et al.*, 2012). Ejaculation usually marks the endpoint of male sexual behavior, and is generally followed by a variable period of decreased male sexual activity, referred to as the post-ejaculatory refractory period (Lenschow and Lima, 2020; Valente, Marques and Lima, 2021).

Sexual behavior can be divided into two phases with apparently different neural control systems: (1) copulation and the accompanying arousal increase, and (2) the ejaculatory process itself. Copulation and arousal increase are thought to be centrally regulated, with the involvement of the autonomic and sensory-somatic nervous systems (Allard *et al.*, 2005; Giuliano and Clement, 2005; Corona *et al.*, 2012). Ejaculation, in contrast, is a two-step reflex triggered by genital input and controlled by autonomic and somatic circuits located within the spinal cord. During the first step, called emission, sperm and seminal fluids are released and accumulated in the prostatic urethra (Newman, Reiss and Northup, 1982; Sheu, Revenig and Hsiao, 2014). The second step, expulsion, is a somatic reflex caused by the activation of spinal motor neurons (MNs) and the associated contraction of the bulbospongiosus muscle (BSM), a large, striated muscle surrounding the base of the penis (Sachs, 1982; Tang *et al.*, 1999; Peikert *et al.*, 2015).

How copulatory sequences and arousal increase are coordinated, how the ejaculatory reflex is inhibited until the arousal threshold and, importantly, how the arrival to the arousal threshold is communicated to the spinal cord allowing the reflex to be triggered, remains unresolved. Important clues come from experiments in anesthetized male rats, where stimulation of the penis (via electrical stimulation of the dorsal penile nerve) was shown to elicit ejaculation in spinalized animals, but not intact ones (Marson and McKenna, 1990, Pescatori *et al.*, 1993). While this result suggests that genital stimulation can trigger the ejaculatory reflex per se, descending inhibitory signals to the spinal cord must modulate the impact of such incoming sensory input to prevent the inadvertent activation of the ejaculatory reflex (Coolen *et al.*, 2004; Carro-Juárez and Rodríguez-Manzo, 2008), contributing to a view of the brain as a "spinal-reflex inhibitor", in addition to a central organizer of sexual behavior (Marson and McKenna,

1992, 1996; Pescatori *et al.*, 1993; Normandin and Murphy, 2011). However, an integral question remains unanswered - what spinal circuit does the descending input modulate?

A key finding in the field stemmed from studies in humans (Coolen *et al.*, 2004; Chéhensse *et al.*, 2017) and rats (Truitt and Coolen, 2002; Coolen *et al.*, 2003; Dobberfuhl *et al.*, 2014): the identification of a group of galanin-expressing (Gal+) interneurons in the lumbar spinal cord that contact and drive the activity of BSM-MNs, the "spinal ejaculation generator" (SEG). Several lines of evidence support the decision to label the Gal+ population as a SEG. While electrical stimulation at the location of the putative SEG evokes ejaculation in anesthetized rats (Borgdorff *et al.*, 2008), its ablation results in complete disruption of the ejaculatory reflex, with no effect on copulatory behavior (Truitt and Coolen, 2002). Furthermore, the SEG seems to be anatomically connected to the sensory branch of the pudendal nerve, indicating that genital information might reach this population (Larsson and Sodersten, 1973; Carro-Juárez and Rodríguez-Manzo, 2005). Thus, in this model, arrival at the ejaculatory threshold may be communicated to the spinal circuitry by the transient interruption of the descending inhibitory input, allowing genital stimulation to activate the SEG and the ejaculatory reflex (Allard *et al.*, 2005). These studies also support the idea that the SEG has no role in the organization of copulation, as its ablation did not impair sexual performance (Truitt and Coolen, 2002). However, this working model remains incomplete, and in some cases controversial, in part because most studies were performed either in humans, where manipulations are limited, or in rats, with methods that have poor anatomical and cellular specificity, and/or low temporal resolution.

Here, we took advantage of the house mouse, a species whose sexual behavior consists of copulatory patterns that resemble human sexual dynamics, in particular with respect to repeated vaginal thrusting preceding ejaculation (in contrast to rat sexual behavior, where ejaculation is dependent on the execution of multiple individual penile insertions, spaced in time, each one with the potential of triggering ejaculation; Dewsbury, 1972; Lenschow and Lima, 2020; Valente, Marques and Lima, 2021). To gain access to the spinal circuitry, we used the pelvic muscle controlling the last step of this complex behavior, the BSM, as a point of entry. Employing genetic-based strategies with high specificity (viruses combined with transgenic mice) and high temporal resolution (optogenetics and electrophysiology), we identified the mouse BSM-MNs, and subsequently their presynaptic partners, a group of Gal+ interneurons in the lumbar spinal cord. We show functional evidence that the Gal+ neurons receive genital sensory input and that their stimulation evokes dominant BSM activity, only after spinalization. Surprisingly, the evoked activity is dependent on the sexual arousal of the male prior to spinalization, indicating that the dynamics of the spinal cord circuitry controlling BSM activity also reflect the internal state of the animal. While Gal+ neurons seem to be active as soon as the male becomes sexually aroused, the genetic ablation of this population leads to profound impact on the copulatory length and structure. These results point towards an unexpected and more intricate role of the spinal cord during sex, beyond the relay of genital information and the control of the ejaculatory reflex.

Results

Anatomical and functional characterization of bulbospongiosus muscle motor neurons (BSM-MNs)

In order to visualize the MNs involved in sperm expulsion, we used the bulbospongiosus muscle (BSM) as an entry point to identify the corresponding spinal cord BSM motor neurons (BSM-MNs). Fluorogold (FG), a well established retrograde tracer (Köbbert *et al.*, 2000), was injected into the BSM of adult mice (N = 12, Figure 1A, B). Serial rostrocaudal reconstruction of the spinal cords revealed a consistent distribution of FG-positive (FG+) BSM-MNs at the dorsomedial part of the ventral horn and close to the dorsal gray commissure (Figure 1B). FG+ somas were observed across several spinal segments, spanning from the lumbar 3 (L3) to the sacral 2 (S2) segments (Supplemental Figure 1), with the majority of cells located between L5 and S1 segments (Figure 1C). Immunohistochemical characterization of the FG+ somas revealed that BSM-MNs are classic alpha MNs, expressing choline acetyltransferase (ChAT) and osteopontin, an alpha MN marker (Misawa *et al.*, 2012), and receive sensory afferent input as demonstrated by the presence of Vesicular Glutamate Transporter 1 (VGLUT1) positive boutons (Figure 1D). Nearly all FG+ BSM-MNs expressed ChAT and VGLUT1 and 80% were osteopontin positive (Figure 1E). The soma size of FG+ MNs is similar to that classically reported for alpha MNs (Figure 1F; Friese *et al.*, 2009).

To establish a causal relationship between the activity of the BSM-MNs and muscle activity, we next employed optogenetic methods to selectively activate these MNs (Boyden *et al.*, 2005) while simultaneously monitoring the activity of the BSM with electromyography (EMG; Figure 1G-M). A retrograde traveling adeno-associated virus (rAAV), carrying the gene for the light activated channel channelrhodopsin (ChR2; rAAV-CAG-ChR2tdTomato, Addgene; Mao *et al.*, 2011), was injected into the BSM of postnatal day 3-6 mouse pups (Figure 1G, upper panel) as the efficiency of viral particles to infect motor endplates is known to drastically drop at later postnatal days (Stepien, Tripodi and Arber, 2010), and raised until sexually mature (2-3 months of age). To activate the ChR2-expressing somas, a laminectomy was performed to allow blue light illumination of several BSM-MNs-containing spinal segments. To assess the specificity of the light stimulation, activity was recorded from both the BSM and a locomotor hindlimb muscle, the *Tibialis Anterior* (TA) (N = 10, Figure 1G). BSM EMG potentials were tightly locked to laser stimulation (Figure 1H BSM trace, Supplemental Figure 2). The largest amplitudes (Figure 1I), shorter latencies (Figure 1K), and lowest light intensities (Figure 1J), were obtained with illumination above the L6 and S1 segments, in agreement with the BSM-MN rostrocaudal density (Supplemental Figure 2). Note that no activity was observed in the TA (Figure 1H, TA trace, Supplemental Figure 2).

In five animals, we achieved single cell juxtacellular recordings from photoidentified BSM-MNs (N = 7 cells; Figure 1N, MN trace; Lima *et al.*, 2009) side by side with BSM EMG recordings. Brief blue light stimulation (10ms, 15mW) at different frequencies (upper panel: 5Hz, middle panel: 10Hz, lower panel: 20Hz) reliably elicited short latency (mean latency to spike: 4.643ms +/- 0.33ms, Figure 1L) action potentials followed by BSM EMG potentials (Figure 1H). Spike and EMG fidelities (calculated as the number of spikes/EMG responses

divided by the number of light pulses) were stable up to 20Hz (Figure 1M). Moreover, light evoked BSM-MN activity led to characteristic pelvic floor movements, tightly locked to the laser (Supplemental Movie 1), and which resemble the movements observed during ejaculation in a sexually behaving male (Supplemental Movie 2; Lenschow and Lima, 2020). Together, these results revealed a population of MNs, primarily located in the L6 and S1 spinal segments, whose optogenetic activation led to characteristic EMG potentials in the BSM and ejaculatory-like movements of the pelvic floor.

Anatomical and functional characterization of the BSM-MNs presynaptic partners

We next aimed at identifying the BSM-MNs presynaptic partners. To do so, we started by injecting the BSM of adult mice with pseudorabies virus (PRV, Kaplan strain; Strack and Loewy, 1990; Boldogkoi *et al.*, 2009; Saleeba *et al.*, 2019) (Figure 2A). Similarly to the FG and retro-AVV injections, PRV-labeled neurons were found primarily in the dorsomedial part of the ventral horn of the L6 segment (Figure 2B). In the rat, BSM-MNs were described to receive input from galanin (Gal+) expressing interneurons, referred to as the putative spinal ejaculation generator (SEG), located around the central canal in the lamina X of the L3/L4 spinal segments (Truitt and Coolen, 2002). In agreement with these results, dense PRV labeling was observed around the central canal in the L2/3 spinal segments that overlapped with post-hoc immunohistochemical labeling of galanin (Figure 2C), revealing the existence of a similar population of Gal+ cells in the mouse.

We took advantage of a mouse line where the Cre recombinase is expressed under the control of the Gal promoter (Gong *et al.*, 2003, 2007) to specifically access this neuronal population. Gal-cre mice were crossed with the reporter mouse line carrying the gene for the red fluorescent protein TdTomato (Madisen *et al.*, 2010) such that in the progeny the fluorescent protein is expressed in Gal+ neurons (Figure 2D). Immunohistochemical staining for galanin in the progeny from the Gal-cre x TdTomato cross confirmed the specificity of this mouse line (Figure 2D & Supplemental Figure 3). TdTomato-positive neurons were found along the rostral caudal axis of the spinal cord, namely in laminae X (around the central canal, N = 10, Figure 2E), with the highest density of cells present at the L2/3 spinal segments (Figure 2E). This location differs from the putative rat SEG, which was described at the L3/4 level (Truitt and Coolen, 2002). However, the mouse Gal+ neurons expressed enkephalin, cholecystokinin, gastrin releasing peptide and substance P, similarly to the rat SEG (Nicholas, Zhang and Hokfelt, 1999; Coolen *et al.*, 2003; Kozyrev, Lehman and Coolen, 2012) as all four peptides were present and overlapped with the Gal+ cells surrounding the central canal in the L2/3 spinal segments (Supplemental Figure 4).

To determine if the results obtained with the PRV injections are due to the existence of a monosynaptic connection between the Gal+ cells and the BSM-MNs (Saleeba *et al.*, 2019), we took a two-pronged approach. First, we aimed to identify the location of the synaptic terminals of the lumbar Gal+ cells by injecting a Cre-dependent AAV carrying a GFP-tagged form of synaptophysin (a synaptic vesicle protein, present in neuronal terminals) into the L2/L3 spinal segments of Gal-cre x TdTomato mice (Figure 2F, N = 7). To allow the visualization of BSM-MNs, the mice were simultaneously injected with FG in the BSM (Figure 2F). GFP-labeled

terminals belonging to the Gal+ cells (green channel, Figure 2G) were found around FG+ BSM-MNs (blue channel, Figure 2G) in all 7 animals (Figure 2H). On average, a total of 79% ± 2% FG+ labeled cells overlapped with synaptophysin-labeled terminals (Figure 2H) indicating that the Gal+ neurons in the L2/3 spinal segments contact the BSM-MNs directly. Furthermore, this approach revealed other projection targets of the Gal+ cells, including the intermediolateral column (IML) and the central autonomic nucleus (CAN) in the lower thoracic and L1 spinal segments (Supplemental Figure 5), as well as the sacral parasympathetic nucleus (SPN) (Supplemental Figure 5). The IML and CAN are known to contain sympathetic preganglionic cells that provide sympathetic outflow mainly through the hypogastric and pelvic nerves to the visceral organs (Hancock and Peveto, 1979; Nadelhaft and McKenna, 1987; Baron and Jänig, 1991; Giuliano *et al.*, 1997). The parasympathetic preganglionic cells clustered in the SPN at the S2-5 spinal segments (Supplemental Figure 5) innervate the pelvic organs, including the prostate (Orr and Marson, 1998), urethra (Vizzard *et al.*, 1995) and penis (Marson and Carson, 1999). The dorsolateral nucleus (DLN) located at the S1/S2 segments, known to consist of MNs innervating the ischiocavernosus muscle, the most important muscle for erection (Schmidt and Schmidt, 1993), also contained GFP-labeled terminals of the Gal+ cells. All the regions containing GFP-labeled terminals were also labeled after PRV injection in the BSM (Supplemental Figure 6), except for the DLN which contains ischiocavernosus MNs. These results suggest that the areas sending information to the Gal+ cells receive reciprocal input and confirm that the PRV initial infection was restricted to the BSM.

To gain physiological evidence supporting direct synaptic connection between the Gal+ cells and the BSM-MNs, we performed *in vitro* whole-cell patch clamp recordings from choleratoxin-B (CTB-594) retrogradely-labeled BSM-MNs in acute spinal cord slices of mouse pups (P2-6) expressing ChR2 under the galanin promoter (Gal-Chr2, progeny of the cross between the Gal-cre mouse and the ChR2 mouse, Madisen *et al.*, 2012). An optical fiber (0.5mm diameter) was placed close to the central canal (Figure 2I) in order to illuminate the terminals of the Gal+ cells. A total of 21 CTB-positive BSM-MNs were recorded in Gal-ChR2 pups (N = 7), out of which 18 reliably responded to laser illumination (Figure 2J-M). Short laser pulses led to dominant excitatory postsynaptic potentials (EPSPs) and/or action potentials in CTB-positive BSM-MNs (see upper traces in Figure 2L,M). Repeating laser stimulation after the superfusion of a high cation containing aCSF, to isolate monosynaptic transmission (Lenschow *et al.*, 2016), led to much smaller EPSPs in BSM-MNs (middle traces in Figure 2L,M). Blocking neural transmission via the pharmacological manipulation of NMDA (through AP5) and AMPA (through DNQX) receptors (lower traces in Figure 2L, M) abolished light-triggered EPSPs in BSM-MNs. CTB-negative large lumbar MNs (N = 16), in contrast to BSM-MNs, did not respond after laser illumination (1 out of 16 responded, Figure 2K, N). Taken together we present evidence for a population of Gal+ neurons present in the laminae X of the L2/3 spinal segments in mice, which is monosynaptically connected to BSM-MNs via glutamatergic transmission. Even though with different spatial distribution, this population shares similar molecular characteristics to the putative rat SEG (Nicholas, Zhang and Hokfelt, 1999; Coolen *et al.*, 2003; Kozyrev, Lehman and Coolen, 2012).

To determine the involvement of the Gal+ cells during sex, we used the expression of the immediate early gene *cFos*, a routinely used molecular tool, to establish a link between behavior and neuronal activity (Krukoff, 1999). For that, we compared the induction of the cFos protein in the Gal+ neurons of the L2/3 spinal segments of male mice that ejaculated (sexual interaction with a receptive female until ejaculation, Ejaculation, N=6), with the induction that occured in males that were either alone in the cage (Cage control, N=7), or males with different degrees of sexual arousal (10 minutes with a receptive female and no penile insertion as mounting was interrupted whenever the male attempted copulation, Aroused, N=5; or five mounts with intravaginal thrusting, 5 Mounts, N=5) (Figure 3 A-D). To specifically quantify the number of Gal+ neurons active, we used the male progeny from the Gal-cre x TdTomato cross and performed post-hoc immunohistochemical quantification of the TdTomato signal and cFos induction in the L2/3 spinal segments for each condition. As expected, given its direct contact to the BSM-MNs, significantly more double positive neurons were found in the Ejaculation group, compared to the other three conditions (Cage control, $p < 0.0001$, Aroused, $p < 0.001$ and 5 Mounts, $p < 0.01$ Student's t-test, Figure 3E). Unexpectedly, we observed similar levels of activation between the Aroused and 5 Mounts groups, and these two conditions exhibited significantly higher levels of double positive neurons when compared to the Cage control ($p < 0.01$, Student's t-test). These results indicate that the Gal+ cells are activated with sexual arousal and/or penile stimulation prior to the ejaculatory threshod, suggesting an involvement of this population in sexual behavior prior to and not just during ejaculation.

Sensory input to the Gal+ neurons and the BSM-MNs

It has been hypothesized that once the ejaculatory threshold is reached, genital input can activate the SEG, triggering the ejaculatory reflex (Allard *et al.*, 2005). This model is supported by anatomical evidence, as previous studies reported connection between the sensory branch of the pudendal nerve and the putative rat SEG (Larsson and Sodersten, 1973; Carro-Juárez and Rodríguez-Manzo, 2005). However, to the best of our knowledge, functional connectivity has never been established. Therefore, next we investigated whether the BSM-MNs and Gal+ cells receive sensory feedback from the penis. We first replicated an experiment previously executed in rats in which the penis is stimulated electrically or through air puffs, in male mice that either were intact (Supplemental Figure 7A) or spinalized (Supplemental Figure 7C) while monitoring the BSM activity in parallel through EMG. Similar to what was reported in the rat, we elicited prominent BSM EMG activity when stimulating (200Hz, 100 pulses, 6V; 5Hz, 3 x 5 pulses of 100ms, 6V) the penis in a spinalized preparation, while penile stimulation in the intact preparation led to scarce BSM activation (Supplemental Figure 7B, D). Penile stimulation triggered BSM responses were significantly larger in amplitude (Supplemental Figure 7E) and duration (Supplemental Figure 7F) in spinalized compared to the non-spinalized preparation, while the onset of BSM responses did not differ (Supplemental Figure 7G). These experiments further support the existence of supraspinal inhibition onto the spinal circuitry, but still fail to address whether penile sensory information is indeed physiologically integrated at the level of Gal+ cells and BSM-MNs. To address this question we used an optogenetic approach and mapped light-induced local field potentials (LFP) of ChR2 infected BSM-MNs in the lumbar spinal cord of adult male mice combined with BSM-EMG recordings (Figure

4A1). Prominent time-locked LFP deflections were observed when illuminating above the BSM-MNs-containing spinal segments (Figure 4A2, blue trace, Vm) which were followed by BSM activity (Figure 4A2, black trace, BSM EMG). Once having mapped the best location of laser induced BSM-MN LFP deflections and BSM EMG activity, the location of the glass pipette capturing LFP deflections was maintained while applying brief air puffs of 5Hz (10ms, 1bar) to the pulled-out penis, or leg as a control (Figure 4A3). Air puff stimulations lead to larger LFP deflections when puffing the penis (Figure 4A3, left panel, blue trace) compared to leg puffs (Figure 4A3, middle panel, yellow trace) and this was consistent at the population level (Figure 4A3, right lower panel). Plotting the light-induced BSM-MNs LFPs versus the penis puff LFP deflections (blue) or the leg puff induced LFP activity (yellow) led to a higher correlation between the light-induced LFPs and the penis puffs (Figure 4A3, right upper panel). These results hint to the BSM-MNs receiving sensory input from the penis. The same experiments were repeated in male mice that expressed ChR2 under the Gal promoter (Gal-ChR2), as we mapped light induced LFP signals at the location of the Gal+ cells (Figure 4B1) while monitoring BSM activity in a spinalized preparation. Optogenetic stimulation at the L2/3 spinal segments evoked prominent BSM responses (Figure 4B2, black trace) in line with time-locked LFP deflections (Figure 4B2, pink trace). We subsequently performed penis air puff stimulations while keeping the LFP capturing pipette at the spot of best light-induced LFPs (Figure 4B1, right panel). Penile sensory stimulation elicited significantly larger LFP responses (Figure 4B3, left panel, pink trace) compared to leg airpuffs (Figure 4B3, middle panel, yellow trace and right lower panel). Moreover, light-induced LFPs were more correlated with penis puff induced LFPs compared to leg puff elicited LFPs (Figure 4B3, right upper panel) indicating that penile sensory inputs can reach the Gal+ cells present at the L2/3 spinal segments.

Electrical stimulation of the spinal cord location harboring the Gal+ neurons leads to BSM activity and suggests peripheral regulation of the refractory period

To further establish the involvement of the Gal+ neurons in the control of the BSM activity in mice, we next investigated whether the artificial activation at the location where this population resides is capable of eliciting BSM activity. First, we performed electrical stimulations along the rostrocaudal lumbar spinal cord by inserting a tungsten electrode at different depths (550um - 850um), while measuring the activity of the BSM in parallel, via EMG recordings (Figure 5A) in sexually naive animals (SN, N = 8). We simultaneously monitored the activity of the TA leg muscle to evaluate the specificity of our protocol (Figure 5A). The location of the stimulating electrode was revealed by electrolytic lesions and immunohistochemical staining for galanin (Figure 5B, upper panel). BSM muscle activity were only successfully triggered (Figure 5B and Supplemental Figure 8) when stimulations (40uA, 200Hz, 100 pulses) were applied close to the location of the Gal+ cluster, in the L2/3 spinal segments (Figure 5C), at a depth of 850 um, which is parallel to the location of the central canal (Figure 5D and Supplemental Figure 8C & D). Electrically triggered BSM responses were significantly higher and longer in spinalized compared to non-spinalized preparations (Supplemental Figure 9) indicating descending inhibition from the brain, in agreement with our results from the mechanical/electrical stimulation of the penis experiments (Figure 4) and prior studies in rats (Marson and McKenna, 1992, 1996). However, in contrast to what was observed in the rat

(Borgdorff *et al.*, 2008), repeated electrical stimulations evoked decreased BSM responses (see Methods Details; Figure 5B; BSM 2nd and 3rd). Quantification of the EMG responses (Figure 5E & F) revealed significantly larger and longer potentials during the first train of stimulation (mean amplitude 0.99mV +/- 3.6mV, 1st vs 2nd amplitude p = 0.04, 1st vs. 3rd amplitude p = 0.02; mean length 8.83ms +/- 1.4ms; 1st vs 2nd length p = 0.09, 1st vs. 3rd length p = 0.02; Mann-Whitney-U Test) when compared to the second (mean amplitude 0.5mV +/- 0.25mV; mean length 4.22s +/- 1.47s) and third trains (mean amplitude 0.06mV +/- 0.04mV; mean length 1.74s +/- 1.31s) of current application, while the onset of the responses did not change (mean onset of 1st 3.9 +/- 1.83s, mean onset of 2nd 6.03 +/- 3.02s, mean onset 3rd 0.54 +/- 0.13s; Figure 5G). The decrease in the response elicited during repeated stimulation was not due to deterioration of the preparation (Supplemental Figure 10).

In addition to the intriguing depressing response observed with repeated electrical stimulations, the electrically elicited BSM activity differed in structure from previously measured EMG responses during ejaculation in freely moving rats (see Borgdorff *et al.*, 2008). Moreover, we did not observe the expulsion of sperm or seminal fluid during any of our experiments in mice. Therefore, to rule out the hypothesis that the lack of sperm emission in mice was due to a technical issue, we reproduced the experiment by Borgdorff *et al.*, 2008 in anesthetized rats. As expected, the application of electrical current (Supplemental Figure 11A) at the L3/4 spinal segments (revealed by electrolytic lesions; Supplemental Figure 11B) led to the characteristic activity pattern in the rat BSM (N = 5; Supplemental Figure 11C) and to the expulsion of sperm (Supplemental Figure 11D).

As mentioned earlier, mice and rats exhibit distinct reproductive strategies, in particular in the number of ejaculations each species can achieve in a short window of time: while rats can ejaculate 7-8 times in a short period before reaching sexual exaustion, mice are more similar to humans and generally enter a refractory period after a single ejaculation, which in the case of Bl6 mice (the genetic background used in this study) can last several days (Valente, Marques and Lima, 2021). We wondered if our inability to elicit stable BSM activity with repeated electrical stimulations in the mouse was related to the state of the male/refractory period. To test this hypothesis we allowed male mice to have sex prior to electrical stimulation experiments. One group had sex until reaching ejaculation (Ejaculation, N = 8; Figure 5H upper panel), while another group of males was allowed to perform 5 mounts with intravaginal thrusting (5 Mounts, N = 7, Figure 5I upper panel). Electrical stimulation of the spinal cord of a male mouse from the Ejaculation group evoked less BSM activity (Figure 5H, lower panel) compared to the BSM activity elicited in the Sexually naive group (Figure 5B, first train of stimulation), and to the BSM activity elicited in a male from the 5 Mounts group (Figure 5I, lower panel). While the mean amplitude of the BSM activity was significantly higher in the 5 Mounts group (Figure 5J), the duration of the BSM activity was significantly shorter in the Ejaculation group, when compared to the other two groups (Figure 5K). Even though there was no difference in the mean amplitude of the BSM events between Sexually naive and the Ejaculation groups (Figure 5J), the number of events was significantly lower in the Ejaculation group compared to the other two (Figure 5M), further suggesting that after ejaculation electrical stimulation of the spinal cord is not capable of eliciting high activity in the BSM. Taken

together, these experiments suggest that electrical stimulation of the mouse spinal cord in the area where the Gal+ neurons were identified, and contrary to the findings observed in the rat, is only able to evoke the second and last phase of the ejaculatory process (expulsion), lacking the power to elicit emission. The internal state-dependent outcome of the electrical stimulations (Sexually naive vs. 5 Mounts vs. Ejaculation) implies that the properties of the neuronal circuits in this region of the spinal cord are modulated by copulation and ejaculation, suggesting that the spinal circuitry might be involved in the control of sexual behavior (corroborating the results from the cFos experiment, Figure 3) and the refractory period in addition to ejaculation.

Optogenetic stimulation of the lumbar Gal+ neurons leads to BSM activity

As electric stimulation experiments inherently lack specificity, to unequivocally establish a link between the activity of the Gal+ cells, BSM-MNs and the BSM, we genetically restricted the neuronal population being stimulated to the Gal+ neurons, by crossing the Gal-cre mouse line with the ChR2 reporter line (Gal-ChR2, Madisen *et al.*, 2012). To activate the Gal+ neurons we placed an optical fiber on top of the spinal cord and delivered brief pulses of blue light along its rostrocaudal axis (Figure 6A, left panel, N = 13). Light delivery (20mW, 200Hz, 100 pulses) led to comparable responses to the ones elicited via electrical stimulation (Figure 6B lower right panel, Figure 6J-L). As expected, BSM activity was only observed in response to illumination restricted to the location with the highest ChR2 expression (revealed by either DiI injections or an electrolytic lesion, Figure 6B, see also Supplemental Figure 12), namely above the L2/3 spinal segments (Figure 6C), the region previously shown to harbor the highest density of Gal+ cells (Figure 2E). Corroborating the results obtained with electric stimulations, optogenetically-evoked BSM responses were markedly higher in amplitude and longer in a spinalized compared to an intact preparation (Supplemental Figure 13) further supporting the idea that the Gal+ cells may be held under tonic descending inhibition (Marson and McKenna, 1992, 1996; Pescatori *et al.*, 1993; Normandin and Murphy, 2011). Optogenetically elicited BSM responses had similar dynamics to electrically evoked ones, this is, they decreased in both amplitude and duration after the first train of laser application (Figure 6I & J). Moreover, apart from observing the tonic discharges in the BSM (Figure 6B, I & L, Supplemental Figure 13D) which were equally elicited with the electrical stimulations, we were able to trigger BSM responses that were timely locked to the light pulses (N = 12; 20mW, 5Hz-50Hz, 15 pulses; Figure 6 H-M). As described above, and in contrast to the optogenetic activation of Gal+ neurons, the optogenetic activation of BSM-MNs evoked stable BSM responses across repeated rounds of illumination (Figure 6N-P), suggesting that the depression of the BSM activity might be due to an alteration in the synaptic transmission between the Gal+ and BSM-MNs, and not changes in the properties of BSM-MNs.

Genetic ablation of lumbar Gal+ neurons disrupts copulatory behavior and arousal build up

So far our results suggest that in addition to its role in sperm expulsion, the population of lumbar Gal+ cells might also be involved in copulation. To determine the function of this spinal population during sexual behavior we used a genetic approach to specifically ablate the Gal+ neurons via the expression of the dipheteria toxin receptor (DTR; Azim *et al.*, 2014). A conditional AAV carrying the construct for DTR (AA8V-FLEX-DTR-GFP, Salk) was injected

in the L2/3 spinal segments of sexually trained males derived from the Gal-Cre x TdTomato cross (Figure 7A; DTR group; N = 12). The control group, of the same genotype and also sexually trained, underwent a sham surgery at the same spinal location (SHAM group; N = 7). After a recovery time and a second session of sexual behavior, both groups (DTR and SHAM) received an intraperitoneal injection of dipheteria toxin (DT). One week after the DT treatment, the effect of the genetic ablation on sexual behavior was tested in the presence of a sexually receptive female. Males of both groups were sacrificed either 90 minutes after ejaculation or 90 minutes after the female was placed inside the testing arena, in cases where the male initiated attempts of copulation but did not ejaculate. In the case of absence of sexual arousal (no display of mount attempts), the trial was interrupted 30 minutes after female in and testing was repeated up to two more times, once a week (Supplemental Figure 14A and see Methods for detailed experimental procedure; Valente, Marques and Lima, 2021). After post-hoc immunohistochemical processing of the spinal cords (Figure 7B & C), the numbers of cFos positive and Gal+ neurons (visualized via the tdTomato protein) in the L2/3 spinal segments were checked. While the number of cFos-positive cells was comparable between the SHAM and DTR group (Figure 7B-D), a significant reduction in the number of Gal+ cells (Figure 7E & G) and in the overlap of Gal+ neurons and cFos cells was observed (Figure 7F & G). In agreement with the previous cFos and electrical stimulation experiments (Figure 3 and 5), and further supporting the involvement of these neurons in a more general control of sexual behavior, the copulatrory sequence (Figure 7H) was strongly affected in the DTR group. While 3 out of 12 DTR animals did not reach ejaculation (but attempted copulation) and only one ejaculated in less than 10 minutes (Figure 7I, lower panel), all SHAM animals reached ejaculation, and only two took longer than 10 minutes to reach ejaculation (Figure 7I, upper panel). Individual raster plots for each animal aligned to the first consummatory act (Figure 7J) illustrate no effect on the latency to mount (Figure 7K), while the latency to ejaculate from first mount was longer (Figure 7L). In order to determine which aspect of the sexual interaction was disrupted, leading to the increase in the latency to ejaculate, we further scrutinized the copulatory sequence, starting with the mounting events that resulted in penile insertion (Mount with thrusting, MT, Figure 7H), which had similar duration across the two groups (Figure 7M and Supplemental Figure 14B). The number of MT was also similar across the two groups (Figure 7N) indicating that a similar amount of genital sensory information was sufficient to trigger ejaculation in both types of males, despite the difference in the latency to ejaculate. In contrast, we observed a difference in the number of mounts that did not result in penile insertion: mount attempts where the male performed several shallow pelvic thrust movements trying to locate the female's vagina (which only occur if sexually aroused, Mounts with probing, MP; Figure 7O; McGill, 1962). Surprisingly, the ejaculation duration was similar for all males that ejaculated (from the last thrust until the male dismounted the female, see Methods; Figure 7P), indicating that if the male reached the arousal threshold, the ejaculatory reflex could be triggered. This is in marked contrast to the results obtained when the Gal+ expressing neurons of the rat, the SEG, were ablated (Truitt and Coolen, 2002). In line with the increased number of MP, the time it took to the first successful penile insertion after the male placed his paws on the female flanks was also significantly longer in the DTR group (Figure 7Q, Supplemental Figure 14C). Finally, we observed that the thrusting rate and the dynamics of the MT were similar across groups (Figure 7R-T) indicating that once penile insertion was

achieved, pelvic thrusting was normal. Taken together, our results indicate that the ablation of the lumbar Gal+ population leads to an increase in the latency to ejaculate and a profound disruption of the copulatory sequence, supporting a more complex involvement of the spinal cord in the control of sexual behavior in mice.

Discussion

Ejaculation has been described as a spinal reflex. This classification entails that the brain plays no part in its execution, but also that the activity of its spinal network is inconsequential to any other behavior, except ejaculation. This dualistic view of the nervous system has been repeatedly challenged, in particular by the existence of some neurological disorders that strongly suggested that the network of spinal neurons should be incorporated into the control system, where central and effector players are in a continuous exchange of information (Frigon and Rossignol, 2006; Guertin, 2013). With this study we bring new evidence corroborating this non-dualistic view, namely in the integration of sensory cues and arousal state in order to ultimately induce ejaculation. Using the penile muscle involved in sperm expulsion as a point of entry, we have characterized a microcircuit in the lumbar spinal cord of male mice consisting of motor neurons innervating the BSM (BSM-MNs) and a galanin-positive (Gal+) cell population that monosynaptically contacts the BSM-MNs, receives sensory input from the penis, controls expulsion and modulates sexual behaviour.

Despite some differences in the identity of the spinal segments harboring the Gal+ neurons (L2/3 segments versus L3/4 in the rat; Truitt and Coolen, 2002), the population described in our study has a similar molecular profile to the previously identified rat Spinal Ejaculator Generator (SEG; Nicholas, Zhang and Hokfelt, 1999; Coolen *et al.*, 2003; Kozyrev, Lehman and Coolen, 2012). Furthermore, even though the existence of functional connectivity between the SEG and the BSM-MNs has been previously suggested (Tang *et al.*, 1999; Borgdorff *et al.*, 2008; Dobberfuhl *et al.*, 2014), to the best of our knowledge, this study, with the dual and genetic based approach, in combination with *in vitro* whole-cell patch-clamp recordings of BSM-MNs while specifically activating Gal+ axons, is the first one to present data that unequivocally establishes the existence of a functional monosynaptic connection between the Gal+ cells and the BSM-MNs. Indeed, besides its direct output to the BSM-MNs, it has been suggested that the Gal+ neurons must also provide input to autonomic centers involved in ejaculation (Marson, Platt and McKenna, 1993; Orr and Marson, 1998; Gerendai *et al.*, 2000, 2003), and other pelvic floor muscles (Marson and McKenna, 1996). Our viral experiments provide strong anatomical evidence for a reciprocal connection between the Gal+ neurons and autonomic nuclei, in addition to the ischiocavernosus MNs, thereby suggesting a potential impact not only in the regulation of emission, but also erection. The output to the ischiocavernosus MNs might be important for the regulation of penile tumescence, which must be finely regulated at the time of ejaculation, as pressure has to momentarily decrease for expulsion to take place (El-Sakka and Lue, 2004).

Electrically induced ejaculation in anesthetized rats was shown to result in very similar motor and physiological activity patterns regardless of an intact connection to the brain (which we

reproduced in our study), but penile stimulation can activate ejaculation only in anesthetized spinalized rats (Pescatori *et al.*, 1993). These results suggested the existence of descending inhibition gating the sensory input from the penis, but that the rat SEG can function independently of the brain once inhibition is removed. We observed something different in the mouse: pronounced BSM activity was only triggered when the Gal+ cells were electrically activated in a spinalized preparation, but not if the connection to the brain was intact. Moreover, penile stimulation in our hands not only was unable to trigger an ejaculation, but also the BSM-induced activity was much smaller than the one observed in a spinalized preparation. Therefore, our results support a model where, at least in the mouse, the Gal+ population and the incoming sensory input is kept under a massive inhibition from the brain, most likely from the ipsilateral paragigantocellular thalamic nucleus (Marson and McKenna, 1990), until the ejaculatory threshold is reached.

We were obviously intrigued by the fact that we could not trigger emission in the mouse with Gal+ and penile stimulation, even though we demonstrated an anatomical connection to autonomic centers, the main players in the emission process (Kolbeck and Steers, 1992). While we cannot completely exclude that the failure to trigger emission is due to our inability to find the appropriate stimulation parameters, we would like to propose that these results are biologically plausible and might actually reflect species differences in the regulation of ejaculation. The mouse copulation pattern, as initially stated, is much similar to the human, marked by repeated vaginal thrusting leading to one ejaculation, but quite divergent from rat sexual behavior during which multiple ejaculations are dependent on the execution of individual penile insertions. The arousal build up in the rat may differ from mice and humans, as it might be independent or much less influenced by genital sensory input, while in the mouse, sensory integration of multiple thrusts is crucial. While the rat results suggest that the descending inhibition only operates at the level of the SEG, our data points for the descending inhibition to modulate the Gal+ neurons and the incoming sensory input to them. The anatomical circuitry seems to be similar in rats and mice, however, the mechanisms by which these circuits operate must be fundamentally different, with the rat spinal circuitry being a "real spinal reflex arc", capable of driving ejaculation with a sensory stimulus, if disconnected from the brain. In contrast, the mouse circuit does not qualify as a proper reflex, as the sensory input is not able to drive emission, nor full blown BSM activity, supporting a constant dialogue between the brain and the spinal cord, for arousal build up and ejaculation. Future comparative experimental efforts should be undertaken to reveal the logic of operation of the hardware in these two different species. The discrepancies outlined in this study may result from different modus operandi, the product of different evolutionary histories.

We observed an unexpected gradual increase in the activity of the Gal+ population with sexual behavior and, even more striking, this populatuion seems to be active as soon as the male becomes sexually aroused. Previous studies in the rat have shown that the activity of the SEG cells increases with mounts and intromissions, but not with mount attempts (Truitt *et al.*, 2003). To our surprise, repeated electrical stimulation was accompanied by a marked decrease in BSM activity, a result that was not due to a deterioration of the preparation. Moreover, if male mice were allowed to have sex and ejaculate just prior to the electric stimulation experiment, BSM

activity was much lower and resembled the activity obtained after multiple rounds. These results indicate the Gal+ neurons are recruited through the entire copulation, corroborating a continuous dialogue with the rest of the body and a possible prominent role of the spinal cord in the control of the refractory period (Turley and Rowland, 2013), contrary to what is currently hypothesized.

Lastly the chemogenetic ablation of the Gal+ population caused a disruption in sexual behavior. Interestingly, and again in contrast to the rat SEG, whose ablation led to a complete abolishment of ejaculation while leaving copulatory patterns intact (Truitt and Coolen, 2002), only 3 out of 12 animals in our study did not ejaculate. However, the session was artificially interrupted after a certain time limit, so we do not know if they would be able to ejaculate if more time was given. Also, and contrary to the rat, we observed an altered sexual behavior in all animals, with an increase in the latency to ejaculate and the number of mounts with probing and a longer duration of the latter, suggesting that immediate sensory penile feedback when the Gal+ cells are ablated is partially disrupted. Two immediate questions arise from these results: how can animals still ejaculate if the Gal+ neurons that contact the BSM-MNs are gone and how and where is the penile sensory feedback treated to reach ejaculation? The first part may be due to a small percentage of Gal+ cells not being ablated, which could suffice to integrate pelvic sensory input and drive ejaculation. But also, redundant spinal circuits may compensate for the Gal+ cell loss. Namely, spinal circuits controlling pelvic floor muscles and organs, which are responsible for sexual behaviour, micturition and defecation, share common connections between the spinal and brain nuclei (Schellino, Boido and Vercelli, 2020). For instance, connections between the sacral parasympathetic nuclei, that control pelvic organ function (i.e. emission), and the BSM-MN nucleus have been described for cats (Nadelhaft, deGroat and Morgan, 1980; Holstege and Tan, 1987) and rats (Hancock and Peveto, 1979). Holstege and Tan (1987), hypothesized that BSM-MNs are a special class of neurons not only of somatic but also autonomic nature and thus, capable of controlling both functions (Holstege and Tan, 1987). Moreover, direct brain spinal projections, namely to the BSM-MNs may drive expulsion of sperm independently of Gal+ cells. Indeed, anatomical evidence points to a direct connection between the hypothalamic paraventricular nucleus (PVN) and the BSM-MNs in the cat (Holstege and Tan, 1987) and rat (Argiolas and Melis, 2005; De Groat, 2016). This pathway seems to regulate erection, but also rat sexual behaviour in general (Argiolas and Melis, 2004). In addition, in rats, ejaculation can be facilitated by an oxytonergic PVN projection onto SEG cells (Oti *et al.*, 2021). Projections from the Barrington's nucleus also known as the pontine micturition center, have been shown to connect to pelvic-related nuclei in the spinal cord (in rats: Nuding and Nadelhaft, 1998; in cats: Holstege *et al.*, 1986; in humans: Huynh *et al.*, 2013) and electrical stimulation of the medial-lateral areas induced emission and expulsion-like responses, respectively (Holstege *et al.*, 1986). Regarding the sensory relay, rat and human studies showed that pressure increase in the prostatic urethra caused by the arrival of sperm and seminal fluid at the time of emission, is sufficient to induce ejaculatory-like contractions in the BSM (Shafik and El-Sibai, 2000; Tanahashi *et al.*, 2012). Rat dorsal penile nerve to BSM-MNs connectivity has been described (Núnez, Gross and Sachs, 1986; Ueyama, Arakawa and Mizuno, 1987; Pascual, Insausti and Gonzalo, 1992) and might be sufficient to relay sensory information, without the Gal+ neurons in our experiments. Regarding the second

question, nobody knows where arousal is controlled and how sensory input impinges on such circuit. But our results point towards an involvement of the spinal network.

Taken together we have identified a cluster of Gal+ cells in the lumbar spinal cord of mice that are directly connected to BSM-MNs and that seem to be involved in the integration of sensory signals during copulation and sexual satiety, thereby taking a more central and intricate involvement in the control of mice copulatory behavior than a simple reflex arc.

Acknowledgments
We thank B. Roska for reagents (PRV) and much valuable advice, and A. Sathyamurthy for technical assistance (immunohistochemistry protocol for cFos in the spinal cord). We thank the Lima lab for their critical input during the course of this project and in particular Nicolas Gutierrez for the support with the Matlab code. We also thank the community at the Champalimaud Research, in particular the Carey Lab for reagents and technical assistance, the ABBE Facility, the Scientific Hardware, Histopathology and Rodent Champalimaud Research Platforms for technical assistances, and Zachary Mainen for reviewing the manuscript. This work was developed with the support from the Champalimaud Foundation, the Institut de Neurosciences Cognitives et Intégratives d'Aquitaine (INCIA), a Human Frontier Science Program Postdoctoral Fellowship (LT000353/2018-L4) (C.L.), a H2020 Marie Skłodowska-Curie Actions Individual Fellowship (799973) (C.L.), a Fundação para a Ciência e a Tecnologia (FCT) PhD Fellowship (PD/BD141576/2018) (A.R.M.), the research infrastructure Congento, co-financed by the Lisboa Regional Operational Programme (Lisboa2020), under the PORTUGAL 2020 Partnership Agreement, through the European Regional Development Fund (ERDF), FCT under the project LISBOA-01-0145-FEDER-022170, an InterEmerging Actions 2020 (301137) (S.Q.L.) and an European Research Council (ERC) Consolidator Grant (772827) (S.Q.L.).

Author contributions
C.L., A.R.M. and S.Q.L. conceptualized the experiments and project ideas. C.L. and A.R.M. conducted all the experiments, part of the histology and most of the data analysis. L.F. helped with histological analysis. B.L. helped with data analysis, namely regarding the behavioral experiments. C.L. with the help of C.Q. and S.B. conducted electrophysiological experiments at the INCIA. C.L., A.R.M. and S.Q. L. wrote the manuscript.

Declaration of interests
The authors declare no competing interests.

Main Figures with legends

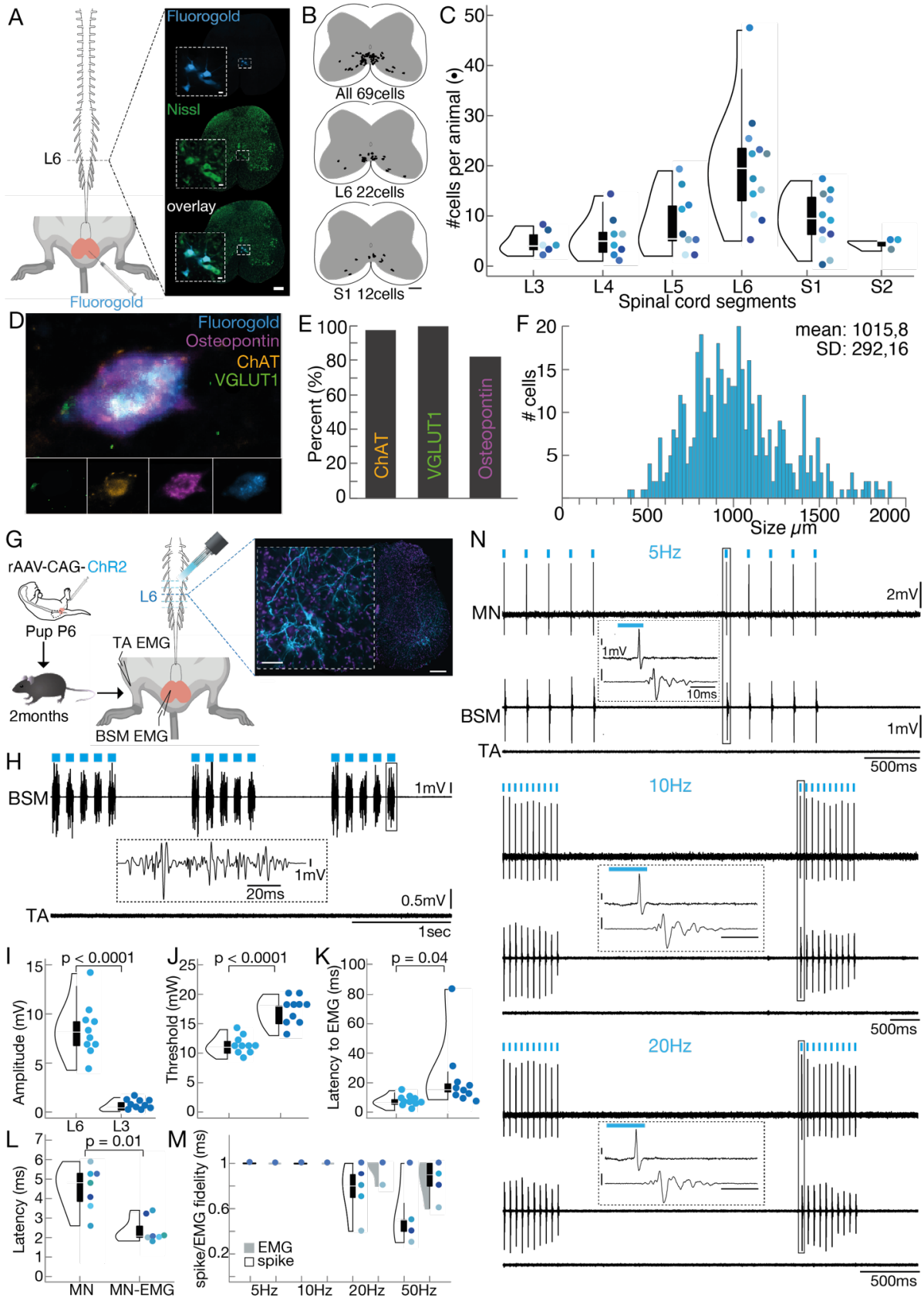

Figure 1: Anatomical and functional characterization of the bulbospongiosus motor neurons (BSM-MNs).

(A) Left panel: Flurogold (FG) was injected into the BSM of adult mice (N=12), leading to labeling across the rostrocaudal lumbosacral spinal cord. Right panel: FG-positive cells (blue) within the lumbar spinal segment 6. Nissl stain (green) was used to identify the spinal cord segment based on the atlas (Watson *et al.*, 2009).

(B) Serial reconstruction of all labeled FG-positive cells between lumbar segment 3 and sacral segment 2 revealed their distribution at the dorsomedial ventral spinal cord, close to the gray commissure. Upper panel: distribution of all labeled FG-positive cells for one animal; middle panel: cell distribution within lumbar segment 6 (L6); lower panel: cell distribution within sacral segment 1 (S1).

(C) Total FG-positive cell numbers along the lumbosacral spinal cord. Different colored dots represent different animals. The majority of cells were found at L6 and S1 spinal segments. Elements of violin plots: center line, median; box limits, upper (75) and lower (25) quartiles; and whiskers, 1.5x interquartile range.

(D) Post-hoc immunohistochemical staining for the alpha MN marker osteopontin (purple), choline transferase transporter (ChAT, orange) and the sensory input marker Vesicular Glutamate Transporter 1 (VGLUT1, green) revealed that all three markers are expressed by FG-positive cells (blue).

(E) Percentages of FG-positive cells expressing ChAT (97.7 ± 2.2 %), VGLUT1 (100%) and osteopontin (81.95 ± 2.2 %).

(F) Cell size distribution of FG-positive cells along the rostrocaudal lumbar spinal cord. Frequency histogram depicting number of MNs in each size bin and size of the MNs (binned in $20um^2$ steps).

(G) Left panel, experimental setup: For functional characterization, a rAAV-CAG-ChR2 was injected into the BSM of pups (P4-P6), later used for optogenetic stimulation when reaching adulthood. For optogenetic stimulation, a fiber was moved on top and along the rostral caudal lumbar spinal cord while monitoring muscle activity in the BSM and a leg muscle (*Tibialis anterior*, TA) using electromyogram (EMG). Right panel: rAAV-CAG-ChR2 expression (light blue) in L6 spinal segment (Nissl stain, purple).

(H) Example BSM and TA EMG trace recorded while optogenetically stimulating above the L6 spinal segment.

(I) Higher BSM EMG amplitudes were triggered when illuminating above the L6 spinal segment (mean amplitude 8.37 ± 1.15 mV), compared to illuminating above the L3 segment (mean amplitude 0.57 ± 0.2). Student's t-test $p < 0.0001$ (violin plots elements: see Methods).

(J) The laser power necessary to elicit BSM potentials was lower above the L6 spinal segment (mean threshold 11.2 ± 0.64 mW), compared to stimulating above the L3 segment (mean threshold 17 ± 0.97 mW). Student's t-test $p < 0.0001$ (violin plots elements: see Methods).

(K) The onset of BSM activity was shorter with illumination above the L6 spinal segment (mean latency to EMG 7.16 ± 1.58 ms) when compared to the L3 segment (mean latency to EMG 23.48 ± 9.43 ms). Student's t-test $p = 0.04$ (violin plots elements: see Methods).

(L) Latencies of triggered responses after laser stimulation are plotted for single BSM-MNs (MN; mean latency 4.6 ± 0.33 ms) and MN to EMG onset (MN-EMG; mean latency 2.25 ± 0.25 ms). Student's t-test $p = 0.01$ (violin plots elements: see Methods).

(M) Fidelity of spike and EMG activity are shown for the different frequencies of stimulation tested (dark gray: EMG fidelity; black: spike fidelity; violin plots elements: see Methods).

(N) Laser stimulation (10mW) at 5Hz (upper panel), 10Hz (middle panel) and 20Hz (lower panel) reliably triggered short latency action potentials in a single BSM-MN. Shortly after the single spikes, BSM EMG potentials were observed (insets) which themselves followed blue laser light applications. No EMG responses were observed in the TA muscle of the leg.

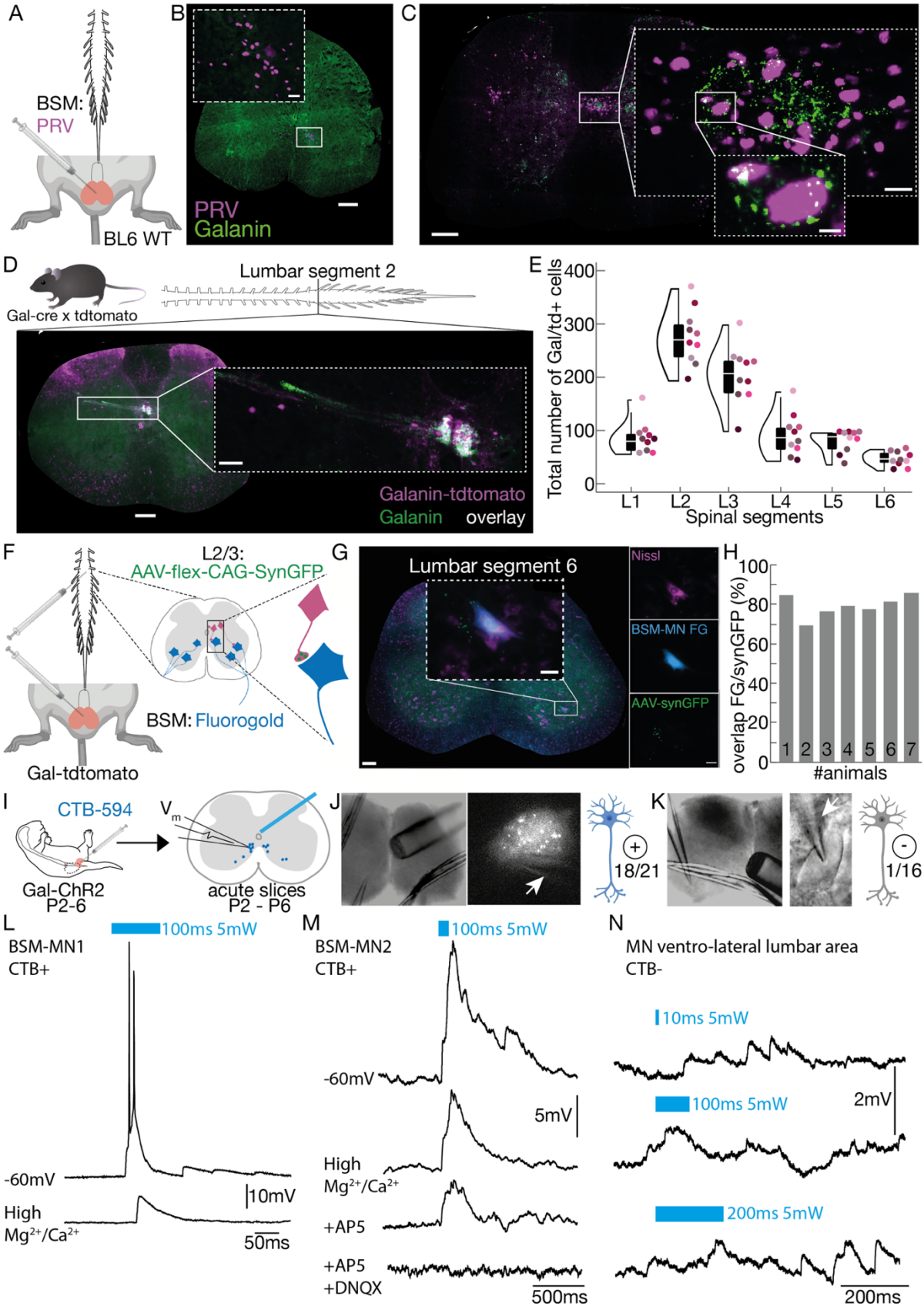
A
BSM:
PRV
BL6 WT
B
PRV
Galanin
C
D
Gal-cre x tdtomato
Lumbar segment 2
Galanin-tdtomato
Galanin
overlay
E
Total number of Gal/td+ cells
400
300
200
100
0
L1
L2
L3
L4
L5
L6
Spinal segments
F
L2/3:
AAV-flex-CAG-SynGFP
BSM: Fluorogold
Gal-tdtomato
G
Lumbar segment 6
Nissl
BSM-MN FG
AAV-synGFP
H
overlap FG/synGFP (%)
100
80
60
40
20
0
1 2 3 4 5 6 7
#animals
I
CTB-594
Gal-ChR2
P2-6
acute slices
P2 - P6
J
+
18/21
K
-
1/16
L
100ms 5mW
BSM-MN1
CTB+
-60mV
10mV
High
Mg2+/Ca2+
50ms
M
100ms 5mW
BSM-MN2
CTB+
-60mV
5mV
High
Mg2+/Ca2+
+AP5
+AP5
+DNQX
500ms
N
MN ventro-lateral lumbar area
CTB-
10ms 5mW
100ms 5mW
2mV
200ms 5mW
200ms

Figure 2: The BSM-MNs receive direct input from a group of lumbar spinal cord Galanin positive (Gal+) neurons.

(A) Experimental setup: PRV injections were done in the BSM of 6 BL6 mice.

(B) PRV-labeled cells were found at the same major location of FG-positive MNs (see Figure1). Scale bar 200um. Scale bar inset 20um.

(C) PRV injections into the BSM led to prominent labeling around the central canal at the L2/3 spinal segments. Post-hoc immunohistochemical staining against galanin revealed that the PRV labeled cluster was intermingled with galanin-positive immunohistochemical signal surrounding the central canal at the L2/3 spinal segments (Green: Galanin, Purple: PRV, Scale bar spinal cord section: 200um, Scale bar inset 1: 20um).

(D) Crossing a Gal-cre line with a tdTomato reporter line, and counterstaining the processed spinal cord sections for galanin, revealed a tight overlap between the tdTomato signal (pink) and the galanin (green) signal (Scale bar spinal cord section: 200um, Scale bar inset: 20um; see also Supplemental Figure 4).

(E) Total cell counts (N = 10) of all Gal-cre x TdTomato positive (Gal-tdT+) cells (y-axis) along the rostral-caudal lumbar spinal cord (x-axis) confirmed the presence of a prominent cluster of Gal-cre TdTomato cells at the L2/3 spinal segments (violin plots elements: see Methods).

(F) Anatomical connection between Gal+ cells and BSM-MNs was investigated through the co-injection of FG into the BSM and a cre-dependent AAV carrying a GFP-tagged synaptophysin (AAV-flex-CAG-SynGFP) into the L2/3 spinal segments of Gal-cre animals (N = 7).

(G) Example image of a spinal cord section obtained from an animal that received FG and AAV-flex-CAG-SynGFP injections. Inset shows a FG-positive BSM-MN that co-localizes with GFP positive postsynaptic boutons.

(H) Quantification of percentage of BSM-MNs showing co-expression of GFP-positive postsynaptic terminals for all 7 injected Gal-cre male mice (mean percentage 79.31 ± 2.1 %).

(I) Experimental setup for establishing the functional connectivity between Gal+ cells and BSM-MNs; *in vitro* whole cell recordings from choleratoxin-B (CTB, tagged with 594 fluorophore) retrogradely labeled BSM-MNs in acute spinal cord slices of pups aged P2-P6.

(J) Example spinal cord slice showing the location of fiber and pipette placement (left panel) during the recording of a CTB-positive cell (middle panel). A total of 21 CTB-positive cells were recorded, of which 18 were connected to galanin positive fibers running through the dorsal gray commissure above the central canal (right panel).

(K) Example spinal cord slice showing the location of fiber and pipette placement (left panel) during the recording of a control cell, a large MN located at the lateral ventral horn and CTB-negative (middle panel). A total of 16 CTB-negative cells were recorded out of which 1 seemed to be connected to galanin positive fibers running through the dorsal gray commissure above the central canal (right panel).

(L) Example whole-cell recording of a CTB-positive BSM-MN. Upper trace: a 100ms laser stimulation led to a short latency Excitatory Postsynaptic Potential (EPSP) and action potentials. Lower trace: High-concentration of Mg+ and Ca2+ in the ACSF lowered the amplitude and latency of the light triggered EPSP.

(M) Second example of a CTB-positive cell is shown, same as L. Lower trace: Application of NMDA and AMPA receptor blockers abolished the light-evoked EPSP, indicating that the neural transmission between Gal+ cells and BSM-MNs is glutamatergic.

(N) Example of a whole-cell recording of a CTB-negative MN. In contrast to the high number of CTB-positive cells responding to laser stimulation, only in 1 out of 16 CTB-negative cells did the illumination (Upper trace: 50ms, Middle trace: 100ms, Lower trace: 200ms) led to an EPSP.

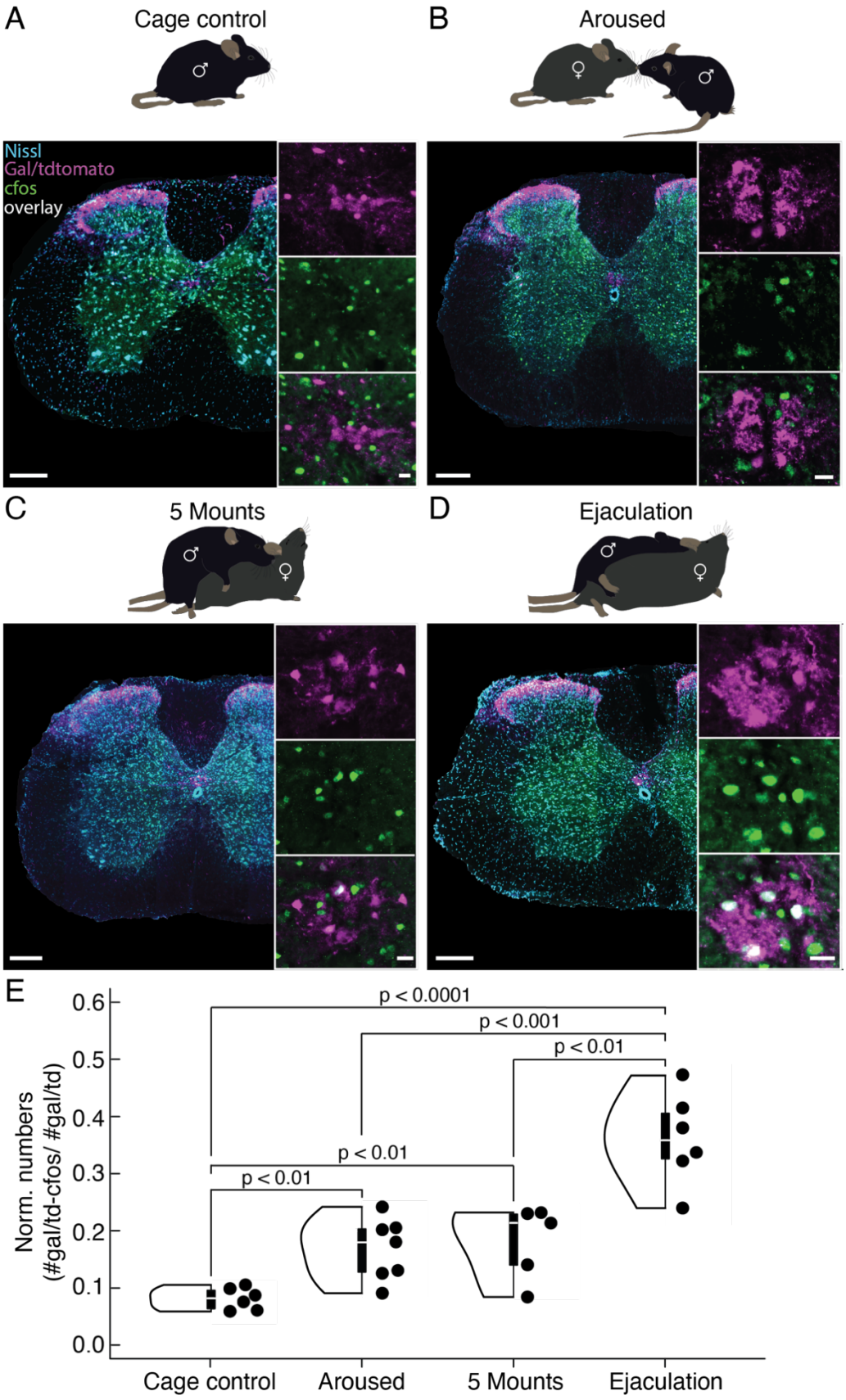
A
Cage control
B
Aroused
Nissl
Gal/tdtomato
cfos
overlay
C
5 Mounts
D
Ejaculation
E
Norm. numbers
(#gal/td-cfos/ #gal/td)
0.0
0.1
0.2
0.3
0.4
0.5
0.6
p < 0.0001
p < 0.001
p < 0.01
p < 0.01
p < 0.01
Cage control
Aroused
5 Mounts
Ejaculation

Figure 3: The lumbar population of Gal+ neurons becomes increasingly active during sexual behavior.

(A) Upper panel: Males in the Cage control group were alone in their home cage or in the behavior box for 10min (N = 6). Lower panel: Example spinal cord section at the L2/3 segments (revealed by Nissl stain, blue). Note no overlap between the cFos signal (green) and the Galanin signal (purple; see larger insets). Scale bar spinal cord section 200um, scale bar inset 20um.

(B) Upper panel: Males in the Aroused group were allowed to interact with a hormonally primed ovariectomised female for 10min, but attempts of copulation were interrupted (N = 7). Lower panel: Example spinal cord section at the L2/3 segments.

(C) Upper panel: Males in the 5 Mounts group: were allowed to perform 5 mounts with vaginal thrusting (N = 5). Lower panel: Example spinal cord section at the L2/3 segments.

(D) Upper panel: Males in the Ejaculation group were allowed to engage in sexual behavior until they ejaculated (N = 6). Lower panel: Example spinal cord section at the L2/3 segments.

(E) Normalized cell numbers (number of double labeled cells, cfos+ and Gal+; divided by the total number of Gal+ cells) for the four groups. Depicted p values from Student's t-test (violin plots elements: see Methods).

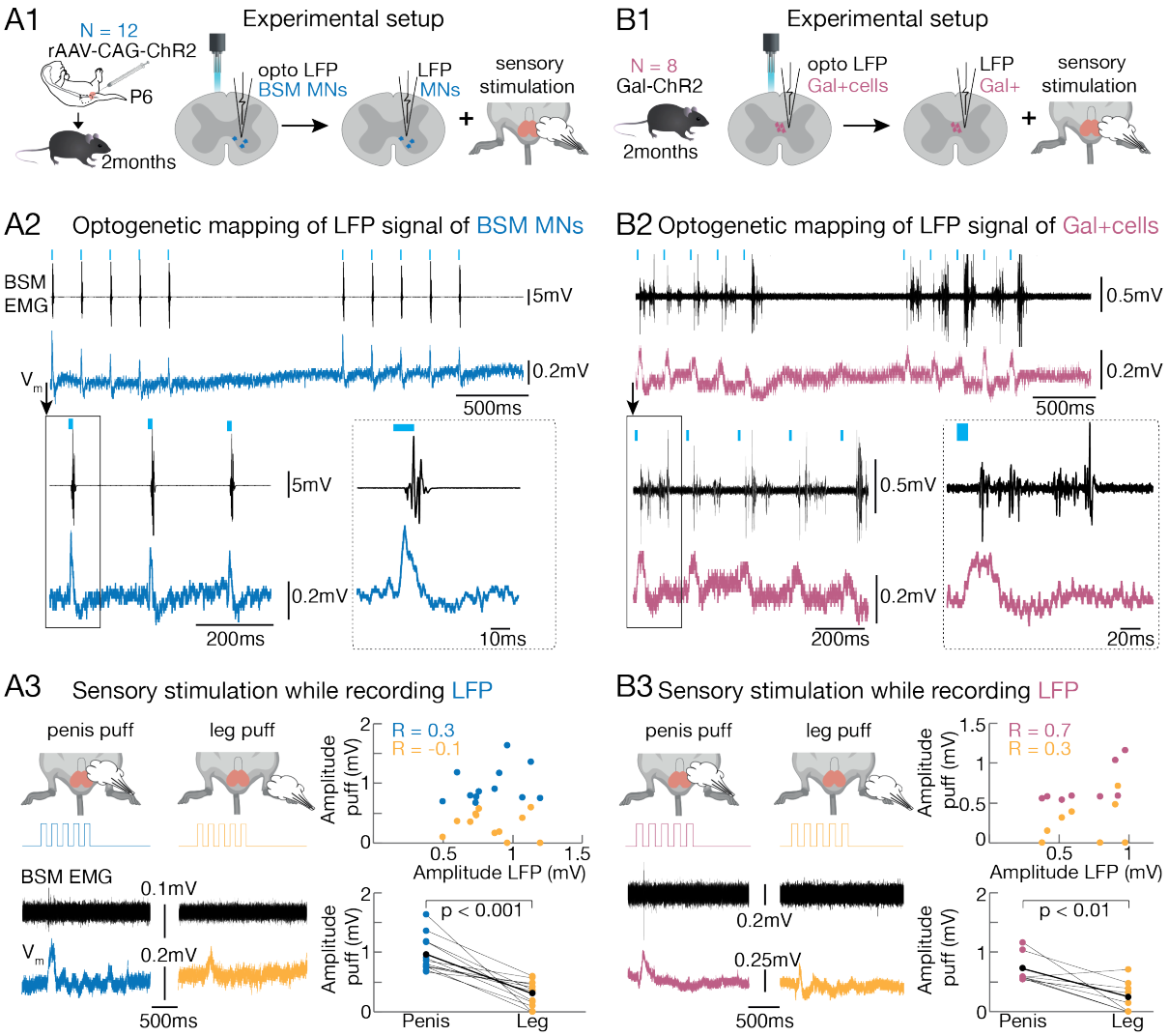
A1
N = 12
rAAV-CAG-ChR2
P6
2months
Experimental setup
opto LFP
BSM MNs
LFP
MNs
sensory
stimulation
B1
Experimental setup
N = 8
Gal-ChR2
2months
opto LFP
Gal+cells
LFP
Gal+
sensory
stimulation
A2
Optogenetic mapping of LFP signal of BSM MNs
BSM
EMG
5mV
Vm
0.2mV
500ms
5mV
0.2mV
200ms
10ms
B2
Optogenetic mapping of LFP signal of Gal+cells
0.5mV
0.2mV
500ms
0.5mV
0.2mV
200ms
20ms
A3
Sensory stimulation while recording LFP
penis puff
leg puff
R = 0.3
R = -0.1
Amplitude puff (mV)
Amplitude LFP (mV)
BSM EMG
0.1mV
Vm
0.2mV
500ms
p < 0.001
Penis
Leg
B3
Sensory stimulation while recording LFP
penis puff
leg puff
R = 0.7
R = 0.3
Amplitude puff (mV)
Amplitude LFP (mV)
0.2mV
0.25mV
500ms
p < 0.01
Penis
Leg

Figure 4: Gal+ neurons and BSM-MNs receive sensory input from the penis.
A1: Light-induced local field potentials (LFPs) were mapped in adult male mice whose BSM-MNs were infected with ChR2 at young age (rAAV-CAG-ChR2 injections into the BSM at P3-P6). Once the position with the most prominent light triggered LFPs was detected, the glass pipette was left at that position and sensory puff stimulations of penis and leg were conducted.
A2: Example traces for optogenetically induced LFP activity of BSM-MNs.. BSM (black) and LFP responses (blue) were tightly locked to the laser onset.
A3: Left panels: The pipette was kept at the position where the highest LFP responses were encountered. Subsequently sensory airpuff stimulation of penis (left, dark blue) and leg (right, yellow) were conducted while monitoring the LFP and EMG in animals whose BSM-MNs were infected with ChR2. Example traces were obtained from the same animal and correspond to the LFP traces depicted in A2. Right upper panel: The highest light-induced LFP responses are plotted against the penis/leg puff induced LFP responses revealing that penis puff induced LFPs (blue) are stronger correlated with the light induced LFP than leg puff induced LFP responses (yellow). Every dot is the pooled data of an animal (N = 12). Right lower panels: Penis puff responses (blue) led to significantly higher amplitudes (mean 0.96 ± 0.27 mV) in LFP than leg puff responses (yellow; mean amplitude 0.31 ± 0.09 mV). Student's t-test $p < 0.001$.
B1: Light-induced LFPs were first mapped in Gal-ChR2 mice. Afterwards the mapping pipette was left at the location where the strongest light triggered LFPs were encountered. Subsequent sensory stimulation of penis and leg were conducted while monitoring LFP and EMG activity in parallel.
B2: Example traces for optogenetically induced LFP activity in Gal-ChR2 animals (purple) while BSM activity (black) was monitored in parallel. Note the light-locked responses of the BSM with parallel timed LFP activity (putative Gal+ population activity around the central canal in L2/3).
B3: Same as A3 but for Gal-ChR2-animals. Left panel: Example traces for penis (pink) and leg (yellow) puff induced LFPs correspond to the traces shown in B2. Right upper panel: Highest light-induced LFP responses are plotted against the penis/leg puff induced LFP responses revealing that penis puff induced LFPs (pink) are stronger correlated with the light induced LFP than leg puff induced LFP responses (yellow). Every dot is the pooled data of an animal (N = 8). Right lower panel: Penis puff responses (pink) led to significantly bigger LFPs (mean amplitude 0.73 ± 0.09 mV) than leg puffs (yellow; mean amplitude 0.25 ± 0.09 mV). Student's t-test $p = 0.0035$.

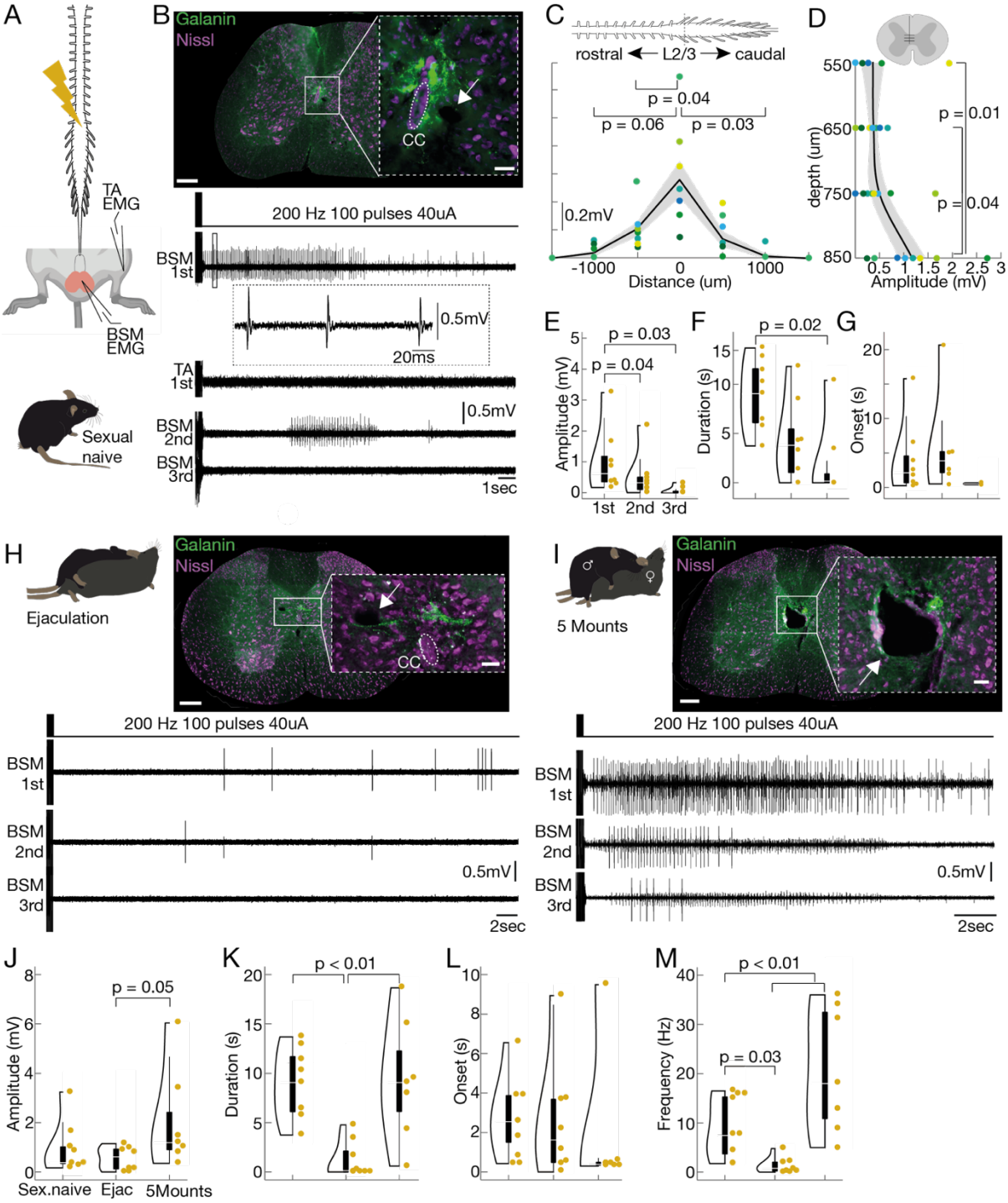

Figure 5: Electrical stimulation of the lumbar spinal cord location harboring the Gal+ neurons leads to BSM activity in an anesthetized preparation.

(A) Electrical stimulations (200Hz, 100 pulses, 40uA) were performed along the rostrocaudal lumbar spinal cord in adult anesthetized and spinalized C57BL6 mice (left panel) while performing EMG recordings in the BSM and a leg muscle (TA - *Tibialis anterior*).

(B) Electrolytic lesions were placed at the location where electrical current applications led to the most prominent BSM potentials (upper panel, see inset and white arrow; Green: immunohistochemical staining for Galanin, Purple: Nissl stain). Lower panel: representative traces of the EMG activity (BSM

and TA) during electrical current application at the lesion site. While the first current application led to high amplitude and high frequency discharges in the BSM (but not in the leg muscle), second current applications led to a reduced response (in this example, BSM activity was not observed during the third current application).
(C) Diagram showing the triggered BSM activity along the rostrocaudal spinal cord axis. Largest BSM responses were encountered at the L2/3 spinal segments (mean amplitude 0.56 ± 0.13 mV). Data refers to individual animals (N = 8). Mean amplitudes: at 500um rostral to L2/3 0.2 ± 0.05 mV; 500um caudal to L2/3 0.14 ± 0.05 mV; at 1000um rostral to L2/3 0.04 ± 0.02 mV;at 1000um caudal to L2/3 0.01 ± 0.003 mV. P-values result from a two-tailed Mann-Whitney-U Test.
(D) BSM amplitudes plotted against the depth of the stimulation sites. Differentially coloured dots refer to individual animals (N = 8). Mean amplitudes: at 550um 0.36 ± 0.23 mV, at 650um 0.37 ± 0.083; at 750um 0.49 ± 0.18 mV; at 850um 1.17 ± 0.27 mV. P-values result from a two-tailed Mann-Whitney-U Test.
(E) Violin plot illustrating the amplitudes of electrically triggered BSM activity (N=8) during the 1st (mean amplitude 0.99 ± 0.36 mV), 2nd (mean amplitude 0.5 ± 0.25 mV) and 3rd (mean amplitude 0.06 ± 0.04 mV) rounds of current application, with boxplots (elements: see Methods). P-values result from a two-tailed Mann-Whitney-U Test.
(F) Same as E, but the duration of the BSM activity is plotted. Mean durations: for 1st stimulation 8.8 ± 1.3 s; after 2nd current application 4.2 ± 1.46 s; after 3rd stimulation 1.74 ± 1.3 s. P-values result from a two-tailed Mann-Whitney-U Test.
(G) Same as E, but the onset with which BSM activity was triggered is plotted. Mean onset of EMG: after 1st current application 3.99 ± 1.83 ms; after 2nd stimulation 6.02 ± 3.01 ms; after 3rd current application round 0.54 ± 0.13 ms. A non parametric anova led to no significance (P = 0.21; Wilcoxon-Signed-Rank Test).
(H) Example BSM EMG traces of 1st, 2nd and 3rd current applications, recorded from an animal that ejaculated prior to the electrical stimulation experiment. Note that the BSM activity pattern during 1st and 2nd round of current application is markedly different from the sexually naive animal (panel B).
(I) Same as H, but traces are obtained from an animal that was allowed to perform 5 mounts with vaginal thrusting prior to the electrical stimulation experiment. BSM activity is comparable to the sexual naive male (panel B).
(J) Violin plot illustrating the amplitudes of electrically triggered BSM activity in sexually naive males (N = 8, mean amplitude 0.99 ± 0.36 mV), males that reached ejaculation (Ejac, N = 8, mean amplitude 0.57 ± 0.16 mV) or executed 5 mounts with vaginal thrusting (N = 7, mean amplitude 2.03 ± 0.76 mV), with boxplots (elements: see Methods). Data refers to the mean amplitude on the stimulation site with the highest response during first rounds of current applications. P-values result from a two-tailed Mann-Whitney-U Test.
(K) Same as J, but the duration of the BSM activity is plotted. Mean duration: in sexual naive animals 8.8 ± 1.3 s; in the Ejac group 1.26 + 0.26 s; in the group with 5 mounts 10.43 + 1.82 s. P-values result from a two-tailed Mann-Whitney-U Test.
(L) Same as J, but the onset of BSM activity is depicted. Mean onset: sexual naive 3.99 ± 1.83 ms; Ejac 2.56 ± 1.04 ms; 5 mounts 0.88 ± 0.48 ms). No significance was found using a non parametric anova, Wilcoxon-Signed-Rank Test; P = 0.2.
(M) Same as J, but the frequency of BSM activity is shown. Mean frequency: sexual naive 8.79 ± 2.2 Hz; Ejac 1.39 ± 0.56 Hz; 5 mounts 20.81 ± 4.8 Hz). P-values result from a two-tailed Mann-Whitney-U Test.

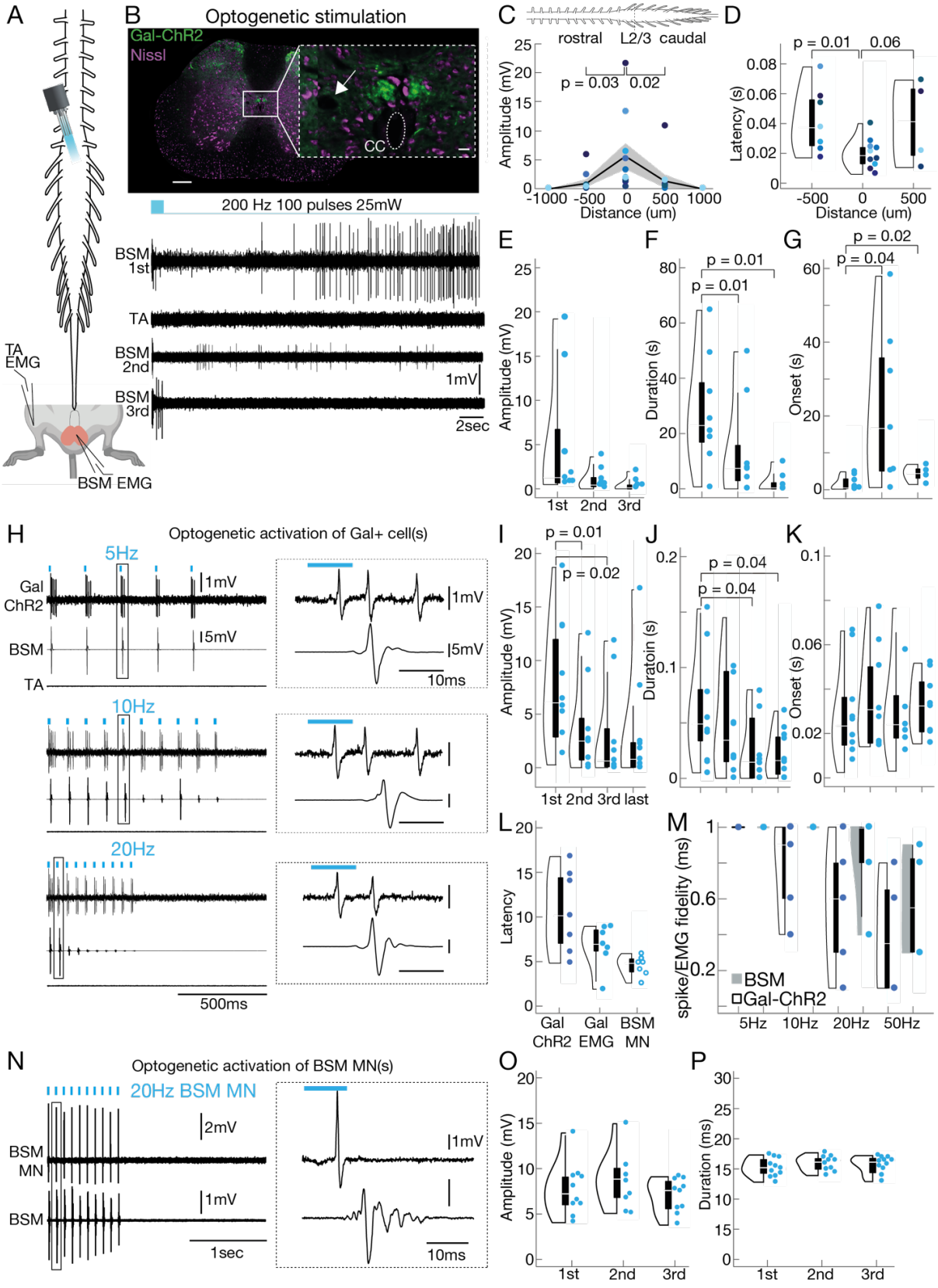
A
B
Optogenetic stimulation
Gal-ChR2
Nissl
CC
200 Hz 100 pulses 25mW
BSM 1st
TA
BSM 2nd
BSM 3rd
1mV
2sec
TA EMG
BSM EMG
C
rostral
L2/3
caudal
p = 0.03
0.02
Amplitude (mV)
Distance (um)
D
p = 0.01
0.06
Latency (s)
Distance (um)
E
Amplitude (mV)
1st
2nd
3rd
F
p = 0.01
p = 0.01
Duration (s)
G
p = 0.02
p = 0.04
Onset (s)
H
Optogenetic activation of Gal+ cell(s)
5Hz
Gal ChR2
BSM
TA
1mV
5mV
10ms
10Hz
20Hz
500ms
I
p = 0.01
p = 0.02
Amplitude (mV)
1st 2nd 3rd last
J
p = 0.04
p = 0.04
Duratoin (s)
K
Onset (s)
L
Latency
Gal ChR2
Gal EMG
BSM MN
M
spike/EMG fidelity (ms)
BSM
Gal-ChR2
5Hz
10Hz
20Hz
50Hz
N
Optogenetic activation of BSM MN(s)
20Hz BSM MN
BSM MN
BSM
2mV
1mV
1sec
10ms
O
Amplitude (mV)
1st
2nd
3rd
P
Duration (ms)
1st
2nd
3rd

Figure 6: Optogenetic activation of the Gal+ neurons leads to BSM activity in an anesthetized preparation.

(A) Optogenetic stimulations (200Hz, 100 pulses, 20mW) were performed on top and along the rostrocaudal lumbar spinal cord in adult anesthetized and spinalized Gal-Chr2 males (left panel) while performing EMG recordings in the BSM and a leg muscle (TA - *Tibialis anterior*).

(B) Electrolytic lesions were placed at the location where optogenetic stimulation led to the most prominent BSM potentials (upper panel, see inset and white arrow; Green: Galanin-ChR2, Purple: Nissl stain). Scale bar of spinal cord section 200um. Inset, 20um. Lower panel: representative traces of the EMG activity (BSM and TA) during optogenetic application on top of the lesion site. Note that it led to a similar activity pattern compared to the electrical stimulations: while the first laser application led to high amplitude and high frequency discharges in the BSM, but not in the leg muscle (TA), the second round of light delivery led to a reduced response, and BSM activity was not detected during the third round of optogenetic stimulation.

(C) Diagram showing the light-triggered BSM activity along the rostrocaudal spinal cord axis. Largest BSM responses were encountered at the L2/3 segments (mean amplitude 5.61 ± 2.31 mV, N=8). Note that responses are more restricted to the L2/3 spinal segments where the cluster of Gal+ cells was found, around the central canal (mean amplitudes: 500um rostral to L2/3 0.99 ± 0.58 mV, 500um caudal to L2/3 1.35 ± 1.06 mV). P-values result from a two-tailed Mann-Whitney-U Test.

(D) Violin plots with boxplots (elements: see Methods) illustrating the latencies with which BSM responses were triggered as a function of distance (N=8). Shorter distances were achieved at 0um which corresponds to the L2/3 spinal segments (0.02 ± 0.006 s). P-values result from a two-tailed Mann-Whitney-U Test.

(E) Violin plots illustrating the amplitudes of optogenetically triggered BSM signal during 1st (mean amplitude 5.5 ± 2.6 mV), 2nd (mean amplitude 1.48 ± 0.86 mV) and 3rd rounds (mean amplitude 0.41 ± 0.23 mV) of laser application, with boxplots (elements: see Methods, N=8). P-values result from a two-tailed Mann-Whitney-U Test.

(F) Same as E, but the duration of BSM activity is plotted. Mean durations: after 1st 29.33 ± 7.28 s; 2nd 15.59 ± 6.43 s; and 3rd 2.27 ± 1.24 s, laser application. P-values result from a two-tailed Mann-Whitney-U Test.

(G) Same as F, but the onsets with which BSM activity was initiated are plotted. Mean onset of BSM EMG: after 1st 1.18 ± 0.02 s; 2nd 25.25 ± 0.1; and 3rd 4.28 ± 0.1 s, laser application. P-values result from a two-tailed Mann-Whitney-U Test.

(H) In addition to tonic BSM responses as observed during the electrical stimulations, optogenetic stimulations also led to timely locked BSM responses, capable of following stimulation frequencies up to 20Hz (N = 12). In a subset of animals (4 out of 12) we recorded photo-identified single Gal-ChR2 neurons (N = 5 cells). Upper left panel: Juxtacellular recording of a Gal-ChR2 cell in parallel with EMG recordings of the BSM (2nd trace) and the TA muscle of the leg (3rd trace) during a 5Hz laser stimulation. Upper right panel: zoom in of the indicated box illustrating the spike and EMG onset. Middle panels: same as upper panel but for a 10Hz and 20Hz laser application of the same cell shown in the upper panel.

(I) Violin plots illustrating the amplitudes of optogenetically time-locked BSM signals (N=12) during 1st (mean amplitude 7.45 ± 1.64 mV), 2nd (mean amplitude 3.59 ± 1.17), 3rd (mean amplitude 2.93 ± 1.26 mV) and last rounds (mean amplitude 3.98 ± 1.98) of laser application, with boxplots (elements: see Methods). P-values result from a two-tailed Mann-Whitney-U Test.

(J) Same as I, but the duration of BSM signals is plotted. Mean durations: after 1st 0.06 ± 0.01 s; 2nd 0.05 ± 0.01; 3rd 0.03 ± 0.01; and last 0.03 ± 0.06 laser application. P-values result from a two-tailed Mann-Whitney-U Test.

(K) Same as I, but the onset with which locked laser light triggered a BSM response. Data refers to 5 averaged onsets. Mean onsets: after 1st 0.03 ± 0.005 s; 2nd 0.03 ± 0.006; 3rd 0.03 ± 0.006; and last 0.03 ± 0.005 s, laser application.
(L) Violin plot with boxplots (elements: see Methods) illustrating the latency for optogenetically triggered spikes in Gal-ChR2 single cells, the latency between spike onset of Gal-ChR2 single cells and BSM EMG onset, and the latency to spike of single photo-identified BSM-MNs. Data refers to 5 single cells.
(M) Same as L, but the Gal-ChR2 spike and Gal-EMG fidelity (with which a laser pulse triggered a single spike or EMG response) is plotted.
(N) Optogenetic activation of photo-identified BSM-MNs (same as Fig. 1). Upper left panel: Juxtacellular recording of a BSM-MNs in parallel with EMG recordings of the BSM (2nd trace) during a 20Hz laser stimulation. Upper right panel: zoom in of the indicated box illustrating the BSM-MNs spike and the EMG onset.
(O) Repeated optogenetic activation of BSM-MNs led to BSM activity of stable amplitude (mean amplitude: after 1st 7.65 ± 0.91 mV; 2nd 8.66 ± 0.93 mV; and 3rd 6.99 ± 0.59 mV laser applications).
(P) Same as O, but the duration of BSM activity in response to optogenetic activation of BSM-MNs is shown (mean durations: after 1st 15.28 ± 0.47 ms; 2nd 15.85 ± 0.39 ms; and 3rd 15.61 ± 0.47 ms laser application).

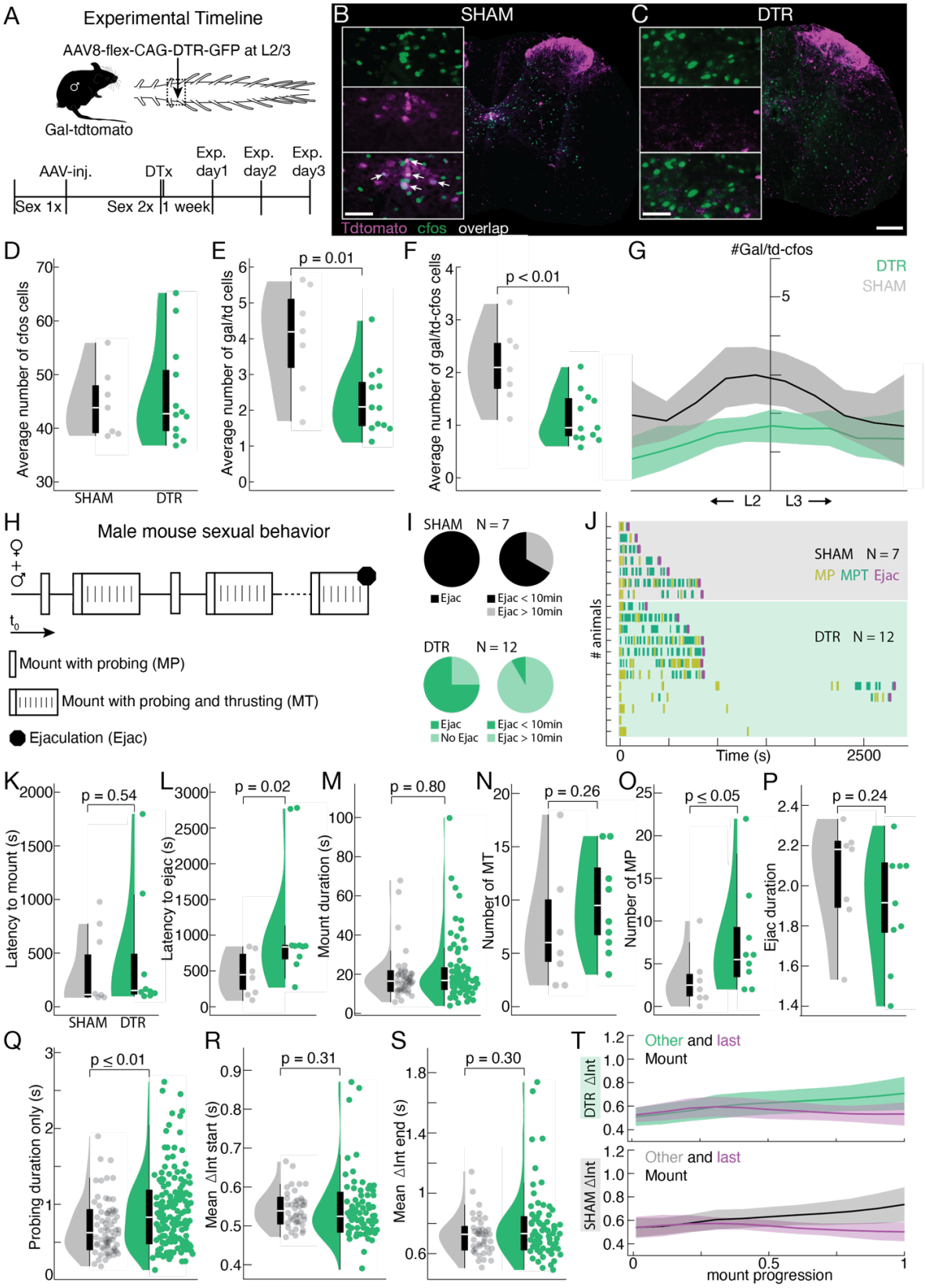
A
Experimental Timeline
AAV8-flex-CAG-DTR-GFP at L2/3
Gal-tdtomato
AAV-inj.
DTx
Exp. day1
Exp. day2
Exp. day3
Sex 1x
Sex 2x
1 week
B
SHAM
C
DTR
Tdtomato cfos overlap
D
Average number of cfos cells
SHAM
DTR
E
p = 0.01
Average number of gal/td cells
F
p < 0.01
Average number of gal/td-cfos cells
G
#Gal/td-cfos
DTR
SHAM
L2
L3
H
Male mouse sexual behavior
Mount with probing (MP)
Mount with probing and thrusting (MT)
Ejaculation (Ejac)
I
SHAM N = 7
Ejac
Ejac < 10min
Ejac > 10min
DTR N = 12
Ejac
No Ejac
Ejac < 10min
Ejac > 10min
J
SHAM N = 7
MP MPT Ejac
DTR N = 12
animals
Time (s)
K
p = 0.54
Latency to mount (s)
L
p = 0.02
Latency to ejac (s)
M
p = 0.80
Mount duration (s)
N
p = 0.26
Number of MT
O
p ≤ 0.05
Number of MP
P
p = 0.24
Ejac duration
Q
p ≤ 0.01
Probing duration only (s)
R
p = 0.31
Mean ΔInt start (s)
S
p = 0.30
Mean ΔInt end (s)
T
Other and last Mount
DTR ΔInt
SHAM ΔInt
mount progression

Figure 7: Genetic ablation of the lumbar Gal+ neurons disrupts male sexual behavior.
(A) Experimental design. Gal-cre x dTomato male mice were sexually trained once before receiving a spinal injection of either a flexed AAV carrying DTR (DTR group) or undergoing a sham surgery (SHAM). Two weeks post-surgery the sexual performance of both groups was tested, after which they received an injection of Diphteria Toxin (DT). One week after DT injection, the impact of the neuronal ablation on sexual behavior was investigated.
(B) Example spinal cord section at the L2/3 segments obtained from an animal of the SHAM group. tdTomato indicating Gal+ neurons (purple) overlap (white) with the immediate early gene cfos (green). Scale bar 200um. Inset 50um.
(C) Same as B but for an animal of the DTR group. Note the poor TdTomato signal (purple) around the central canal at the L2/3 spinal segments.
(D) Violin plots of cFos cells quantified in the L2/3 spinal segments for the SHAM (gray, mean number 44.6 ± 2.4) and DTR (green, mean number 46.2 ± 2.1) animals. P = 0.7 resulting from a student's t-test (violin plots elements: see Methods).
(E) Same as D, but the averaged number of Gal-cre x TdTomato cells is depicted. Note the significantly lower number of Gal-cre x TdTomato cells in the DTR animals (mean number of tdTomato+ cells 2.3 ± 0.28) compared to the SHAM group (4.0 ± 0.6). P = 0.01 resulting from a student's t-test.
(F) Same as D, but the averaged number of Gal-cre x TdTomato cells co-expressing cfos is plotted. A significant difference was observed across groups (mean number of Gal-cre xTtdTomato+/cfos+ cells in DTR 1.1 ± 0.14 and SHAM 2.1 ± 0.3 animals, p = 0.01 resulting from a student's t-test).
(G) Cumulative curve of Gal-cre x TdTomato cell numbers along the L2/3 spinal segments for SHAM and DTR animals.
(H) Schematic representation of male sexual behavior: Mounts with probing (MP), correct positioning of the paws on the female flanks and shallow pelvic thrusting movements trying to locate the vagina; Mounts with thrusting (MT), after the initial probing period of shallow thrusting the male inserts the penis inside the female and executes several deeper thrusts until he dismounts; several MT are executed until the ejaculatory threshold is achieved .
(I) Pie chart indicating percentages of animals (black/gray SHAM; green/light green DTR) that ejaculated, and ejaculated in less than 10 minutes.
(J) Raster plot aligned to the first consummatory act (MP or MT). Each line represents an animal: SHAM animals on a shaded gray; DTR animals on a shaded green background. Purple line marks Ejaculation (Ejac). Animals are ordered by latency to ejaculate, after separating animals that ejaculated or not.
(K) Violin plot showing the latency to mount (MP or MT) for SHAM (mean latency 392 ± 181 s) and DTR (mean latency 435 ± 248 s) animals. No significant difference was detected, p = 0.54, Mann-Whitney U-test (violin plots elements: see Methods).
(L) Same as K, but the latency to ejaculate from the first consummatory act (MP or MT) is plotted (mean latency to ejac for SHAM animals 427.2 ± 146 s). Note that DTR animals take significantly longer to reach ejaculation (mean latency to ejac 1170.8 ± 392 s). P = 0.002 resulting from a Mann-Whitney U-test.
(M) Same as K, but for the mount duration (all MT events) which is comparable across groups (mean mount duration of SHAM animals 18.9 ± 2 s and DTR animals 21.1 ± 2 s). P = 0.8 resulting from a Mann-Whitney U-test.
(N) Number of MTs for SHAM (mean number 7 ± 2.7) and DTR (mean number 9.3 ± 2) animals. P = 0.29 resulting from a Mann-Whitney U-test (violin plots elements: see Methods).
(O) Number of MPs for SHAM (mean number 3 ± 1.6) and DTR (mean number 7.6 ± 2.7) animals. P = 0.03 resulting from a Mann-Whitney U-test (violin plots elements: see Methods).

(P) The time window for ejaculation is plotted (from the last thrust until separating from the female). Mean ejac duration for SHAM animals 16 ± 3 s vs. mean DTR 15.4 ± 2.3 s. P = 0.8 resulting from a Student's t-test (violin plots elements: see Methods).
(Q) Probing duration for all MT (time from first to the last shallow thrust, before penile insertion). Mean probing duration for SHAM 0.7 ± 0.04 s vs. DTR 0.91 ± 0.04 s. P = 0.002 resulting from a Mann-Whitney U-test (violin plots elements: see Methods).
(R) Violin plots of all inter-thrust intervals of the first four thrusts of a MT (mean for SHAM 0.54 ± 0.01 s vs. DTR 0.54 ± 0.01 s). P = 0.31resulting from a Mann-Whitney U-test (violin plots elements: see Methods).
(S) Same as R, but the inter-thrust interval of the last four thrusts in a MT is plotted (mean for SHAM 0.69 ± 0.03 s vs. DTR 0.76 ± 0.03). P=0.15 resulting from a Mann-Whitney U-test.
(T) Mean interval with standard deviation is plotted in relation to mount progression for all other MT (light green DTR; gray SHAM) and the last MT leading to ejaculation (purple); a similar pattern of deceleration and acceleration is observed across the two groups (McGill, 1962).

Supplemental Figures

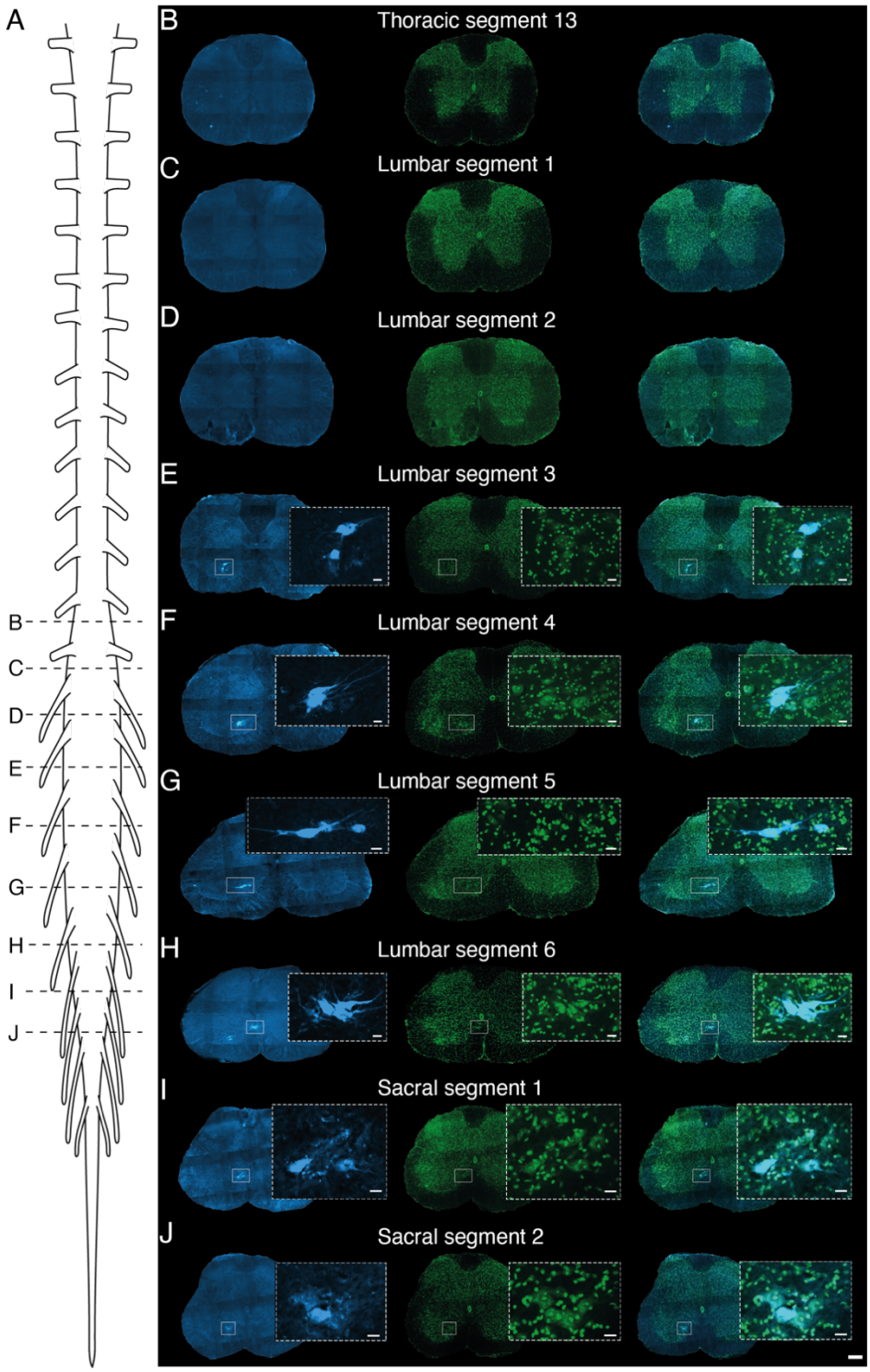

Supplemental Figure 1: Anatomical distribution of the bulbospongiosus muscle motor neurons (BSM-MNs).

(A) Spinal cord scheme illustrating segments that are shown in B-J.

(B - J) Left panels: Blue channel revealing FG labeled BSM-MNs (E -J). Middle panel: Green channel illustrating the Nissl stain in order to identify the spinal cord segments. Right panel: Overlap of both channels. Scale bar 200um. Inset scare bar: 50um.

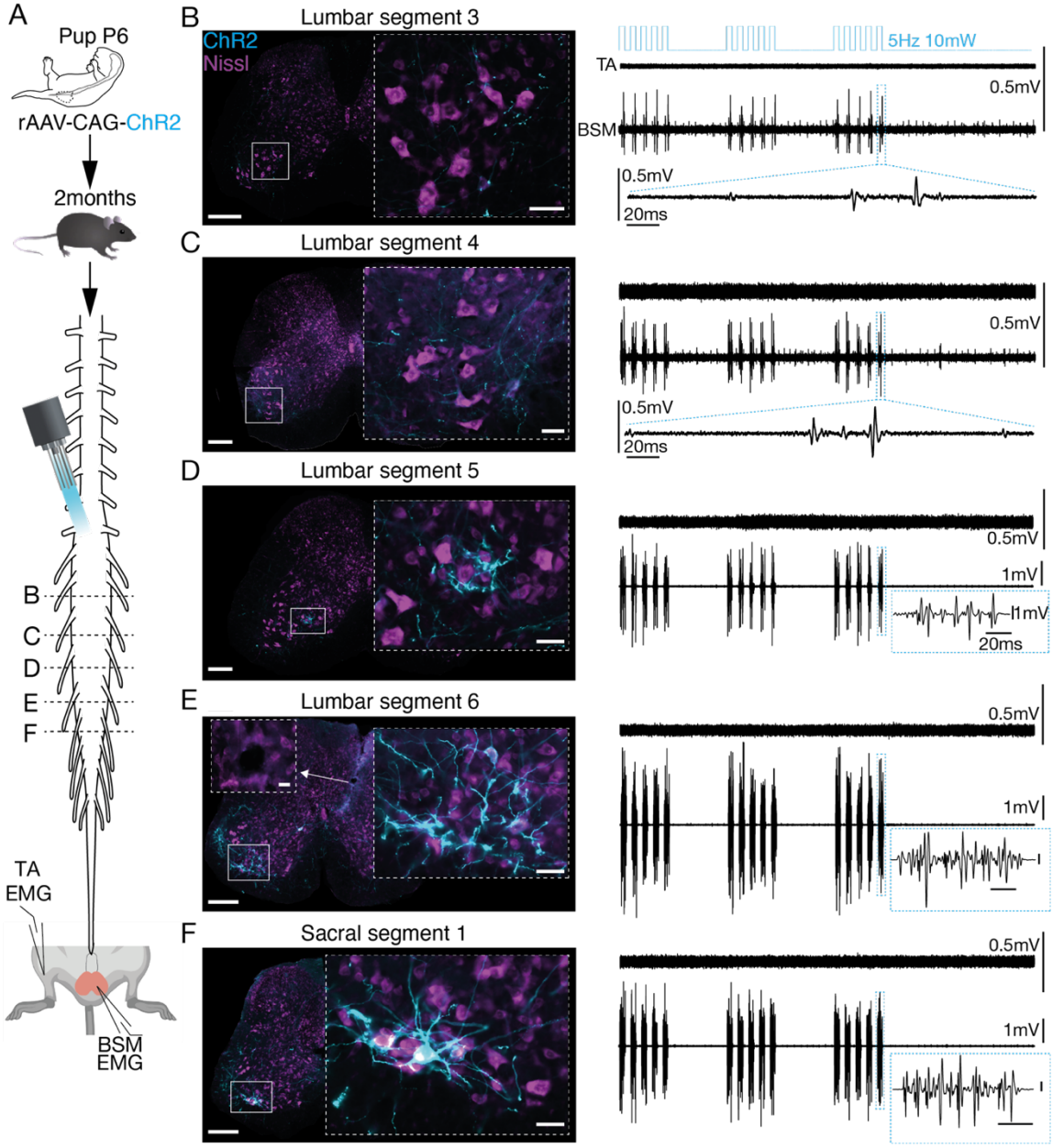

Supplemental Figure 2: Optogenetic stimulation of the BSM-MNs along the rostrocaudal axis of the spinal cord.

(A) Experimental setup. Left panel: BL6 mice pups (aged postnatal day 3-6) received an injection of a rAAV-CAG-ChR2 on the BSM. Pups were raised until 2-3 months of age, to perform optogenetic stimulation on top of the spinal cord (rostral to caudal) while in parallel monitoring EMG activity in the BSM.

(B) Leftpanel: Representative spinal cord segment (lumbar segment 3, L3) of a 2 month old mouse that was infected at the age of P4-P6 with a rAAV-CAG-ChR2 (blue) in the BSM. Identification of spinal cord segments based on the atlas was achieved via a Nissl stain (purple). Right panel: corresponding EMG recordings (upper trace: leg; lower trace: BSM) observed while shining blue light on top of the spinal cord segment shown in the left panel. EMG recordings were aligned to histology by placing an electrolytic lesion at the spot with the largest BSM response recorded (see panel E). Scale bar 200um. Scale bar inset 20um.

(C-F) Same as B for the remaining spinal cord segments depicted in A (see dotted lines, from L3-S1). Note that the biggest responses in the BSM EMG were triggered at the location where most BSM-MNs were infected (L6, S1).

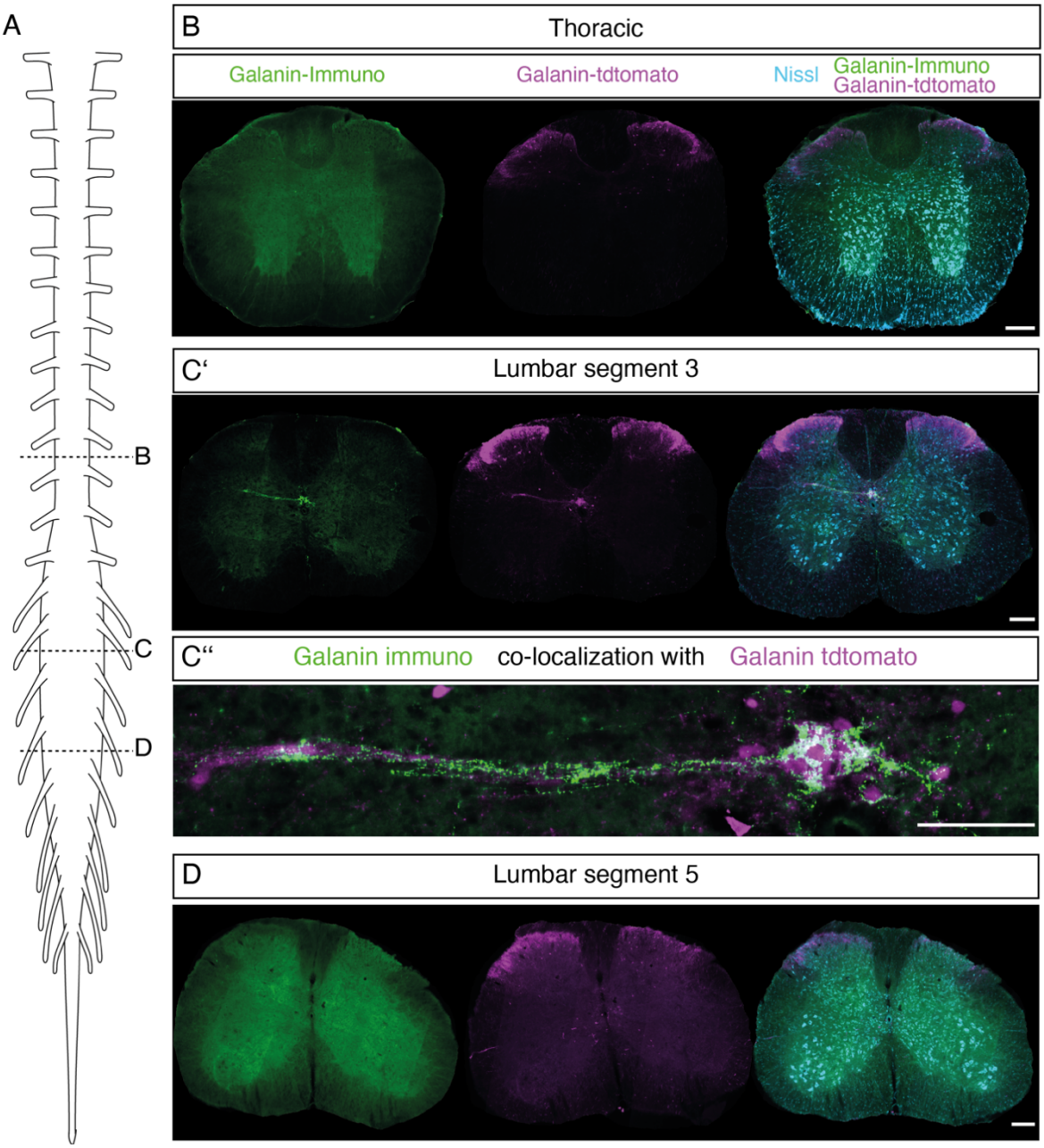

Supplemental Figure 3: The Gal+ population is mostly present at the L2/3 spinal segments.
(A) Scheme of spinal cord.
(B) Example staining, in the thoracic part depicted in A, for Galanin (left, green) in a Gal-cre x TdTomato animal (purple, middle). The Nissl stain (cyan) served as an identification parameter for the spinal cord segments. Note that there is no Galanin signal around the central canal. Scale bar 200um.
(C') Same as B but for the L3 segment3. Note the presence of a prominent cluster of Galanin expressing cells (shown with the immunostaining, green, and the tdTomato signal, purple, of the Galanin-reporter line) around the central canal.
(C") Overlay of the Galanin immunohistochemical signal (green) with the tdTomato signal in the Gal-cre x TdTomato cross reveals an overlap of both signals (see zoom in). Scale bar 100um.
(D) Same as B but for the L5 spinal segment. Note again the absence of Galanin positive cells around the central canal.

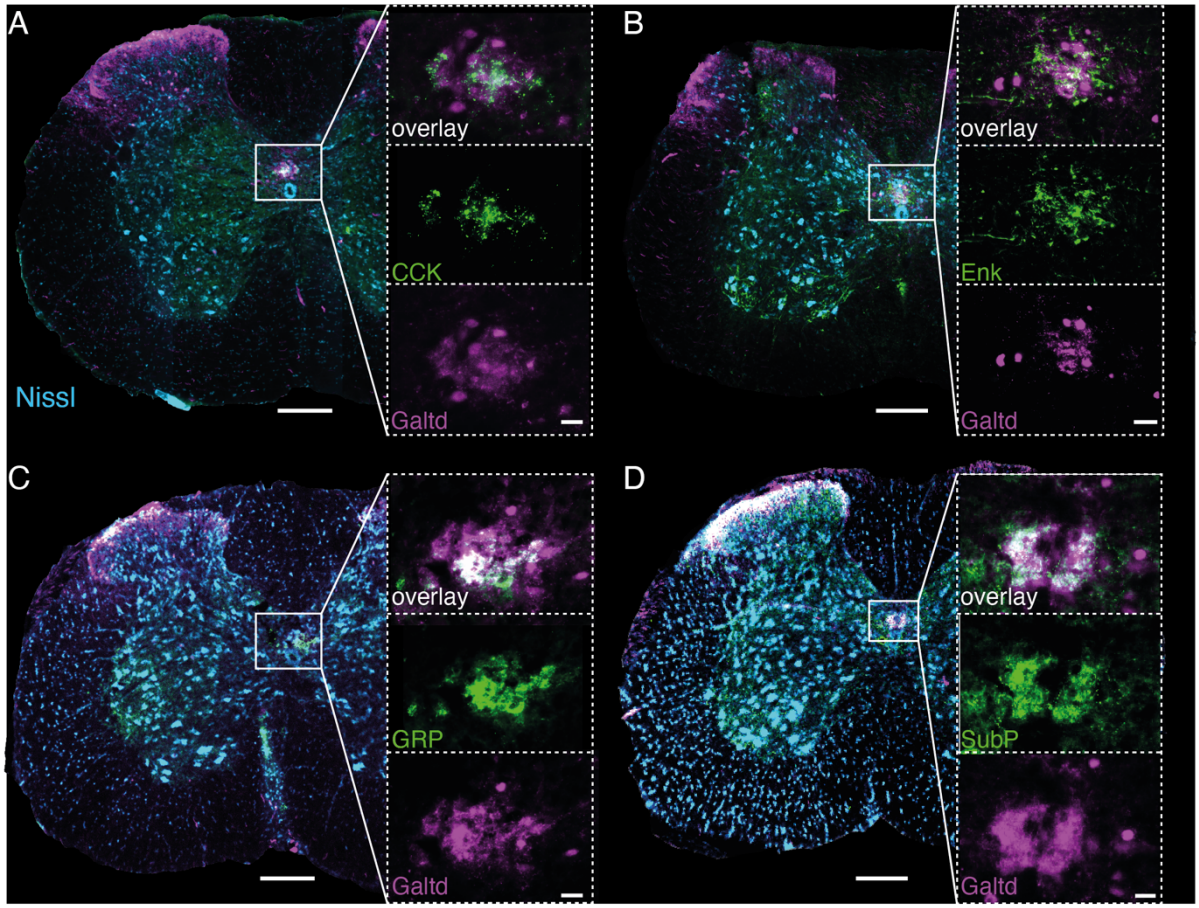

Supplemental Figure 4: Immunohistochemical characterization of the lumbar Gal+ population.
(A) Immunohistochemical staining for Cholecystokinin (green) in the L2/3 spinal segments obtained from a Gal-cre x dTomato (Gal-td, pink) male mouse. A Nissl stain (light blue) was performed to identify the spinal cord segment. Scale bar spinal segment 200um. Scale bar insets 20um.
(B) Same as A but immunohistochemical processing was done for Enkephalin (Enk).
(C) Same as A but a post-hoc staining for Gastrin-releasing peptide (GRP) was performed.
(D) Same as A but immunohistochemical staining against Substance P (SubP) was performed.

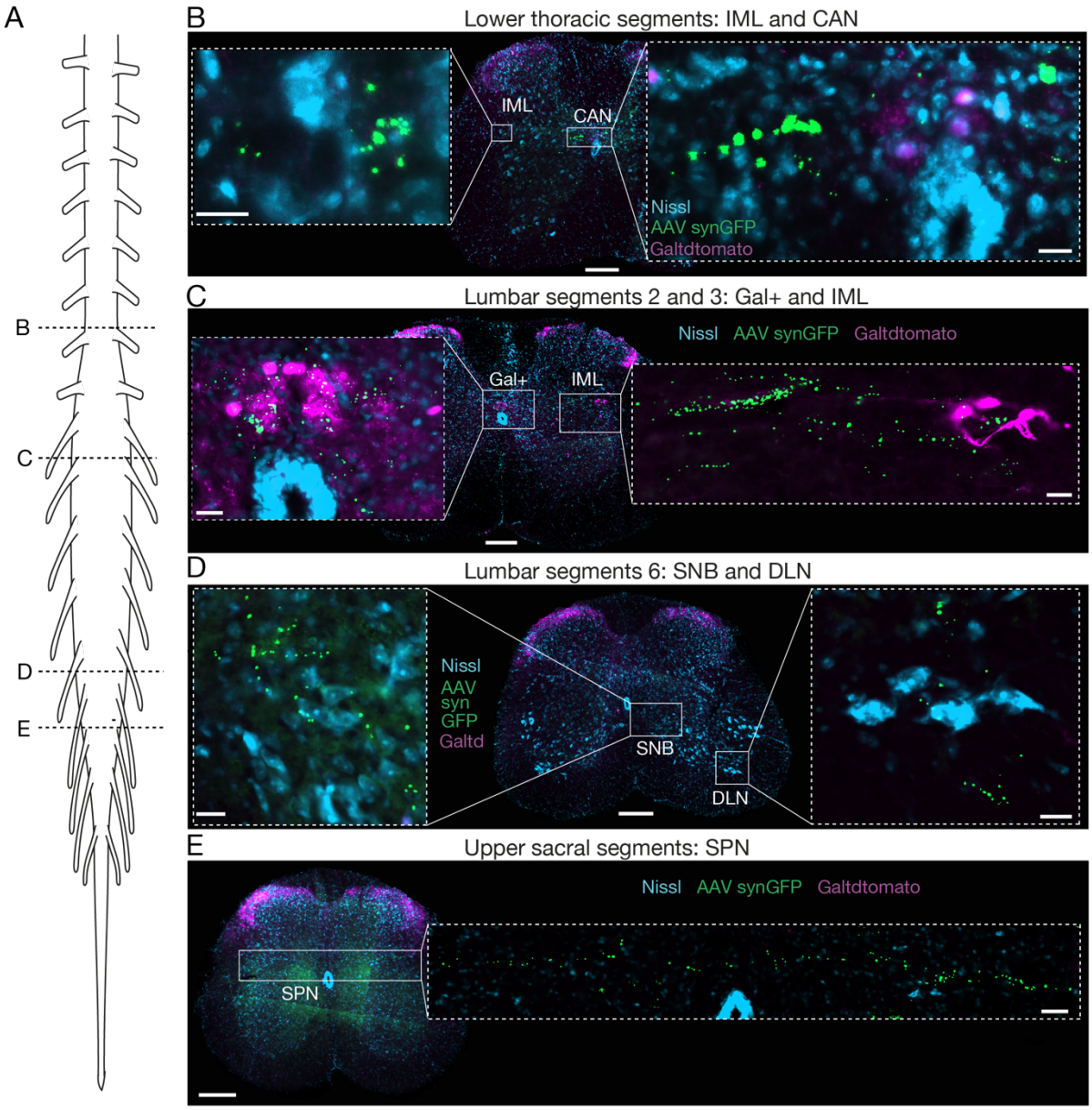

Supplemental Figure 5: Spinal projection targets of the Gal+ cells revealed with a marker for postsynaptic bouts (synaptophysin delivered through an AAV-flex-CAG-SynGFP) .

(A) Scheme of spinal cord.

(B) GFP-labeled synaptic terminals of Gal+ cells were found at the location of the central autonomic nucleus (CAN) and intermediolateral nucleus (IML) at lower thoracic segments. Both nuclei are known to contain sympathetic preganglionic cells. Scale bar 200um. Scale bar insets 20um.

(C) Prominent GFP-labeled boutons were found at the location of Gal+ cells and at the IML of the L2/3 spinal segments. Scale bar 200um. Scale bar inset 50um.

(D) At the L6 segment, GFP-positive synaptic terminals were dominantly found at the spinal nucleus of bulbocavernosus (SNB) that contains the BSM-MNs and at the dorsolateral nucleus (DLN) which contains the MNs controlling the ischiocavernosus muscle.

(E) In upper sacral segments GFP-positive terminals were diffusely found in regions containing parasympathetic preganglionic cells (SPN, sacral parasympathetic nucleus).

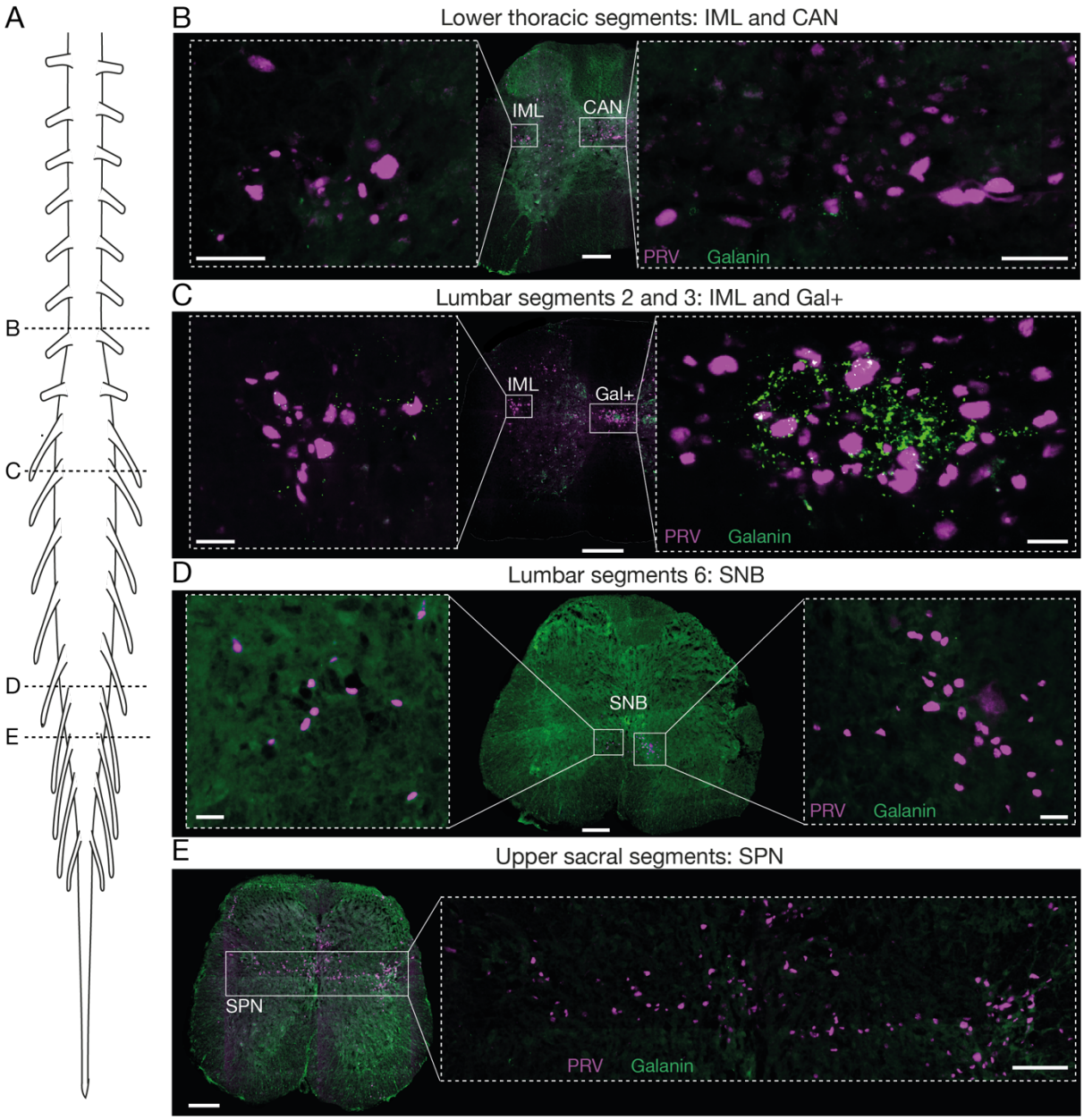

Supplemental Figure 6: PRV injections into the BSM reveal similar anatomical sites as the ones obtained with the injection of AAV-flex-CAG-SynGFP at the location of the Gal+ cells.

(A) Spinal cord scheme.

(B) PRV-positive labeled cells were found at the location of the intermediolateral (IML) and central autonomic nucleus (CAN) at lower thoracic segments. Scale bar 200um. Scale bar inset 20um.

(C) Prominent PRV labeling was encountered at the central canal and at the IML in L2/3 segments. Scale bar 200um. Scale bar inset 20um.

(D) Clusters of PRV cells were present only in the spinal nucleus bulbocavernosus (SNB), that contains the BSM-MNs, at the L6 segment, but not on the dorsolateral nucleus (DLN), containing the MNs controlling the ischiocavernosus muscle, which shows the specificity of the PRV approach to trace the MNs innervating the BSM. Scale bar 200um. Scale bar inset 50um.

(E) In the upper sacral segments, PRV labeling could be seen along the spinal parasympathetic centers (SPN). Scale bar 200um. Scale bar inset 100um.

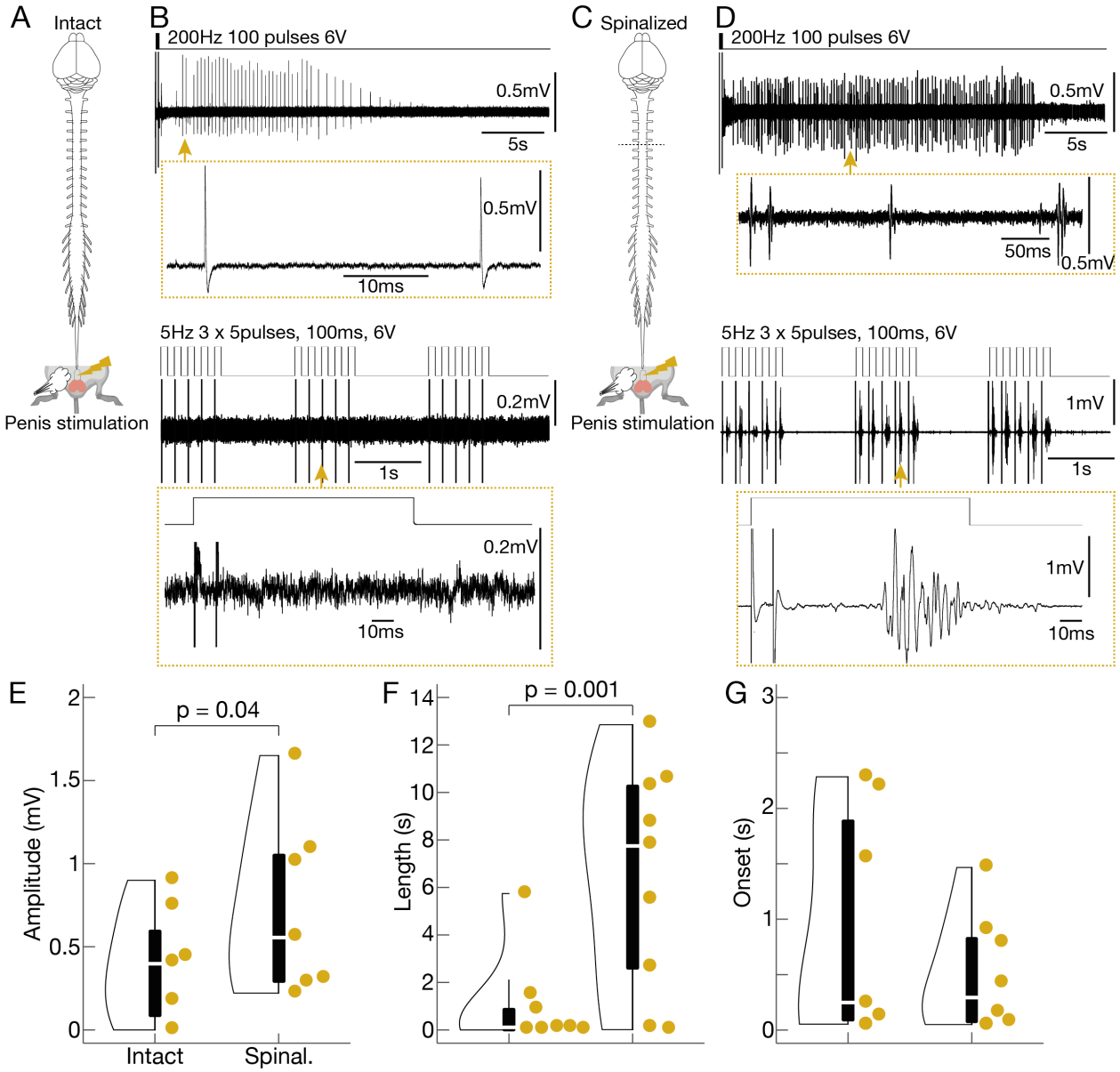

Supplemental Figure 7: Mechanical and electrical stimulation of the penis leads to more pronounced BSM EMG activity in a spinalized anesthetized *in vivo* preparation

(A) Experimental design: stimulation of the penis was achieved with either current application using a nerve cuff electrode or with an airpuff, pointed to the penis that was pulled out. The anesthetized preparation was intact, meaning that the connection with the brain was kept.

(B) Example EMG traces obtained in an animal in which the connection to the brain was kept intact and electrical stimulation was applied to the penis. Upper panel: train stimulation. Lower panel: 5Hz stimulation. Note that the train stimulation triggered modest BSM responses while the 5Hz stimulation did not trigger any activity in the BSM EMG.

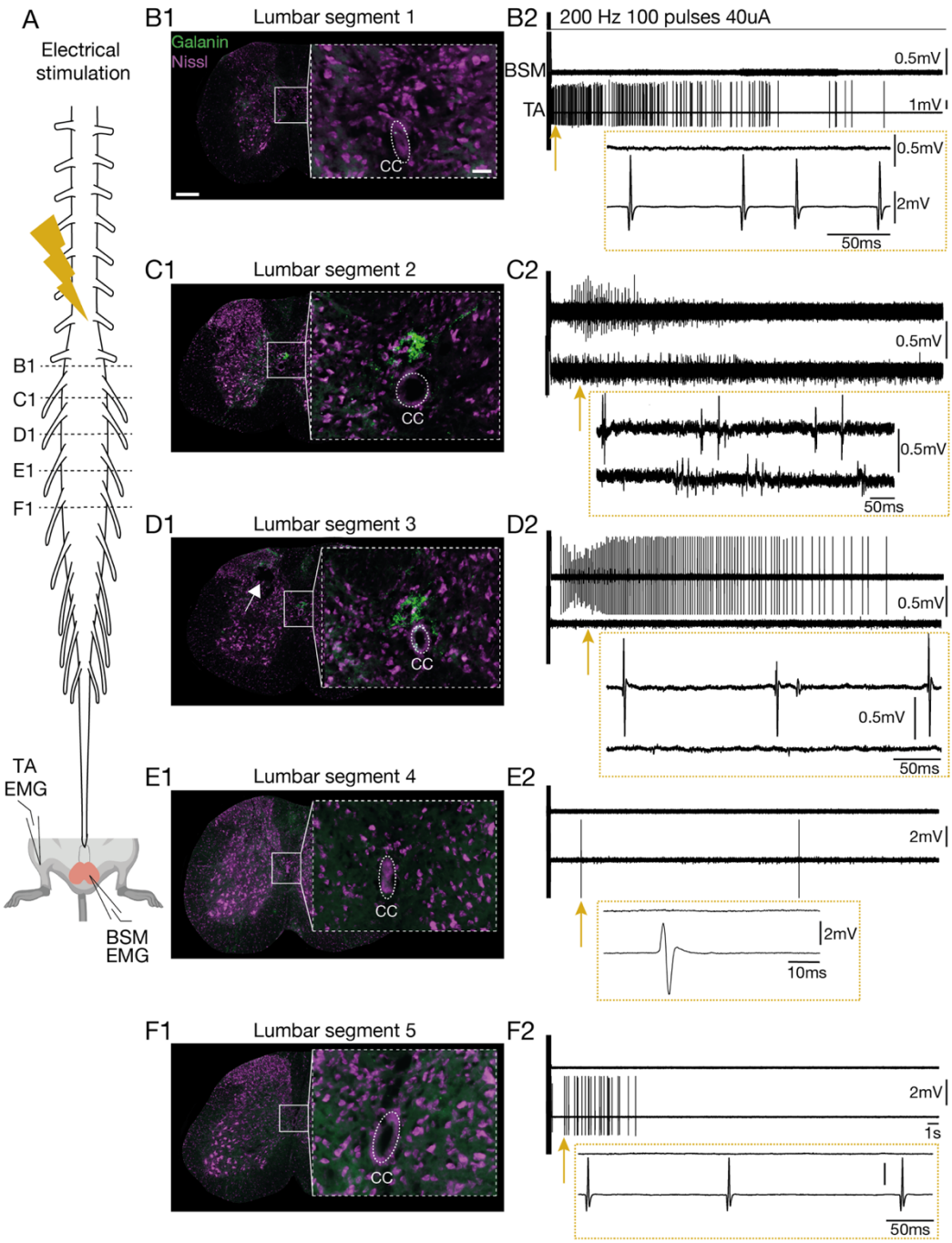

Supplemental Figure 8: Electrical stimulation along the rostrocaudal lumbar spinal cord in an anesthetized preparation.

(A) Experimental design: anesthetized animals were clamped into the spinal frame and the spine was opened. A tungsten electrode was inserted along the rostrocaudal axis at different depths and current was applied while BSM activity was monitored in parallel.

(B1 - F1) Representative post-hoc histological sections along the rostrocaudal axis of the spinal cord are shown. Note the electrolytic lesion at the L3 segment. Green: Galanin. Purple: Nissl.

(B2 - F2) Representative electrophysiological traces with BSM (lower trace) and leg (upper trace, TA, *tibialis anterior*) responses triggered at the stimulation site shown in B1 - F1. Note that BSM responses were most prominent at locations (C2, D2) where Galanin labeling was observed post hoc around the central canal (C1, D1) while TA responses randomly occurred along the rostrocaudal axis.

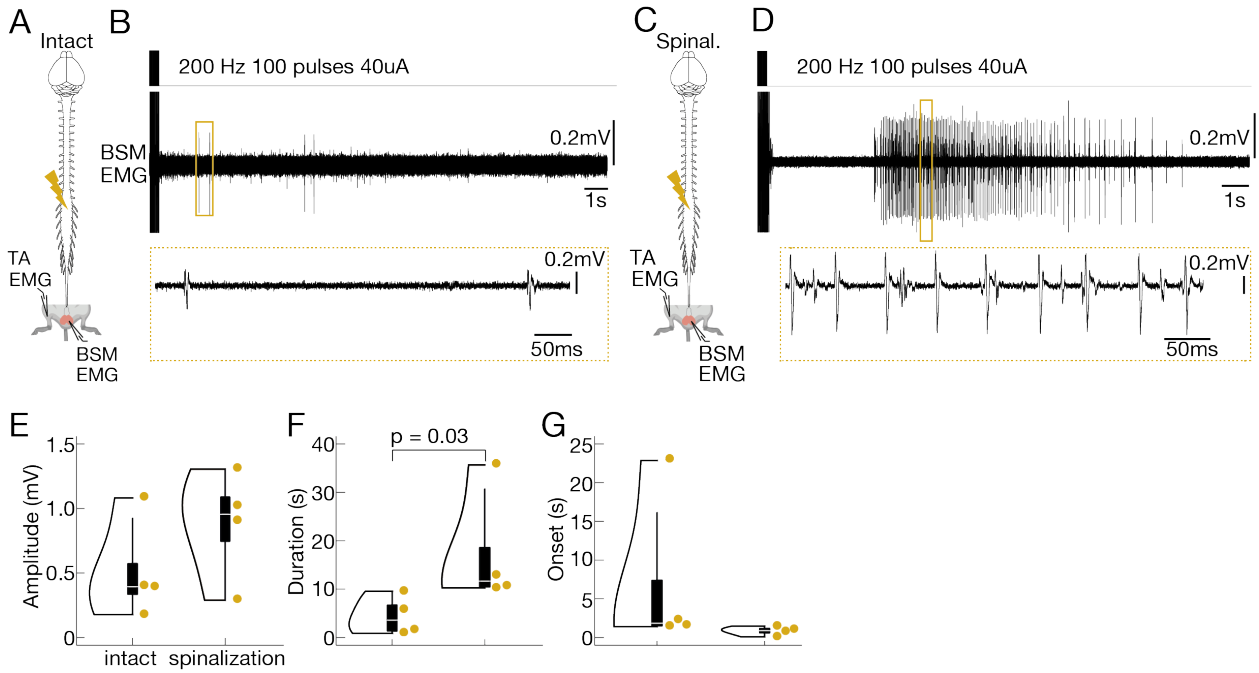

Supplemental Figure 9: Electrically triggered BSM responses in a spinalized vs non-spinalized preparation.

(A) Experimental design: electrical stimulations were conducted in an anesthetized mice in which the connection to the brain has been kept intact while in parallel monitoring BSM activity using EMG recordings.

(B) Example EMG trace obtained in an animal in which the connection to the brain was kept intact and electrical stimulation was applied with a tungsten electrode.

(C) Same as A, but a spinalization was performed between thoracic segments 5 and 6.

(D) Same as C, but EMG trace is recorded from an animal in which a spinalization was performed prior to stimulation. Note the difference in BSM activity.

(E) Violin plots showing the BSM EMG amplitude triggered with electrical stimulation in intact anesthetized mice (mean amplitude 0.51 ± 0.19 mv) compared to spinalized mice (0.87 ± 0.21 mV). P = 0.48 resulting from a Mann-Whitney U-Test.

(F) Same as E but the duration of the BSM EMG activity is plotted, which was markedly longer in the spinalized (mean duration 17.33 ± 0.21 s) vs. intact (mean duration 4.41 ± 2.02 s) anesthetized preparations. P = 0.03 resulting from a Mann-Whitney U-Test.

(G) Same as E but the onset of triggered BSM responses is depicted (mean onset for intact 7.0 ± 5.28 s; vs mean onset for spinalized 0.84 ± 0.28 mice). P = 0.05 resulting from a Mann-Whitney U-Test.

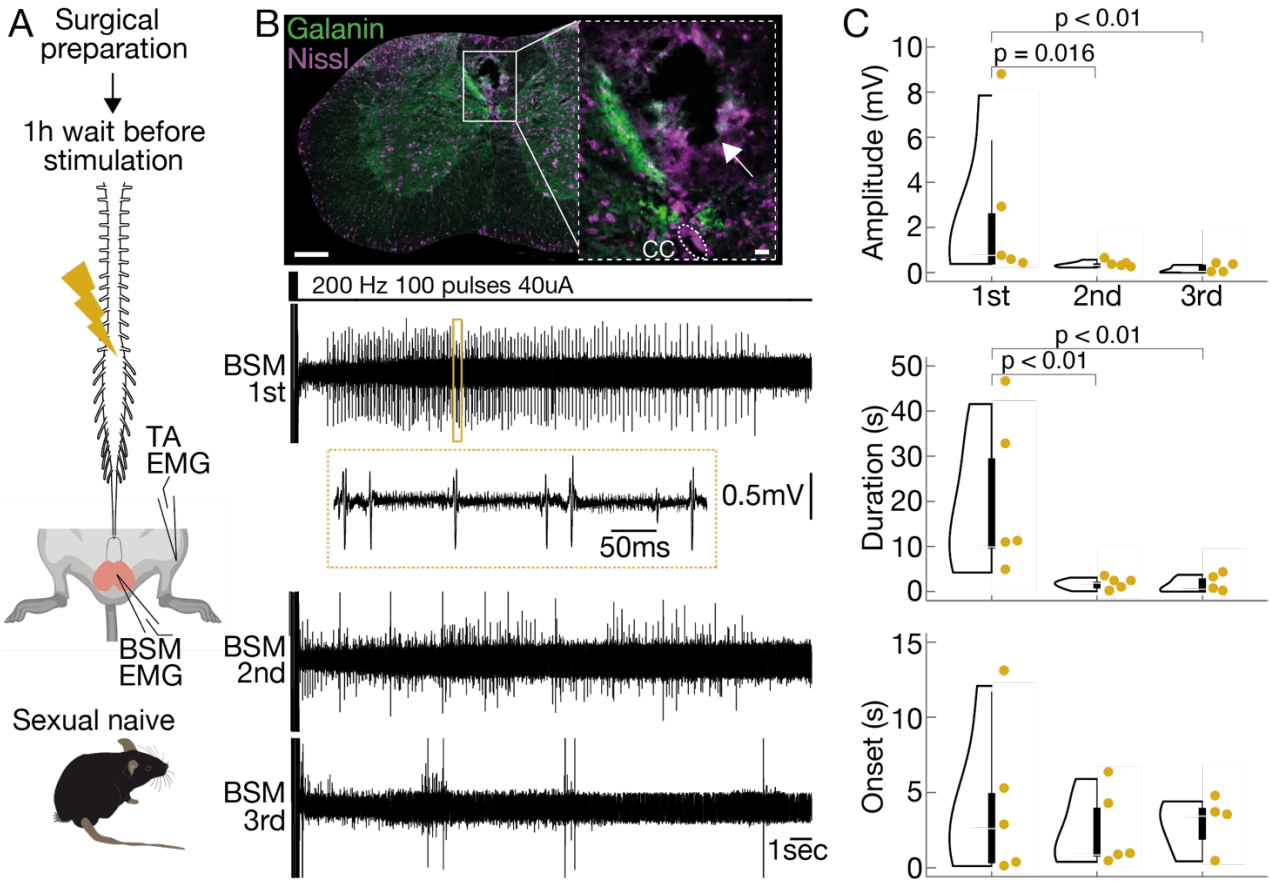

Supplemental Figure 10: Electrically triggered BSM activity does not depend on the duration of the spinal aperture.

(A) Experimental design: anesthetized animals were clamped into the spinal frame and the spine was exposed. Before starting with the electrical stimulation protocol, a waiting window of 1h was respected in order to reveal that the observed depression in the BSM activity with repeated trains of stimulation was not due to deterioration of the prep (due to the interval between opening the spinal cord and the application of the last stimulation protocol).

(B) Upper panel: Histological section showing the electrolytic lesion (white flash) that has been placed at the location on which electrical stimulation triggered the highest BSM activity. Green: Galanin. Purple: Nissl. Scale bar 200um. Scale bar inset: 50um. Lower panel: Electrical stimulation protocol (200Hz, 100 pulses, 40uA) led to pronounced BSM activity (BSM 1st) at the location of Galanin clusters. The same depression in BSM activity (as depicted in main Figure 5) was observed during the 2nd and 3rd rounds of stimulation.

(C) Quantitative analysis of BSM responses triggered after 1h of waiting time. Amplitude (upper panel; mean amplitudes: 1st 2.48 ± 1.39 mV; vs. 2nd 0.35 ± 0.06 mV; vs. 3rd 0.13 ± 0.08 mV; 1st vs. 2nd P = 0.016 and 1st vs. 3rd P = 0.0078 resulting from a Mann-Whitney U-Test) and duration (middle panel; mean durations: 1st 18.9 ± 7.08 s; vs. 2nd 1.61 ± 0.51; vs. 3rd 1.4 ± 0.76 s; 1st vs. 2nd P = 0.007 and 1st vs. 3rd P = 0.008 resulting from a Mann-Whitney U-Test) of BSM activity decreased upon 2nd and 3rd stimulation rounds while the onset with which BSM activity was elicited remained stable (lower panel; mean onsets: 1st 4.01 ± 2.2 s; vs. 2nd 2.38 ± 1.08 s; vs. 3rd 2.75 ± 0.9 s; P = 0.98 resulting from a Kruskal Wallis test).

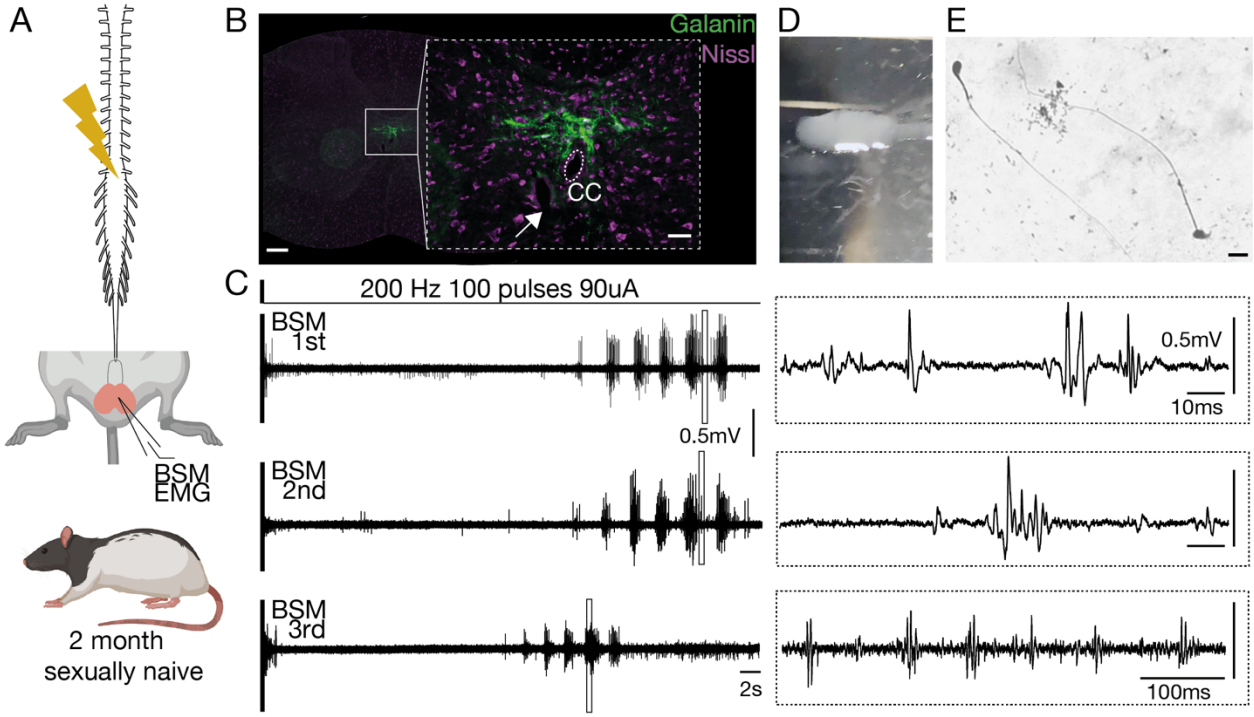

Supplemental Figure 11: Repeated electrical stimulation of the rat spinal cord at the location of the ejaculation generator leads to stable BSM activity and to the emission and expulsion of sperm.

(A) Similar to the mice experiment, the tungsten electrode was moved along the rostrocaudal axis of the spinal cord in an anesthetized rat (sexually naive, 2 months) while the BSM activity was monitored in parallel using an EMG.

(B) Histological section of the L3 spinal segment where BSM activity was elicited and ejaculation triggered by current application. Note a similar expression pattern of Galanin (green) around the central canal (CC) when compared to mice. An electrolytic lesion (white arrow) was placed at the shown location. Purple: Nissl stain. Scale bar 200um, inset 50um.

(C) Example BSM EMG trace for the first current application at the location shown in B, note the characteristic rhythmic pattern in the BSM with a long onset. The 2nd and 3rd current application (BSM 2nd, BSM 3rd) led to a very similar activity pattern in the BSM, contrary to mice.

(D) Current applications at the L3/4 spinal segments not only led to a characteristic activity pattern in the BSM, but also to the expulsion of sperm. Cloudy liquid (sperm) was collected on an objective slide which was diluted for post-hoc staining.

(E) Sperm was made visible by performing a Papnicolaou staining protocol. Scale bar 10um.

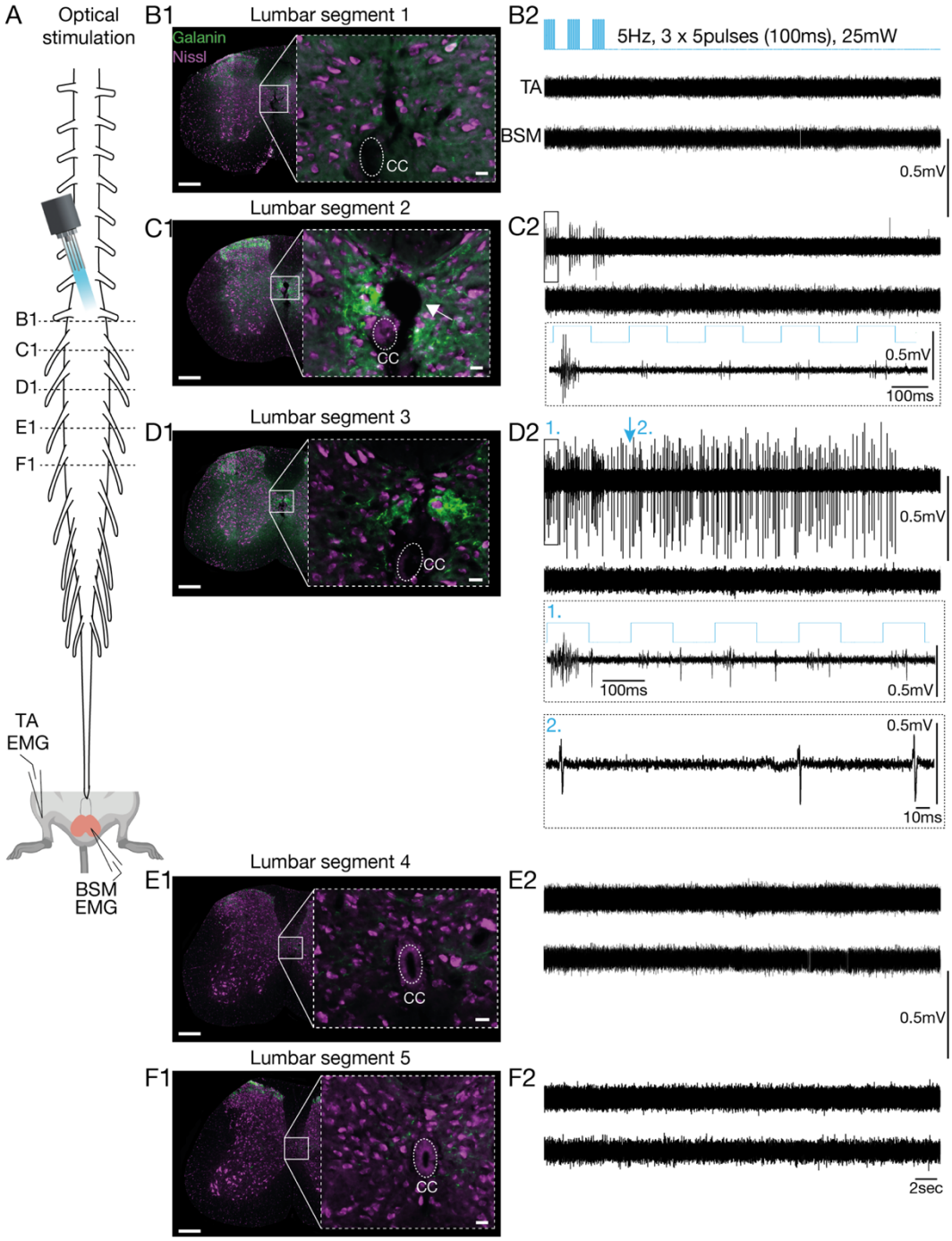

Supplemental Figure 12: Optogenetic stimulation of the Galanin expressing neurons in an anesthetized preparation.

(A) Experimental design: anesthetized Gal-ChR2 animals were clamped into the spinal frame and the spine was opened. An optical fiber was placed on top of the spinal cord and moved along the rostral caudal axis to deliver blue light while in parallel BSM activity was monitored.

(B1 - F1) Representative post-hoc histological sections along the rostral caudal axis of the spinal cord are shown. Note the electrolytic lesion at the lumbar segment 2 which corresponds to the location where the biggest and longest BSM responses were triggered. Green: Galanin ChR2. Purple: Nissl.

(B2 - F2) Representative electrophysiological traces with BSM and leg (TA, *Tibialis Anterior*) responses triggered at the optogenetic stimulation site shown in B1 -F1. Note that BSM responses were most prominent at locations (C2, D2) where Galanin ChR2 labeling was observed post hoc around the central canal (C1, D1) while TA responses were never observed.

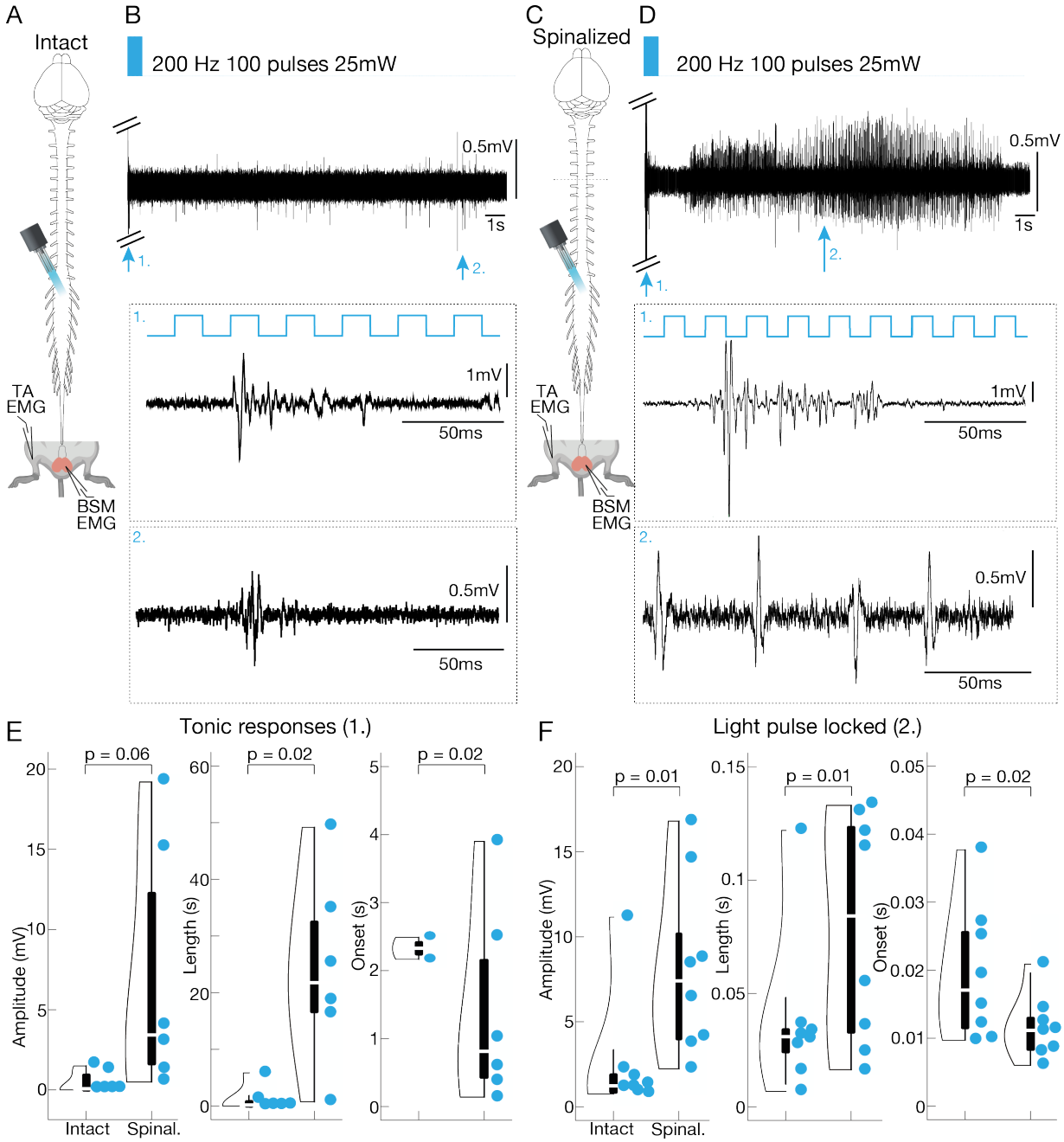

Supplemental Figure 13: Optogenetically triggered BSM responses in a spinalized vs non-spinalized preparation.

(A) Experimental design: optogenetic stimulations were conducted in an anesthetized mice in which the connection to the brain has been kept intact while in parallel monitoring BSM activity using EMG recordings.

(B) Example EMG trace obtained in an animal in which the connection to the brain was kept intact and optogenetic stimulation was applied with an optrode on the spinal cord surface (above the midline).

(C) Same as A but a spinalization was performed between thoracic segments 5 and 6.

(D) Same as B but EMG trace is recorded from an animal in which a spinalization was performed prior to stimulation. Note the difference in BSM activity.

(E) BSM EMG amplitude (left), length (middle) and onset (right) triggered with an optogenetic train stimulation in intact anesthetized mice compared to spinalized mice. Note that amplitudes (mean amplitude intact 0.45 ± 2.6 mV vs. mean amplitude spinalized 7.13 ± 2.6 mV; P = 0.06 resulting from a Student's t-test) and lengths (mean length intact 1.13 ± 6.7 s vs. mean length spinalized 24.1 ± 7.01 s; P = 0.007 resulting from a Student's t-test)

were markedly increased after spinalization while the onset with which BSM responses were triggered was shortened after spinalization (mean onset intact 2.32 ± 0.5 s vs. mean onset spinalized 1.42 ± 0.6 s; P = 0.02 resulting from a Student's t-test).

(F) Same as E but parameters are depicted for the 5Hz optogenetic stimulations (see Figure 5 and supplemental Figure 12). The same phenomena was observed. Light triggered BSM responses showed an increase in amplitude (left; mean amplitude intact 2.5 ± 1.24 mV vs. mean amplitude spinalized 8.11 ± 1.83 mV; P = 0.01 resulting from a Student's t-test) and length (middle; mean length intact 0.04 ± 0.01 s vs. mean length spinalized 0.08 ± 0.02 s; P = 0.05 resulting from a Student's t-test) and a decrease in onset (right; mean onset intact 0.02 ± 0.003 s vs. mean onset spinalized 0.01 ± 0.003 s; P = 0.02 resulting from a Student's t-test) after the connection to the brain was cut.

A

SHAM ANIMALS ✓ Sex ✗ No Sex

Animals	1st session	2nd session	3rd session
1	✓		
2	✓		
3	✗	✓	
4	✓		
5	✗	✓	
6	✗	✗	✓
7	✓		

DTR ANIMALS ✓ Sex ✗ No Sex

Animals	1st session	2nd session	3rd session
1	✓		
2	✓		
3	✓		
4	✓		
5	✓		
6	✗	✗	✓
7	✓		
8	✗	✓	
9	✗	✗	✓
10	✓		
11	✗	✓	
12	✓		

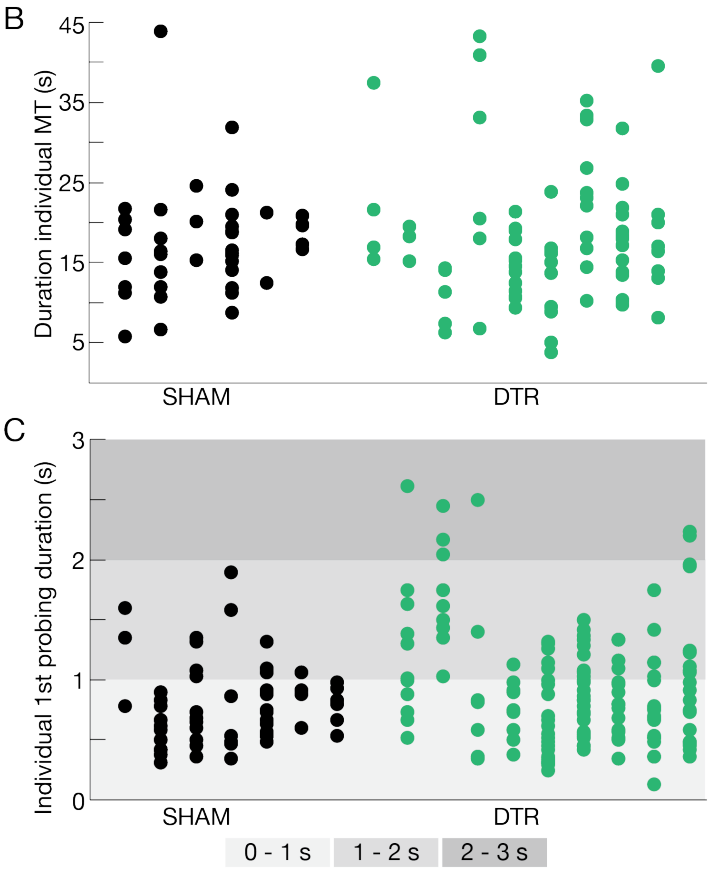

Supplemental Figure 14: SHAM and DTR animals have similar behavior patterns over several sessions.
(A) Animals were tested for 3 weeks in a row to assess their capability to perform sexual behavior after surgery. Both SHAM (left) and DTR (right) animals took different amounts of sessions to initiate the behavior, but eventually all showed sexual behaviours (mounts, probing, thrustings, and in most cases ejaculation) in the span of three weeks.
(B) Duration of individual mounts with thrusts (MT, in seconds) per animal. SHAM and DTR animals show identical values.
(C) Duration of the first probing event per mount (MP, in seconds) per animal. DTR animals show a higher amount of mounts with longer probing durations (namely with more than 2 seconds duration).

Methods

Lead contact

Further information and requests for resources and reagents should be directed to and will be fulfilled by the lead contact, Susana Q. Lima (susana.lima@neuro.fchampalimaud.org)

Materials availability

This study did not generate new unique reagents.

Experimental model and subject details

All experimental procedures were carried out in strict accordance with the guidelines of the European Committee Council Directive and were approved by the Animal Care and Users Committee of the Champalimaud Neuroscience Program, the Portuguese National Authority for Animal Health (Direcção Geral de Veterinária; approval number 0421/000/000/2022) and by the local ethic committee of the University of Bordeaux and the French Agriculture and Forestry Ministry for handling animals (approval number 2016012716035720). For tracing from the BSM (FG and PRV) and electrical stimulation experiments, BL6 (Mus musculus domesticus, C57BL/6J) male mice aged 3-6 months were used. For tracing from the spinal cord, the cFos experiment and the DTR ablation, Gal-cre x TdTomato (Mus musculus domesticus, B6;129S6-Gt(ROSA)26Sortm9(CAG-tdTomato)Hze/J) male mice aged 3-6 months old were obtained from Jackson Laboratories. For the spinal cord optogenetic stimulation and airpuff/electrical sensory stimulation of the penis, Gal-ChR2 (Mus musculus domesticus, B6;129S-Gt(ROSA)26Sortm32(CAG-COP4*H134R/EYFP)Hze/J) male mice aged 3-6 months old were obtained from Jackson Laboratories. For electric stimulation of the spinal cord, Long Evans (Crl:LE Long-Evans) male rats were ordered from Charles Rivers. For the pup muscle injections, BL6 male mice pups aged P3-P6 were used. For the pup optogenetic and electrophysiology experiment, Gal-ChR2 male mice pups aged P2-P6 were used. Finally, as a sexual stimuli, after ovariectomy and hormonal priming, BL6 female mice aged 3-6 months were used. All the animals were bred and maintained in our animal facility. Except for the optogenetic experiment in pups, all animals were weaned at 21 days and housed in same-sex groups in stand-alone cages (1284L, Techniplast, 365 × 207 × 140 mm) with access to food and water ad libitum. Mice were maintained on an inverse 12:12 light/dark cycle and experiments were performed during the dark phase of the cycle, phase of higher animal activity. After initiation of sexual behaviour training or immediatly after surgery, male mice were kept single-housed until the experiment was over.

Bulbospongiosus muscle (BSM) injections

Mice were anesthetized with 3% isoflurane in oxygen and put into the mouthpiece of a stereotaxic device (Kopf, Tujunga, CA, USA). After that, mice were turned into a supine position to facilitate access to the BSM. After shaving the anogenital area and cleaning with Betadine (MEDAPharma) and 70% ethanol, a small incision in the scrotum area was made. At this point, an analgesic (buprenorphine, 0.05-0.1mg/kg, intraperitoneal injection) was administered. The BSM was exposed after removing fat and conjunctive tissue. Pulled capillaries (length 3 1/2 inches [9 cm]; inner diameter 0.53, outer diameter 1.14 mm; tip

diameter 40 µm; DrummondScientific, Broomall, PA, USA) were used to inject 1,5 ul of 2% Fluorogold (FG) at a rate of 13.8 nL per pulse, and a frequency of 0.2 Hz . In total, 5 BSM sites were injected with FG (three in the dorsal and two in the ventral portion of the BSM). A waiting time of 5 min prior to and 10 min after injection was kept. The glass pipette was pulled out slowly and the skin sutured. All mice were single housed post-surgery until perfusion. A total of 12 male mice was used for anatomical investigation of BSM motor neurons using FG.
Another 6 male mice were injected with PRV-Ka-gEI-mCherry (PRV; Boldogkoi *et al.*, 2009) in the BSM. The male was similarly anesthetized with 3% isoflurane in oxygen and put into the mouthpiece of a stereotaxic device. After that, mice were turned into a supine position to access the BSM, and after disinfecting, a small incision was made to expose the muscle. Using a glass pipette as described above, 1 ul of PRV was injected once into the BSM at a rate of 13.8 nL per pulse, and a frequency of 0.2 Hz. A waiting time of 5 min prior to and 10 min after injection was kept, after which the pipette was pulled and the incision sutured. All mice were single housed post-surgery until perfusion.

Spinal cord stereotaxic virus injections and histology

Mice were anesthetized with 3% isoflurane in oxygen and spinally fixed into a stereotaxic frame using adapted vertebrae clamps (Kopf, Tujunga, CA, USA). During surgery, anesthesia was maintained using 1.5% isoflurane. Injection sites (lumbar segments 2/3) were targeted by using vertebral landmarks as described in (Harrison *et al.*, 2013). Muscle and fat tissue were gently removed in order to get a better sight onto the spinal cord. The injection pipette was inserted in between the thoracic vertebrae T11 and T12 before having made a small puncture into the dura mater that allowed for better insertion of the injection pipette. Pulled capillaries (length 31/2 inches [9 cm]; inner diameter 0.53, outer diameter 1.14 mm; tip diameter 40 µm; DrummondScientific, Broomall, PA, USA) were used to inject the AAVs at 100 µm medial from the midline, at a depth of 750-850 µm from the spinal cord surface at a rate of 0.1 Hz with 2.3-4.6nL per pulse. For the AAV1-CAG-floxed-SynGFPrev-WPRE (N=7), 30nL were injected, whereas for the pAAV8-FLEX-DTR-GFP (N=12), 150-300 nL were injected either in one or two locations of the spinal cord. Before and after the pressure injection a waiting time of 10 min was kept. Afterwards, the pipette was retracted, eventual bleeding stopped and the skin sutured. Furthermore, as a control for the DTR experiment, sham injections were performed (N=7). Using the same method described above, the animals were anesthetized and spinal clamped to a stereotaxic frame. After fat and tissue removal to expose the vertebrae, a glass pipette without virus was lowered to the spinal cord at the Gal+ cells location. The pipette was kept inside the spinal cord for a total of 25 min, after which it was carefully removed and the animal was sutured. Analgesic (burprenorphine 0.1 mg/kg) was administered post surgery at all times. After sufficient time for viral expression (2 weeks for the pAAV8-FLEX-DTR-GFP and 3 weeks for the AAV1-CAG-floxed-SynGFPrev-WPRE) and eventual behavioral experiments (DTR experiment), animals were deeply anesthetized and perfused transcardially with saline, followed by a cold 4% paraformaldehyde solution (PFA) in 0.01mol/L PBS. Spinal cords were removed from the spine and kept for 1h in 4% PFA before transferring them for another hour into 0.01M PBS. Subsequently spinal cords were stored overnight in 30% sucrose, 0.1% azide in order to cryo-protect the tissue. Spinal cords were embedded in frozen section medium and frozen for half an hour at -80°C in 2-methylbutane solution before mounting them

in the cryostat. Spinal cord sections which did not undergo subsequent immunohistochemical staining were cut and mounted on a poly-lysine-coated glass slide at 50 µm, sections with post-hoc immunohistochemical staining were cut and mounted at 30 µm.

Nissl stain

The slides were washed 2 times in 0.01M PBS to remove the excess of frozen section medium. After that the sections were rehydrated for 40 min in PBS 0.1M, pH 7.2 (PBS 10x) and permeabilized for 10min with 0.1% Triton-X (T9284-100ML, SigmaAldrich) in PBS 10x. The tissue was washed 2 times 5 min with PBS 10x before incubating them for 20 min with a 1:100 Neurotrace staining solution (in PBS 10x; (NeuroTrace™ 500/525 Green Fluorescent Nissl Stain, N21480, ThermoFisher Scientific; or NeuroTrace™ 530/615 Red Fluorescent Nissl Stain, N21482, ThermoFisher Scientific; or NeuroTrace™ 640/660 Deep-Red Fluorescent Nissl Stain, ThermoFisher Scientific). Subsequently the tissue was washed with 0.1% Triton-X in PBS 10x for 10 min. After washing 2 times 5 min with PBS 10x, the slides were rinsed with distilled water, dried and coverslipped with Mowiol.

Immunohistochemistry

Immunohistochemical labeling was performed using standard procedures. Briefly, spinal cord sections, which were labeled either for Gastrin releasing peptide (Gastrin Releasing Peptide (GRP) (Porcine) - Antibody, Phoenix Pharmaceuticals, H-027-13), Substance P (Anti-Substance P Receptor Antibody, Sigma-Aldrich, AB15810), Enkephalin (Anti-Enkephalin/ENK antibody, Abcam, ab85798), CCK (Polyclonal Rabbit anti-Human CCK / Cholecystokinin Antibody, LSBio, LS-C190673), Osteopontin (Mouse Osteopontin/OPN Antibody, R&D Systems, AF808), VGLUT1 (VGLUT 1 antibody, Synaptic Systems, 135 304) or Galanin (Anti-Galanin Antibody, Milipore, AB2233), were firstly washed 2 times 5 min with PBS 0.01M to remove the excess OCT. Afterwards, they were washed 2 times 10 min with PBS 10x and preincubated for 1.5 hours at room temperature in a blocking solution (PBS 10x, 1% bovine serum albumin, and 0.3% Triton X-100). Afterwards, primary antibodies were diluted in the same blocking solution at a proportion of 1:100. The primary antibody was incubated on the glass slides overnight at room temperature. Incubation with the primary antibody was followed by 5 times 10 min washing with PBS 10x. Subsequently, we proceeded to detect the primary antibody with a secondary antibody coupled to different fluorophores (Alexa Fluor 488, 594 or 647, Abcam/Thermo Fisher Scientific). The secondary antibody was diluted (1:500) in blocking solution and the reaction was allowed to proceed for 2 hours in the dark at room temperature. In some cases, a Nissl stain was performed as described above. After the staining procedure, sections were washed 5 times 10 min with PBS 10x, rinsed with distilled water, dried and coverslipped with Mowiol mounting medium. Immunohistochemical staining for the immediate early gene cFos deferred slightly from the above described procedure. Namely, after washing with PBS 0,01M and PBS 10x, the sections were incubated in a different blocking solution (PBS 10x, 0.3% Triton X-100, 4% normal donkey serum, 1% bovine serum albumin) for 1h at room temperature. The primary antibody (rabbit anti-cFos, Synaptic Systems, 226 003), diluted 1:500 in blocking solution was added for 2 overnights at 4ºC. Afterwards, the sections were washed 3 times 5 min in PBS 10x, 0.3% Triton X-100, and the secondary antibody (Alexa Fluor 488 or 647, ThermoFisher Scientific) was added in blocking

solution for 2h at room temperature. Finally, the sections were washed 3 times 5 min in PBS 10x, 0.3% Triton X-100, rinsed with distilled water, dried and coverslipped with Mowiol mounting medium. As described before, some slides were also counterstained with Nissl.

Electrophysiology

In vivo electrical stimulations and optogenetic stimulations

For acute electrophysiological experiments, mice (N = 8) and rats (N = 4) were anesthetized by injection of an initial dose of 100 mg/kg ketamine and 7.5 mg/kg xylazine. Respiration, blink and pinch reflex were observed throughout the experiment and, if needed, animals were injected with an extra shot (25%) of ketamine/xylazine mixture or a 25% dose of ketamine alone. The animal's back, scrotum and right leg were shaved and cleaned with ethanol. Electromyogram electrodes were inserted into the BSM or tibialis anterior (TA) muscles and glued using Vetbond. The back skin was cut along the rostral caudal axis and the spine was fixed into stereotaxic spinal clamps (Kopf). Muscle and conjunctive tissue was removed before performing a laminectomy along the rostral caudal axis. Spinalization was performed in between the thoracic segments 5 and 6. For electrical stimulations, a 1MΩ tungsten electrode (World Precision Instruments) was lowered at each microstimulation site (ranging from ~550 µm to ~950 µm of depth in the dorsal ventral axis, in each spinal cord segment), and currents ranging from 50 µA to 140 µA were injected using a stimulus isolator (Model no. A365RC, World Precision Instruments) while possible movements were documented. Various stimulation protocols were tested (single, 5Hz, 50Hz). Eventual activity in the BSM and TA was monitored via EMG recordings using a custom-made amplifier (x 1000) and filtered at 2 kHz. Data acquisition and analysis were performed using spike2 software (CED Cambridge). Tungsten electrodes were moved along the rostral caudal axis of the spinal cord and electrolytic lesions were placed at the location where the biggest EMG responses were encountered.

In a subset of animals undergoing electrical stimulations (N = 15), sexual behavior (see below) was performed prior to the acute recordings. Animals either ejaculated (N = 8) or performed 5 mounts with intromission (N = 7), before they were anesthetized.

During control experiments, the animals were prepared as above but a waiting time of 1h was kept before the first stimulation in order to control that the observed effects are not due to a rundown of the preparation.

For optogenetic stimulations of the Gal+ cells (N = 13 of Gal-ChR2 male mice) and BSM-MNs (N = 10 of BL6 mice infected with an AAV expressing ChR2 on the BSM) the experimental procedure was similar except the fact that an optrode was moved on top of the spinal cord, in the rostral caudal axis, while monitoring EMG recordings and documenting movements. Likewise, an electrolytic lesion was placed at the position where the light pulses led to the most prominent BSM EMG responses. We tested a variety of stimulation protocols (single, 5Hz, 10Hz, 20Hz, 50Hz, 100Hz) and laser powers (5mW - 40mW).

In vivo juxtacellular recordings of photoidenfied cells

Single in vivo juxtacellular recordings were performed as described in (Lima *et al.*, 2009). Briefly, a glass electrode (resistance ranging from 4 to 6 MΩ) made of borosilicate glass tubes (Hilgenberg) was first lowered at the position where optogenetic stimulations led to the highest activity in the BSM. Pipettes were filled with a ringer solution. Extracellular local field

potential recordings were captured while shining the light. Subsequently, cells were searched for by applying a negative current pulse and using an audio monitor (Grass Technologies, AM10) while steps were made in 1.5 µm increments with a micromanipulator (Luigs & Neumann SM-5, Germany) and potential increases in resistance were carefully observed. When spiking activity was detected, electrophysiological recordings were performed in line with optogenetic stimulation protocols (single, 5Hz, 10Hz, 20Hz, 50Hz) and EMG monitoring. Recordings were amplified (Dagan BVC-700A, Dagan, Minneapolis, MN), low-pass filtered at 10 kHz and sampled at 50 kHz by a data-acquisition interface (Power 1401, CED, Cambridge, England) and controlled and analyzed by the spike2 software (CED, Cambridge, England).

In vitro patching of identified BSM MNs in new born male Gal-ChR2 animals

New-born male Gal-ChR2 mice aged postnatal day (P2) to P6 were used in accordance with the guidelines of the French Agriculture and Forestry Ministry for handling animals. The protocol was approved by the local ethics committee of the University of Bordeaux (approval number 2016012716035720). To record specifically from identified MNs innervating the BSM, a crystal of cholera toxin β-subunit conjugated to AlexaFluor 594 (Thermo Fisher Scientific, C34777) was inserted into the BSM with an insect pin 20–24 h before slice preparation procedure in cryo-anesthetized mouse pups. Following the labeling process, spinal cord slices were prepared using the following procedure: mice were anesthetized using isoflurane until all reflexes were gone. After decapitation, the spinal cord was dissected out in an ice-cold sucrose-based saline solution containing the following: 2 mM KCl, 0.5 mM CaCl2, 7 mM MgCl2, 1.15 mM NaH2PO4, 26 mM NaHCO3, 11 mM glucose and 205 mM sucrose. The saline was bubbled with 95% O2, 5% CO2. Transverse slices (350 µm) of the lower lumbar enlargement and first sacral segments were cut with a vibratome and then transferred to a holding chamber. Slices were allowed to recover in oxygenated aCSF (130 mM NaCl, 3 mM KCl, 2.5 mM CaCl2, 1.3 mM MgSO4, 0.58 mM NaH2PO4, 25 mM NaHCO3, 10 mM glucose) for at least 1 hour at 30 °C. Whole-cell current-clamp recordings from BSM-MNs, identified by their 594 fluorescence, were made under visual control with a Multiclamp 700B amplifier. Recording glass microelectrodes (4–7 MΩ) were filled with the following: 120 mM K-gluconate, 20 mM KCl, 0.1 mM MgCl2, 1 mM EGTA, 10 mM HEPES, 0.1 mM CaCl2, 0.1 mM GTP, 0.2 mM cAMP, 0.1 mM leupeptin, 77 mM d-mannitol and 3 mM Na2-ATP, with a pH of 7.3. All of the experiments were performed at room temperature (~23 °C). Data acquisition and analysis were performed using the Axograph software. Experiments were discarded if series resistance increased more than 20% during a given recording period. Polysynaptic transmission was decreased using a high cation solution containing 7.5 mM CaCl2 and 8 mM MgSO4 (Liao and Walters, 2002). Throughout recording episodes, GABAergic and glycinergic inputs were blocked with gabazine and strychnine (1 µM each), respectively (Clarac *et al.*, 2004; Taccola, Marchetti and Nistri, 2004). A stimulating optrode connected to an optogenetic laser box (Prizmatrix) was placed above the central canal at the dorsal gray commissure and light pulses were applied at different lengths. Excitatory postsynaptic currents (EPSCs) were recorded from MNs held at −60 mV in current clamp mode. The input resistance of MNs (Rin) was determined from the slope of the voltage-current curve within the linear portion of current traces. AHP parameters were measured after single

action potential evoked by short depolarizing current steps (7 ms, 0.25 nA) in current clamp conditions in MNs held at −60 mV by injection of bias current.

Pup viral injections

In order to infect the BSM-MNs with the light activated channel, channelrhodopsin (ChR2), young animals needed to be used as it has been shown that viral tracers are not able to infect the motor end plate beyond a certain age (Stepien, Tripodi and Arber, 2010). Pups (P3-P6) were briefly separated from their litter and mother, and placed in a freezer. After all reflexes were gone, pups were placed on ice and a small incision below the penis was made in order to access the BSM. Pulled capillaries (length 3 1/2 inches [9 cm]; inner diameter 0.53, outer diameter 1.14 mm; tip diameter 15-20 µm; DrummondScientific, Broomall, PA, USA) were used to inject 1µl of retroAAV-CAG-hChR2-H134R-tdTomato (28017-AAVrg, Addgene) into the BSM at a rate of 18.4 nl/pulse per second.

After injection, the incision was glued and the pups placed onto a heating pad. Once all reflexes were recovered, the pups were put back to their litter and mother. Injected pups were raised until 2-3 months of age before performing the acute optogenetic experiments as described above.

Sensory stimulation of the penis and local field potential recordings of photo-identified cells

For sensory stimulation of the penis in parallel with BSM activity monitoring by EMG, the surgical procedure was performed as described above (*In vivo electrical stimulations and optogenetic stimulations*). In order to stimulate the penis electrically (by wrapping a nerve cuff electrode around the penis) or mechanically (by locally applying an airpuff) the penis was gently pulled out. Electrical (6V) and mechanical (0.5 - 1 mbar) stimulations of the penis were done at either 200 Hz (100 pulses) or 5 Hz (3 x 5 pulses, 100ms). Stimulation protocols were first run in an anesthetized male mouse with an intact brain spinal connection before disrupting the latter by performing a spinalization between the thoracic segments 9 and 10. Electrical and/or mechanical stimulation protocols were then repeated in the anesthetized preparation (N = 7).

For local field potential (LFP) recordings of optogenetically tagged Gal+ or BSM MNs, a glass electrode (resistance ranging from 4 to 6 MΩ) made of borosilicate glass tubes (Hilgenberg) was lowered at the position of the Gal+ cells or the BSM-MNs and optogenetic stimulations were performed until encountering the maximal light triggered LFP response. Subsequently the glass pipette was left in the place at which the highest light triggered LFP response of BSM-MNs or Gal+ cells was encountered. Finally the penis and leg were mechanically stimulated with a locally applied airpuff (5Hz; 5 pulses, 100ms) while monitoring LFP responses and EMG responses in BSM and TA muscles. Analysis was performed in spike2 and data plotted in Excel and Matlab.

Behavior

Sexual priming prior electrical stimulations

Male mice were single-housed and trained in sexual behaviour, with a primed ovariectomised female, until ejaculation was reached in 3 sessions. Afterwards, the animals were divided into

two groups: one group was allowed to perform 5 mounts with intromissions (N = 7) and the second group was allowed to perform the whole repertoire of sexual behavior until reaching ejaculation (N = 8). Immediately after the behavior, the animals were anesthetized and used for *in vivo* electrical stimulations as described above.

cFos experiments

Male Gal-cre x TdTomato mice were single-housed and trained in sexual behaviour, with a primed ovariectomised female, until ejaculation was reached in 3 sessions. After one week, the animals underwent a behavioral paradigm and divided into three different groups: in the first group, animals were allowed to socially interact with a female for 10 min (Aroused, N=7), without performing mounts or intromissions; the second group of male mice performed five mounts with intromissions (5 Mounts, N=5), after which the female was removed; in the third group, the animals were allowed to reach ejaculation (Ejaculation, N=6). In another group of animals (Cage control) male mice were either alone in their home cages, without sexual encounters (N=3), or had the same sexual training but were then alone in the behaving box for 10min (N=3), in order to assess the baseline neuronal activity in the spinal cord (no differences in the cFos count was observed in these two control conditions). After the behavior session, male mice were placed back in their home cages for 90 minutes to allow for sufficient cFos expression. Finally, the animals were deeply anesthetized and perfused transcardially with saline, followed by a cold 4% PFA in 0.01mol/L PBS. Spinal cords were removed from the spine and kept for 1h in 4% PFA before transferring them for another hour into 0.01M PBS. Subsequently spinal cords were stored overnight in 30% sucrose, 0.1% azide in order to cryo-protect the tissue. Spinal cords were embedded in frozen section medium for half an hour at -80°C in 2-methylbutane solution before mounting them in the cryostat. The spinal cords were sectioned at 30µm for post-hoc immunohistochemical staining as described above.

DTR experiments

Male Gal-cre x TdTomato animals (2-3 months old) were single-housed and trained for sexual behaviour until ejaculation was reached once. After that, the animals were spinally injected with an AA8V-FLEX-DTR-GFP (N = 12) at the location of the SEG cells (allowing for the specific expression of the Diphtheria Toxin Receptor), or had a sham surgery (N = 7), as described above, and allowed to recover for 2 weeks. Afterwards, the animals underwent another round of sexual behaviour training to confirm that they were still reliably ejaculating. After this, the animals received an intraperitoneal injection of 50 ng/g (0.1 mL/10 g) of Diphtheria Toxin (DT, Sigma, D0564-1MG). One week after, the animals were transferred to an experimental box, where they had a 10 min habituation, after which a primed ovariectomised female was introduced. The animals were allowed to perform the full repertoire of sexual behaviour and after ejaculation was reached, or 90min after female introduction passed when sexual behaviours were observed, the animals were returned to their homecage. If the animals did not initiate behaviour, the experiment was stop after 30min and they underwent the sexual experimental paradigm for two more weeks. In the final session, or after ejaculation, the animals were returned to their homecage and a 90 min interval was kept before perfusion, for cFos expression to occur. Finally, the animals were deeply anesthetized, transcardially perfused

and the spinal cords collected for histological processing as described above (*cFos experiments*).

Ovariectomy and hormonal priming

All female mice (N=20) used as sexual stimuli were ovariectomised. Briefly, female mice were anesthetized using 3% isoflurane in oxygen and placed into a mouth piece allowing for continuous isoflurane anesthesia. After all reflexes were gone, an incision was made at the center of the lower back. The skin was separated from the muscle towards both sides of the back. After that, on one side, leveled with the hindlimb, the ovary fat pad was located and a small incision was made in the muscle above this area. The ovary was gently pulled and the connection between the ovary and the uterus was cut using a cauterizer. The same procedure was repeated for the second ovary. Finally, the incision in the back was sutured and the animal was allowed to fully recover on a heating pad. After two weeks of recovery, the animals underwent hormonal priming during which they received an estrogen (1 mg/ml, Sigma E815 in sesame oil) injection 2 days prior to the sexual behavior experiment and a progesterone (5 mg/ml, Sigma P0130 in sesame oil) injection 4h before the experiment was scheduled. Hormonal priming with estrogen and progesterone was conducted before each experiment.

Quantification and Statistical Analysis

Histological analysis

After immunohistochemical labeling of cFos (as described above), the spinal cord sections were imaged using a Slide Scanner (Zeiss AxioScan.Z1, Zeiss Microscopy). The obtained images were processed using the Zen Software (Zen 2.6, Zeiss Microscopy), and tiff images of each channel (488 for the cFos, cy3 for the Gal-cre TdTomato cells and cy5 for the Nissl staining) were exported. These tiff files were, together with the corresponding image of the spinal segment from the mouse spinal cord atlas (Watson *et al.*, 2009), opened in Photoshop (Adobe Photoshop, Adobe). Once the overlap between the spinal atlas outlines and the immunohistochemical tiff image was adjusted, the cells present in laminae X (around the central canal and the location of the Gal+ cells) of the spinal cord were manually counted by placing dots on each cell. The manual counting procedure was done for both channels, the cFos in green and tdtomato in red. Custom written Matlab code was finally used to count the dots and identify overlaps between the two channels. Counting of cFos and Gal-cre x TdTomato positive cells was done blindly.

Behavioral Analysis

The DTR behavioral experiments were carefully recorded using two point gray cameras (Teledyne FLIR), at 60 frames per second. The cameras acquired a top and front video of the cage and were controlled using a bonsai script (Bonsai Visual Reactive Programming). Afterwards, the videos were analyzed using Python Video Annotator (developed at the Champalimaud Foundation). A wide range of behaviors was annotated, namely: sniffing of the anogenital area of the female; mount attempts (when the male was not able to perform intromissions) mounts with probing (shallow pelvic movements when the male is trying to intromit but still has not inserted the penis); mounts with intra-vaginal thrustings; intra-vaginal thurstings (when the male successful inserted the penis in the female's vagina); and finally

ejaculation (time between the beginning of shivering and the moment the male dismounted the female). The duration, in frames, for each behavior was then aligned to the camera timestamps, acquired during video recording. Analysis of behavioral timestamp data was performed using a python script in Spyder 3.3.6 (Python).

Statistical Analysis

Statistical analysis was performed with homemade code in Matlab and Python (scipy and statsmodels). All error ranges represent standard error of the mean. For two-sample comparisons of a single variable, Student's t test was used, unless in cases when the underlying distributions were non-Gaussian (Shapiro-Wilk test, $p<0.05$), where a two-tailed Mann-Whitney-U Test was performed. When multiple variables were compared, a Kruskal Wallis test or a Wilcoxon-Signed-Rank test were used since the data did not follow a Gaussian distribution. Probabilities of the null hypothesis $p<0.05$ were judged to be statistically significant. Elements of violin plots: center line, median; box limits, upper (75) and lower (25) quartiles; and whiskers, 1.5x interquartile range.

To estimate the inter-thrust interval (ITI) versus mount progression (Figure 7T), the thrust number was divided by the total number of thrusts in the mount, what we call mount progression. Then data from all the mounts and all the sessions from the different groups was pulled together and a non-parametric kernel regression was performed. The shadow region corresponds to the standard deviation.

Data and code availability

• All data reported in this paper will be shared by the lead contact (S.Q.L.) upon request.
• This paper does not report original code.
• Any additional information required to reanalyze the data reported in this paper is available from the lead contact (S.Q.L.) upon request.

References

Allard, J. et al. (2005) 'Spinal cord control of ejaculation', World Journal of Urology, 23(2), pp. 119–126. doi: 10.1007/s00345-004-0494-9.

Argiolas, A. and Melis, M. R. (2004) 'The role of oxytocin and the paraventricular nucleus in the sexual behaviour of male mammals', Physiology and Behavior, 83(2), pp. 309–317. doi: 10.1016/j.physbeh.2004.08.019.

Argiolas, A. and Melis, M. R. (2005) 'Central control of penile erection: Role of the paraventricular nucleus of the hypothalamus', Progress in Neurobiology, 76(1), pp. 1–21. doi: 10.1016/j.pneurobio.2005.06.002.

Azim, E. et al. (2014) 'Skilled reaching relies on a V2a propriospinal internal copy circuit', Nature. Nature Publishing Group, 508, pp. 357–363. doi: 10.1038/nature13021.

Balcombe, J. (2009) 'Animal pleasure and its moral significance', Applied Animal Behaviour Science, 118(3–4), pp. 208–216. doi: 10.1016/j.applanim.2009.02.012.

Baron, R. and Jänig, W. (1991) 'Afferent and sympathetic neurons projecting into lumbar visceral nerves of the male rat', Journal of Comparative Neurology, 314(3), pp. 429–436. doi: 10.1002/cne.903140302.

Boldogkoi, Z. et al. (2009) 'Genetically timed, activity-sensor and rainbow transsynaptic viral tools', Nature Methods, 6(2), pp. 127–130. doi: 10.1038/NMETH.1292.

Borgdorff, A. J. et al. (2008) 'Ejaculation Elicited by Microstimulation of Lumbar Spinothalamic Neurons', European Urology, 54(2), pp. 449–456. doi: 10.1016/j.eururo.2008.03.043.

Boyden, E. S. et al. (2005) 'Millisecond-timescale, genetically targeted optical control of neural activity', Nature Neuroscience, 8(9), pp. 1263–1268. doi: 10.1038/nn1525.

Cappelleri, J. C. et al. (2007) 'Clinically meaningful improvement on the Self-Esteem And Relationship questionnaire in men with erectile dysfunction', Quality of Life Research, 16, pp. 1203–1210. doi: 10.1007/sl.

Carro-Juárez, M. and Rodríguez-Manzo, G. (2005) 'Role of genital sensory information in the control of the functioning of the spinal generator for ejaculation', International Journal of Impotence Research, 17(2), pp. 114–120. doi: 10.1038/sj.ijir.3901277.

Carro-Juárez, M. and Rodríguez-Manzo, G. (2008) 'The spinal pattern generator for ejaculation', Brain Research Reviews, 58(1), pp. 106–120. doi: 10.1016/j.brainresrev.2007.12.002.

Carson, C. and Gunn, K. (2006) 'Premature ejaculation: definition and prevalence', International Journal of Impotence Research, 18(SUPPL. 1), pp. 5–13. doi: 10.1038/sj.ijir.3901507.

Chéhensse, C. et al. (2017) 'Human spinal ejaculation generator', Annals of Neurology, 81(1), pp. 35–45. doi: 10.1002/ana.24819.

Clarac, F. et al. (2004) 'The in vitro neonatal rat spinal cord preparation: a new insight into mammalian locomotor mechanisms', Journal of Comparative Physiology, 190(5), pp. 343–357. doi: 10.1007/s00359-004-0499-2.

Coolen, L. M. et al. (2003) 'Afferent connections of the parvocellular subparafascicular thalamic nucleus in the rat: Evidence for functional subdivisions', Journal of Comparative Neurology, 463(2), pp. 132–156. doi: 10.1002/cne.10739.

Coolen, L. M. et al. (2004) 'Central regulation of ejaculation.', Physiology & Behavior, 83(2), pp. 203–215. doi: 10.1016/j.physbeh.2004.08.023.

Corona, G. et al. (2012) 'The hormonal control of ejaculation', Nature Reviews Urology, 9(9), pp. 508–519. doi: 10.1038/nrurol.2012.147.

Dewsbury, D. A. (1972) ‘Patterns of copulatory behavior in male mammals’, The Quarterly review of biology, 47(1), pp. 1–33.

Dobberfuhl, A. D. et al. (2014) ‘Identification of CNS neurons innervating the levator ani and ventral bulbospongiosus muscles in male rats’, Journal of Sexual Medicine, 11(3), pp. 664–677. doi: 10.1111/jsm.12418.

El-Sakka, A. I. and Lue, T. F. (2004) ‘Physiology of penile erection.’, The Scientific World Journal, 4, pp. 128–134. doi: 10.1100/tsw.2004.58.

Friese, A. et al. (2009) ‘Gamma and alpha motor neurons distinguished by expression of transcription factor Err3’, Proceedings of the National Academy of Sciences of the United States of America, 106(32), pp. 13588–13593.

Frigon, A. and Rossignol, S. (2006) ‘Experiments and models of sensorimotor interactions during locomotion’, Biological Cybernetics, 95(6), pp. 607–627. doi: 10.1007/s00422-006-0129-x.

Georgiadis, J. R., Kringelbach, M. L. and Pfaus, J. G. (2012) ‘Sex for fun: a synthesis of human and animal neurobiology’, Nature reviews. Urology. Nature Publishing Group, 9(9), pp. 486–498. doi: 10.1038/nrurol.2012.151.

Gerendai, I. et al. (2000) ‘Central nervous system structures labelled from the testis using the transsynaptic viral tracing technique’, Journal of Neuroendocrinology, 12(11), pp. 1087–1095. doi: 10.1046/j.1365-2826.2000.00560.x.

Gerendai, I. et al. (2003) ‘Identification of neurones of the brain and spinal cord involved in the innervation of the ductus deferens using the viral tracing method’, International Journal of Andrology, 26(2), pp. 91–100. doi: 10.1046/j.1365-2605.2003.00392.x.

Giuliano, F. et al. (1997) ‘Erectile response to hypothalamic stimulation in rats: role of peripheral nerves’, American Journal of Physiology - Regulatory Integrative and Comparative Physiology, 273, pp. 1990–1997. doi: 10.1152/ajpregu.1997.273.6.r1990.

Giuliano, F. and Clement, P. (2005) ‘Neuroanatomy and physiology of ejaculation.’, Annual review of sex research. United States, 16, pp. 190–216.

Gong, S. et al. (2003) ‘A gene expression atlas of the central nervous system based on bacterial artificial chromosomes’, Nature, 425(6961), pp. 917–925. doi: 10.1038/nature02033.

Gong, S. et al. (2007) ‘Targeting Cre recombinase to specific neuron populations with bacterial artificial chromosome constructs’, Journal of Neuroscience, 27(37), pp. 9817–9823. doi: 10.1523/JNEUROSCI.2707-07.2007.

De Groat, W. C. (2016) Autonomic nervous system: Central urogenital control, Reference Collection in Neuroscience and Biobehavioral Psychology. Elsevier. doi: 10.1016/B978-0-12-809324-5.01816-2.

Guertin, P. A. (2013) 'Central pattern generator for locomotion: anatomical, physiological, and pathophysiological considerations', Frontiers in Neurology, 3(183), pp. 1–15. doi: 10.3389/fneur.2012.00183.

Hancock, M. B. and Peveto, C. A. (1979) 'Preganglionic neurons in the sacral spinal cord of the rat: an HRP study', Neuroscience Letters, 11(1), pp. 1–5. doi: 10.1016/0304-3940(79)90046-6.

Harrison, M. et al. (2013) 'Vertebral landmarks for the identification of spinal cord segments in the mouse', NeuroImage. Elsevier B.V., 68, pp. 22–29. doi: 10.1016/j.neuroimage.2012.11.048.

Holstege, G. et al. (1986) 'Anatomical and physiological observations on supraspinal control of bladder and urethral sphincter muscles in the cat', Journal of Comparative Neurology, 250(4), pp. 449–461. doi: 10.1002/cne.902500404.

Holstege, G. and Tan, J. (1987) 'Supraspinal control of motoneurons innervating the striated muscles of the pelvic floor including urethral and anal sphincters in the cat', Brain, 110(5), pp. 1323–1344. doi: 10.1093/brain/110.5.1323.

Huynh, H. K. et al. (2013) 'Pontine Control of Ejaculation and Female Orgasm', Journal of Sexual Medicine, 10(12), pp. 3038–3048. doi: 10.1111/jsm.12300.

Köbbert, C. et al. (2000) 'Current concepts in neuroanatomical tracing', Progress in Neurobiology, 62(4), pp. 327–351. doi: 10.1016/S0301-0082(00)00019-8.

Kolbeck, S. C. and Steers, W. D. (1992) 'Neural regulation of the vas deferens in the rat: An electrophysiological analysis', American Journal of Physiology - Regulatory Integrative and Comparative Physiology, 263, pp. 331–338. doi: 10.1152/ajpregu.1992.263.2.r331.

Kozyrev, N., Lehman, M. N. and Coolen, L. M. (2012) 'Activation of Gastrin-releasing Peptide Receptors in the Lumbosacral Spinal Cord is Required for Ejaculation in Male Rats', Journal of Sexual Medicine, 9(5), pp. 1303–1318. doi: 10.1111/j.1743-6109.2012.02688.x.

Krukoff, T. L. (1999) 'c-fos Expression as a Marker of Functional Activity in the Brain BT - Cell Neurobiology Techniques', in Boulton, A. A., Baker, G. B., and Bateson, A. N. (eds). Totowa, NJ: Humana Press, pp. 213–230. doi: 10.1385/0-89603-510-7:213.

Larsson, K. and Sodersten, P. (1973) 'Mating in male rats after section of the dorsal penile nerve', Physiology and Behavior, 10(3), pp. 567–571. doi: 10.1016/0031-9384(73)90223-0.

Leitzmann, M. F. et al. (2004) 'Ejaculation Frequency and Subsequent Risk of Prostate Cancer', Jama, 291(13), pp. 1578–1586. doi: 10.1001/jama.291.13.1578.

Lenschow, C. et al. (2016) 'Sexually Monomorphic Maps and Dimorphic Responses in Rat Genital Cortex', Current Biology. Elsevier Ltd, 26(1), pp. 106–113. doi: 10.1016/j.cub.2015.11.041.

Lenschow, C. and Lima, S. Q. (2020) 'In the mood for sex: neural circuits for reproduction', Current Opinion in Neurobiology. Elsevier Ltd, 60, pp. 155–168. doi: 10.1016/j.conb.2019.12.001.

Liao, X. and Walters, E. T. (2002) 'The use of elevated divalent cation solutions to isolate monosynaptic components of sensorimotor connections in Aplysia', Journal of Neuroscience Methods, 120(1), pp. 45–54. doi: 10.1016/S0165-0270(02)00189-9.

Lima, S. Q. et al. (2009) 'PINP: A new method of tagging neuronal populations for identification during in vivo electrophysiological recording', PLoS ONE, 4(7), pp. 1–10. doi: 10.1371/journal.pone.0006099.

Lucio, R. A. et al. (2012) 'The physiology and ecophysiology of ejaculation', Tropical and Subtropical Agroecosystems, 15(SUPPL. 1), pp. S113–S127.

Madisen, L. et al. (2010) 'A robust and high-throughput Cre reporting and characterization system for the whole mouse brain', Nature Neuroscience. Nature Publishing Group, 13(1), pp. 133–140. doi: 10.1038/nn.2467.

Madisen, L. et al. (2012) 'A toolbox of Cre-dependent optogenetic transgenic mice for light-induced activation and silencing', Nature Neuroscience, 15(5), pp. 793–802. doi: 10.1038/nn.3078.

Mao, T. et al. (2011) 'Long-Range Neuronal Circuits Underlying the Interaction between Sensory and Motor Cortex', Neuron. Elsevier Inc., 72(1), pp. 111–123. doi: 10.1016/j.neuron.2011.07.029.

Marson, L. and Carson, C. (1999) 'Central Nervous System Innervation of the Penis, Prostate, and Perineal Muscles: A Transneuronal Tracing Study', Molecular urology. United States, 3(2), pp. 43–50.

Marson, L. and McKenna, K. E. (1990) 'The identification of a brainstem site controlling spinal sexual reflexes in male rats', Brain research, 515, pp. 303–308.

Marson, L. and McKenna, K. E. (1992) 'A role for 5-hydroxytryptamine in descending inhibition of spinal sexual reflexes', Experimental Brain Research, 88(2), pp. 313–320. doi: 10.1007/BF02259106.

Marson, L. and McKenna, K. E. (1996) 'CNS cell groups involved in the control of the ischiocavernosus and bulbospongiosus muscles: A transneuronal tracing study using pseudorabies virus', Journal of Comparative Neurology, 374(2), pp. 161–179. doi: 10.1002/(SICI)1096-9861(19961014)374:2<161::AID-CNE1>3.0.CO;2-0.

Marson, L., Platt, K. B. and McKenna, K. E. (1993) 'Central nervous system innervation of the penis as revealed by the transneuronal transport of pseudorabies virus.', Neuroscience, 55(1), pp. 263–280. doi: 10.1016/0306-4522(93)90471-Q.

Maunder, L., Schoemaker, D. and Pruessner, J. C. (2017) 'Frequency of Penile–Vaginal Intercourse is Associated with Verbal Recognition Performance in Adult Women', Archives of Sexual Behavior, 46, pp. 441–453. doi: 10.1007/s10508-016-0890-4.

McGill, T. E. (1962) 'Sexual behavior in three inbred strains of mice', Behavior, 19(4), pp. 341–350.

Misawa, H. et al. (2012) 'Osteopontin Is an Alpha Motor Neuron Marker in the Mouse Spinal Cord', Journal of Neuroscience Research, 90, pp. 732–742. doi: 10.1002/jnr.22813.

Nadelhaft, I., deGroat, W. C. and Morgan, C. (1980) 'Location and Morphology of Parasympathetic Preganglionic Neurons in the Sacral Spinal Cord of the Cat Revealed by Retrograde Axonal Transport of Horseradish Peroxidase', Journal of Comparative Neurology, 193, pp. 265–281.

Nadelhaft, I. and McKenna, K. E. (1987) 'Sexual Dimorphism in Sympathetic Preganglionic Neurons of the Rat Hypogastric Nerve', Journal of Comparative Neurology, 256, pp. 308–315.

Newman, H. F., Reiss, H. and Northup, J. D. (1982) 'Physical basis of emission, ejaculation, and orgasm in the male', Urology, XIX(4), pp. 341–350.

Nicholas, A. P., Zhang, X. and Hokfelt, T. (1999) 'An immunohistochemical investigation of the opioid cell column in lamina X of the male rat lumbosacral spinal cord', Neuroscience Letters, 270, pp. 9–12.

Normandin, J. J. and Murphy, A. Z. (2011) 'Serotonergic lesions of the periaqueductal gray, a primary source of serotonin to the nucleus paragigantocellularis, facilitate sexual behavior in male rats', Pharmacology Biochemistry and Behavior, 98(3), pp. 369–375. doi: 10.1016/j.pbb.2011.01.024.Serotonergic.

Nuding, S. C. and Nadelhaft, I. (1998) 'Bilateral projections of the pontine micturition center to the sacral parasympathetic nucleus in the rat', Brain research, 785, pp. 185–194.

Núnez, R., Gross, G. H. and Sachs, B. D. (1986) 'Origin and Central Projections of Rat Dorsal Penile Nerve: Possible Direct Projection to Autonomic and Somatic Neurons by Primary Afferents of Nonmuscle Origin', Journal of Comparative Neurology, 247, pp. 417–429.

Orr, R. and Marson, L. (1998) 'Identification of CNS neurons innervating the rat prostate: A transneuronal tracing study using pseudorabies virus', Journal of the Autonomic Nervous System, 72, pp. 4–15.

Oti, T. et al. (2021) 'Oxytocin Influences Male Sexual Activity via Non- synaptic Axonal Release in the Spinal Cord', Current Biology. Elsevier Ltd., 31(1), pp. 103–114. doi: 10.1016/j.cub.2020.09.089.

Pascual, J. I., Insausti, R. and Gonzalo, L. M. (1992) 'Pudendal nerve topography in the rat spinal cord projections studied with the axonal tracer wheat germ agglutimnin conjugated-

horseradish peroxidase', The Journal of Urology. The American Urological Association Education and Research, Inc., 147(3), pp. 718–722. doi: 10.1016/S0022-5347(17)37365-2.

Peikert, K. et al. (2015) 'The Male Bulbospongiosus Muscle and Its Relation to the External Anal Sphincter', Journal of urology, 193, pp. 1433–1440. doi: 10.1016/j.juro.2014.10.050.

Pescatori, E. S. et al. (1993) 'Electrical stimulation of the dorsal nerve of the penis evokes reflex tonic erections of the penile body and reflex ejaculatory responses in the spinal rat', The Journal of Urology. The American Urological Association Education and Research, Inc., 149(3), pp. 627–632. doi: 10.1016/S0022-5347(17)36168-2.

Sachs, B. D. (1982) 'Role of striated penile muscles in penile reflexes, copulation, and induction of pregnancy in the rat', Journal of reproduction and fertility, 66, pp. 433–443.

Saleeba, C. et al. (2019) 'A Student's Guide to Neural Circuit Tracing', Frontiers in Neuroscience, 13(897), pp. 1–20. doi: 10.3389/fnins.2019.00897.

Schellino, R., Boido, M. and Vercelli, A. (2020) 'The Dual Nature of Onuf's Nucleus : Neuroanatomical Features and Peculiarities, in Health and Disease', Frontiers in Neuroanatomy, 14(572013), pp. 1–13. doi: 10.3389/fnana.2020.572013.

Schmidt, M. H. and Schmidt, H. S. (1993) 'The ischiocavernosus and bulbospongiosus muscles in mammalian penile rigidity', Sleep, 16(2), pp. 171–183.

Shafik, A. and El-Sibai, O. (2000) 'Mechanism of ejection during ejaculation: identification of a urethrocavernosus reflex', Archives of Andrology, 44, pp. 77–83.

Sheu, G., Revenig, L. M. and Hsiao, W. (2014) 'Physiology of Ejaculation', in Men's Sexual Health and Fertility. Springer New York, pp. 13–29. doi: 10.1007/978-1-4939-0425-9.

Stepien, A. E., Tripodi, M. and Arber, S. (2010) 'Monosynaptic Rabies Virus Reveals Premotor Network Organization and Synaptic Specificity of Cholinergic Partition Cells', Neuron. Elsevier Inc., 68(3), pp. 456–472. doi: 10.1016/j.neuron.2010.10.019.

Strack, A. M. and Loewy, A. D. (1990) 'Pseudorabies Virus: A Highly Specific Transneuronal Cell Body Marker in the Sympathetic Nervous System', The Journal of neuroscience, 10(7), pp. 2139–2147.

Taccola, G., Marchetti, C. and Nistri, A. (2004) 'Modulation of rhythmic patterns and cumulative depolarization by group I metabotropic glutamate receptors in the neonatal rat spinal cord in vitro', European Journal of Neuroscience, 19, pp. 533–541. doi: 10.1111/j.1460-9568.2003.03148.x.

Tanahashi, M. et al. (2012) 'Characterization of bulbospongiosus muscle reflexes activated by urethral distension in male rats', American Journal of Physiology - Regulatory Integrative and Comparative Physiology, 303, pp. 737–747. doi: 10.1152/ajpregu.00004.2012.

Tang, Y. et al. (1999) ‘Spinal and Brain Circuits to Motoneurons of the Bulbospongiosus Muscle: Retrograde Transneuronal Tracing With Rabies Virus’, The Journal of comparative neurology, 414, pp. 167–192.

Truitt, W. A. et al. (2003) ‘Activation of a subset of lumbar spinothalamic neurons after copulatory behavior in male but not female rats’, The Journal of neuroscience, 23(1), pp. 325–331. Available at: http://www.ncbi.nlm.nih.gov/pubmed/12514231.

Truitt, W. A. and Coolen, L. M. (2002) ‘Identification of a potential ejaculation generator in the spinal cord’, Science, 297, pp. 1566–1569. doi: 10.1126/science.1073885.

Turley, K. R. and Rowland, D. L. (2013) ‘Evolving ideas about the male refractory period’, BJU International, 112, pp. 442–452. doi: 10.1111/bju.12011.

Ueyama, T., Arakawa, H. and Mizuno, N. (1987) ‘Central distribution of efferent and afferent components of the pudendal nerve in rat’, Anatomy and Embryology, 177, pp. 37–49.

Valente, S., Marques, T. and Lima, S. Q. (2021) ‘No evidence for prolactin’s involvement in the post-ejaculatory refractory period’, Communications Biology. Springer US, 4(10), pp. 1–10. doi: 10.1038/s42003-020-01570-4.

Vizzard, M. A. et al. (1995) ‘Transneuronal labeling of neurons in the adult rat brainstem and spinal cord after injection of pseudorabies virus into the urethra’, Journal of Comparative Neurology, 355(4), pp. 629–640. doi: 10.1002/cne.903550411.

Watson, C. et al. (2009) ‘Atlas of the Mouse Spinal Cord’, in Watson, C., Paxinos, G., and Kayalioglu, G. B. T.-T. S. C. (eds) The spinal cord. San Diego: Academic Press, pp. 308–379. doi: https://doi.org/10.1016/B978-0-12-374247-6.50020-1.

Zer-Krispil, S. et al. (2018) ‘Ejaculation Induced by the Activation of Crz Neurons Is Rewarding to Drosophila Males’, Current Biology. Elsevier Ltd., 28(9), pp. 1445–1452. doi: 10.1016/j.cub.2018.03.039.